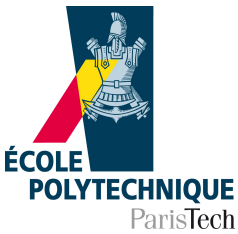

Transient Instability Mechanisms by Frequency Coalescence in Fluid Structure Systems*

*Mécanismes Transitoires d'Instabilités par Confusion de Fréquence dans des Systèmes Fluides-Structures

Muhamad SHEHRYAR

Laboratoire d'Hydrodynamique (LadHyX)

École Polytechnique

Palaiseau, France

Thèse présentée pour obtenir le grade de

Docteur de l'École Polytechnique,
Spécialité Mécanique

En vue d'une soutenance le 3 Décembre 2010 devant le jury composé de :

Laurent JOLY	Rapporteur	ISAE, Toulouse
Ian TAYLOR	Rapporteur	University of Strathclyde
Benoit OESTERLE	Examinateur	Université de Nancy I
Gérard GRILLAUD	Examinateur	CSTB, Nantes
Xavier BOUTILLON	Examinateur	École Polytechnique
Pascal HEMON	Directeur de thèse	École Polytechnique

my parents and my wife

Acknowledgement

it all started with an e-mail:

... ... Please let me know if I can apply for a PhD position
in your laboratory ... ...

who knew those simple words would bring me the three years of work experience which I shall cherish for the rest of my life. It wasn't long after that I was at LadHyX working with Pascal Hémon.

From the first coffee that I had at LadHyX up till now when I add these final words to my thesis, Pascal has always been there, bearing with me all the way. Going lengths and taking pain to respond to my silly questions. I wouldn't have learnt probably half of what I know today had it not been for his keen interest and personal concern. He pointed me in the right direction and inspired me to learn more and do better. Words cannot explain my deep gratitude and profound respect that he earned over the last three years. Pascal, thank you for letting me work with you and pushing me all the way to this stage.

Emmanuel, your towering personality (and I mean literally a towering personality) and your signature laugh have always been my inspiration. Discussing problems with you was always an enlightening experience. Had it not been your encouragement doing a large part of this thesis would have been very boring. Xavier Amandolèse, thank you for patiently listening to me and for all the sincere advice that I needed the most.

Patrick, if I want to be like anyone in this world, that is you. Asking you all the wild questions on our way to the cafeteria used to be the best part of the whole day.

I must thank Christelle and Franz for tolerating me through the thesis writing phase and for not throwing me out during my allergies. Franz, thank you so much for all the jokes and fun. By the way, plant on the office table, seriously, what were you thinking? Christelle, I hope your cat gets well soon.

Benoit, thank you for all the coffees that we had at the lab. I couldn't have learnt LaTeX without your support. You saved me valuable time with all the tricks in Matlab. Thank you so much for always taking out time to help me.

Successful completion of this thesis would not have been possible had it not been for the constant IT support by Daniel Guy and Alexandre Rosinisky. Thérèse, I remember when you showed me the Bureau de Badge, listened to all my broken French and did not embarass me. Credit for the unique working environment at LadHyX goes to all the PhD Students, GianLu, Cristobal, Elena, Xavier, Johnny, Yu, thank you guys for the great company. Shyam, you have been an awsome smoking partner.

While all the results discussed in this report have been obtained experimentally using the facilities at LadHyX, I was paid a monthly stipend by the Higher Education Commission, Governement of Pakistan. Thank you Sir's' for letting me persue this PhD.

Finally, someone I can't live without, SADDAF, thank you for staying up late for me all these years, for being with me every day and every night, for encouraging me all the way, for praying for me and for all the love. I couldn't have done this without you.

Abstract

This thesis concerns the transient mechanism in fluid structure systems with two coupled degrees of freedom, submitted to frequency coalescence instabilities. Three different solid objects are studied in the order of increasingly streamlined cross sections, namely a square cylinder, a streamlined bridge deck section and a symmetric airfoil. This report is divided into two parts. First part is reserved for the long term behavior of all the three fluid structure systems. The square cylinder is allowed to oscillate freely in a high mass ratio environment. Experiments are repeated, firstly without the memory effect and then with the memory effect over the entire reduced velocity range. Data points obtained from the first case represent validity of the experimental procedure. The later case demonstrates the existence of hysteresis in the reduced amplitude curve. A comparison is developed with a standard wake oscillator model. Long term stability parameters for a bridge deck and a symmetric airfoil are measured and validated using simple theoretical tools detailed in Part-I. Part-II of the thesis report is dedicated to the transient behavior. Growth rate of oscillations amplitude for the square cylinder is measured for the first case, as mentioned above. Experimental results are provided showing the effect of frequency ratio and the amplitude of initial excitation on the maximum energy amplification for the bridge deck. The bridge deck behavior is studied first, under the effect of a mechanical excitation and then under the effect of an excitation induced by an abrupt gust. The airfoil is studied in a linear and a non-linear structural environment subjected to an abrupt gust. Experimental evidence of the existence of by-pass transition to flutter instability in case of the non-linear setup is provided and discussed. A new combination of the quasi steady theory and the Kussner's aerodynamic admittance function is proposed to validate the results obtained for the linear airfoil setup. Some discussion and a few ideas about the future work are included in the end.

Keywords

Vortex Induced Vibrations, Limit Cycle Oscillations, Hysteresis, Lock-in, Growth Rate, Transient Growth, Frequency Ratio, Bridge Deck, Airfoil, By-pass Transition, Aerodynamic Damping / Stiffness.

Résumé

Cette thèse porte sur les mécanismes transitoires de systèmes fluide-structure à deux degrés de liberté, soumis à des instabilités par confusion de fréquence. Trois différents objets solides sont étudiés dans l'ordre des sections de plus en plus aérodynamique: un cylindre carré, un profil de pont et un profil d'aile symétrique. Deux grandes parties composent ce manuscrit. La première concerne le comportement à long terme des trois systèmes. Le cylindre carré oscille librement sous l'effet du vent. Les expériences sont réalisées d'abord sans effet mémoire, puis avec l'effet mémoire, sur la gamme complète de vitesse réduite. La seconde série d'expériences démontre l'existence d'une hystérésis sur l'amplitude réduite. Une comparaison avec un modèle classique est présentée. Les paramètres de stabilité à long terme pour le profil de pont et le profil d'aile symétrique sont mesurés et validés à l'aide d'outils théoriques simples. La seconde partie du rapport de thèse est consacrée au comportement transitoire. Le taux de croissance de l'amplitude des oscillations du cylindre carré est mesuré. Le comportement du profil du pont est étudié d'abord sous l'effet d'une excitation mécanique, puis sous l'effet d'une excitation par une rafale de vent. Les résultats expérimentaux sont fournis montrant l'effet du rapport de fréquence et de l'amplitude de l'excitation initiale sur l'amplification d'énergie par croissance transitoire. Le profil d'aile symétrique est étudié dans un montage linéaire puis non-linéaire soumis aux effets d'une rafale soudaine. L'existence de la transition by-pass vers l'instabilité de flottement dans le cas du système non-linéaire est démontrée à l'aide des résultats expérimentaux. Une combinaison de la théorie quasi-stationnaire et de la fonction de Küssner est proposée et en très bon accord avec les résultats des mesures. Le rapport conclut par des discussions et quelques idées sur les travaux futurs.

Mots clés

Vibrations Induite par détachement des tourbillonaires, Cycle limite, l'Hystérésis, Lock-in, Taux de croissance, Croissance transitoire, la raport de fréquence, Profil du pont, Profil d'aile, Croissance by-pass, Amortissement / Rigidité aérodynamique.

Contents

List of Figures

List of Tables

Nomenclature

A	Coupling force scaling, wake-oscillator model
A_i	Aeroelastic coefficients for torsional motion
b	Span of the airfoil, bridge deck and square cylinder
B	Chord of the bridge deck section
c	Chord of the airfoil
c	Structural damping, square cylinder set-up
C_c	Critical damping, square cylinder set-up (N.s/m)
C_D	Drag coefficient
$C(k)$	Theodoresen circulation function
C_L	Lift coefficient, square cylinder set-up
C_{L_o}	Lift coefficient measured on a fixed cylinder subjected to vortex shedding
C_M	Moment coefficient
C_{M_a}	Added mass coefficient
C_z	Lift coefficient airfoil and bridge deck set-ups
C'_z	Derivative of lift coefficient, $C'_z = \frac{\partial}{\partial \alpha} C_z$
d	Distance between the center of gravity *'G'* and axis of rotation *'O'* (m)
D	Side of the square cylinder (m)
$E(t)$	Total energy as a function of time (J)
E_o	Initial energy (J)
E_{max}	Maximum energy (J)
$E_{nl}(t)$	Energy term due to the non-linear feature in the airfoil set-up (J)
$\left(\frac{E_{max}}{E_o}\right)_c$	Maximum normalized energy at critical mean velocity, U_c
f	Frequency of the LCO for square cylinder (Hz)

f_o	Un-damped natural frequency of the square cylinder (Hz)
f_α, f_z	Pure natural frequencies (Hz), airfoil and bridge deck set-ups
f_1, f_2	Frequencies in bending and in torsion, airfoil and bridge deck set-ups
f_w	Vortex shedding frequency ($f_w = f_o S t U_r$)
f^*	Reduced frequency of the LCO ($f^* = \frac{f}{f_o}$)
$F'(t)$	Fluctuating lift component (N)
F_z	Lift force (N)
F_x	Drag force (N)
g	Gap value in the non-linear airfoil set-up
H_i	Aeroelastic coefficients for flexural motion
J_o	Moment of inertia around O, $\left(kg.m^2\right)$, airfoil and bridge deck set-ups
k	Stiffness (N/m), Square cylinder set-up
k_a, k_z	Stiffness (N.m/rad) and (N/m), airfoil and bridge deck set-ups
K	Reduced circular frequency, $K = \frac{2\pi}{U_r}$.
L	Circulatory lift
m	Mass (kg)
M	Mass parameter, square cylinder setup, $M = \frac{C_{Lo}}{2}\frac{1}{2\pi^2 St^2 \mu}$.
M_o	Pitching moment at the axis of rotation O, (Nm), airfoil and bridge deck set-ups
q	Reduced vortex lift coefficient, $q = 2\frac{C_L}{C_{Lo}}$
r_F	Frequency ratio, $r_F = \frac{f_z}{f_\alpha}$, bridge deck set-up
r_s	Structural damping, square cylinder set-up
Re	Reynold's number
$S(k)$	Sears admittance function
S_c	Scruton number, $S_c = 2\eta\mu$
S_G	Skopp-Griffin parameter, $S_G = 4\pi^2 St^2 S_c$
St	Strouhal number, $St = \frac{f_w}{U} D$
u	Horizontal component of up-stream gust (m/s)
U	Wind velocity (m/s)
$\overline{U}$	Mean wind velocity (m/s)
U_c	Critical wind velocity (m/s)

U_{cnl}	Non-linear critical wind velocity (m/s)
U_r	Reduced velocity ($U_r = \dfrac{\overline{U}}{Df_o}$)
w	Vertical component of up-stream gust (m/s)
z_M	Oscillation amplitude at lock-in
$z(t)$	Pure vertical motion, (m), airfoil and bridge deck set-ups
$z(t)$	Amplitude of the transverse vortex induced oscillations for square cylinder set-up
Z^*	Reduced RMS amplitude of LCO ($Z^* = \dfrac{\hat{z}}{D}$)
α	Angular displacement, (rad), airfoil and bridge deck set-ups
δ	Growth rate of the oscillations square cylinder set-up (%)
δk	Additional stiffness in the non-linear airfoil set-up
ϵ	Near wake Van der Pole parameter
η	Damping ratio, square cylinder set-up ($\eta = \dfrac{c}{C_c}$)
η_α, η_z	Reduced structural damping (%)
γ	Added damping coefficient (%)
$\lambda_\alpha, \lambda_z$	Pure eigen values (rad^2/s^2)
μ	Dimensionless mass ratio, $\mu = \dfrac{m}{\rho D^2 b}$
ν	Kinematic viscosity (m^2/s)
ω_α, ω_z	Pure angular frequencies (rad/s)
$\Omega = \Omega_f$	Vortex shedding angular frequency, $\Omega_f = 2\pi St\dfrac{U}{D}$
Ω_s	Structural angular frequency, square cylinder set-up, $\Omega_s = \sqrt{\dfrac{k}{m}}$
$\Phi(\tau)$	Wagner's aerodynamic indicial admittance function
$\Psi(\tau)$	Kussner's aerodynamic indicial admittance function
ρ	Air density (kg/m^3)
τ	Non-dimensional time, $\tau = \dfrac{2U}{c}t$
φ	Phase angle between the vortex shedding frequency and the cylinder oscillating frequency
ξ	Reduced structural damping for square cylinder, $\xi = \dfrac{r_s}{2m\Omega_s}$

Chapter 1

Introduction

From an eagle soaring in the sky to long curly rivers tracing their paths through valleys and fields to the perfectly synchronized dancing corn fields taking their queue from the wind, almost everything that goes on around us in nature involves a solid structural body interacting with a freely flowing fluid. Either its flesh and bone of a bird or solid rock, structures of many different types interact with air or water all the time. Its not just nature; most of human activities from driving to work on a busy week day to wave surfing during the vacations constitute un-deniably; uncountable examples of fluid structure interaction systems. The importance of this field of science cannot be over stated.

1.1 Motivation

In nature as a fluid interacts with a solid object, the mere interface between the two mediums results in a net force being exerted on the solid surface. A flexible solid surface may deform under the load. A rigid solid may displace from its original position given the magnitude of the applied force is large enough. Either case results in a reactionary force changing the fluid flow in return. Our discussion during the course of this study however, shall be limited to rigid oscillating solids in a uniform fluid flow. This action and reaction mechanism results in a highly coupled fluid structure system in the sense that any small change in the characteristics of one would result in a proportional change in the dynamic characteristics of the other.

Given the extremely un-predictable behavior of various important parameters in nature; if such a highly interactive coupled system is left un-checked, the magnitude of energy exchanged between the two mediums may rise to dangerous levels. The

system may self-destruct. Luckily, enough research has already been done in this field of science to allow us a fairly good understanding of the under lying mechanisms of instabilities likely to be generated under such circumstances.

From a scientific point of view, a system is normally considered to have just two degrees of freedom to ensure simplicity. Each degree of freedom has its proper natural frequency. A system shall be at a greater risk of annihilation if the two frequencies are close together or even approach one another under the effect of a rapidly changing dynamic variable. The reason being, as the two frequencies approach one another, the fluid and the structure motion gets increasingly synchronized. The extent of energy transfer increases resulting in higher amplitude of structure oscillations. The amplitude may increase to a limit where the structure may suffer fatigue and consequently failure.

In a fluid structure interaction system this dynamic variable is usually the mean free stream fluid velocity. As long as the two frequencies are far apart, there is no such threat to the integrity of the system. The system is said to be stable. Frequency interaction in a two degree of freedom system can be depicted by one of the following schematics:

(a).

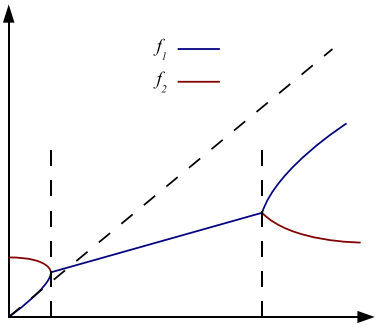

Type-I: Limited Frequency Coalescence

(b).

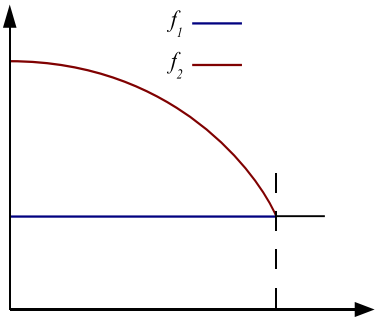

Type-II: Un-limited Frequency Coalescence, Class 1

(c).

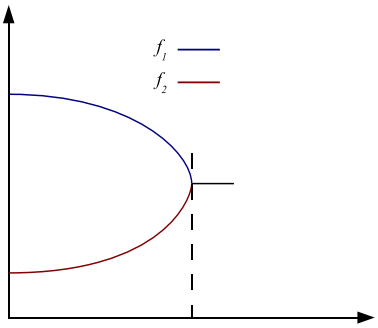

Type-II: Un-limited Frequency Coalescence, Class 2

Figure 1.1: Frequency Coalescence Mechanisms Fluid Structure Systems.

TYPE - I: Limited Frequency Coalescence

The first type of frequency interaction mechanism prevails in instances like when a solid object is immersed, partially or completely, in a flow stream. Presence of the solid in the flow stream generates complex fluid flow phenomena down stream, namely vortex generation and shedding at a natural frequency which is a function of the mean flow stream velocity. Lets call this frequency f_2 as in the Fig.1.1. As f_2 approaches the natural frequency of the solid, namely f_1, the solid oscillations start dominating the down stream vortex shedding. The two frequencies coalesce into a single frequency which is close to but different from the natural frequency of the solid object. The two frequencies are said to have *'Locked-in'*[1]. As the frequencies coalesce, amplitude of the system oscillations increases dramatically. As the mean free stream velocity approaches a second critical value, the two frequencies split again. Hence, the name 'limited frequency coalescence'. As the two frequencies split, the amplitude of the system oscillations returns to its previous values. The system seemingly evolves towards just a single degree of freedom oscillation mechanism. The present study encompasses only the lock-in phenomena. Higher velocity range beyond the frequency lock-in shall not be discussed here.

TYPE - II: Un-Limited Frequency Coalescence

Let us start by understanding that as the two frequencies coalesce in this case, the system under consideration becomes unstable unlike the Type-I mechanism. Amplitude of the oscillations grows exponentially. The solid object is said to *'flutter'*. Any further increase in the magnitude of the mean free stream velocity only takes the system deeper into the unstable region, hence the name 'un-limited frequency coalescence'. However, as long as the mean free stream velocity is below this critical value the system is stable unless it is excited to the un-stable state by external means as shall be discussed later. This mechanism can be further sub-divided into two classes, Fig.1.1. In case of Class-1, one of the frequencies of the system remains quasi-constant while the other frequency varies. Smoothly as the mean free stream velocity is low but comparatively abruptly as it approaches the system critical velocity. The *'critical velocity'* in such cases is defined as the velocity where the

1. Sarpkaya (1979) defines lock-in in such cases as when the frequencies of vortex shedding and the body oscillations collapse into a single frequency close to the natural frequency of the body, Fig.1.1. This 'frequency lock-in' phenomena is known to range over $\pm 25\% \approx \pm 30\%$ of the natural vortex shedding frequency.

frequencies coalesce. In Class-2 however, ideally both the frequencies mirror each other's behavior, Fig.1.1(c). This clear distinction in behavior within Type-II can be attributed to the existence of strong structural coupling between the two degrees of freedom in Class-2. In case of Class-1 usually in real life scenarios, structural coupling between the two degrees of freedom is avoided by manipulating various structural parameters. It can not however be eliminated entirely given the aerodynamic effects which reveal themselves in detailed theoretical modelling of such problems. All the pertinent structural parameters and the added aerodynamic terms shall be identified and discussed in the following chapters.

In man made systems, Type-I limited frequency coalescence mechanism prevails largely in human inventions like sky-scrapers, chimney stacks and riser tubes etc. The Type-II, Class-1 un-limited frequency coalescence mechanism exists more often in civil constructions like bridge decks. Aircraft structures generally exhibit the Type-II, Class-2 mechanism. We shall investigate all these cases in more detail in the chapters which follow. Figs.1.1(a, b & c) correspond to Figs.1.2(a, b & c) respectively.

(a).

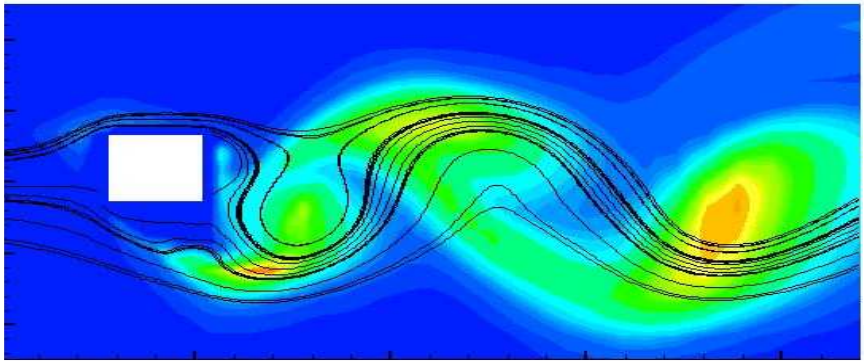

(b).

(c).

Figure 1.2: Fluid Structure Interaction Systems. (a). Flow Past a Bluff Body (b). Suspension Bridge at Porte de Millau France (c). Airbus A380 landing at Sydney Airport November 2006.

1.2 Limited Frequency Coalescence

Vortex-induced vibration of structures is of practical interest in many fields of engineering. It can cause vibrations in heat exchanger tube bundles, it influences the dynamics of riser tubes bringing oil from the sea bed to the surface, it is important for the design of civil structures such as chimney stacks as well as for the design of marine and land vehicles. It can also cause large amplitude motions of tethered structures in the ocean. These examples are just a few from the large spectrum of problems where vortex-induced-vibrations (VIV) are important.

Vibrations induced by vortices shedding down-stream of a bluff body submerged in an incident flow have been a subject of vast scientific investigations for a long time now, Fig.1.3. Wilkinson (1974), Otsuki *et al.* (1974) and Mizota & Nakamura (1975) presented some experimental data on the forced oscillations of square section cylinders. Sarpkaya (1979) presented a selective review of the then existing knowledge bank about vortex induced oscillations. Sarpkaya and the references there in remark that in case of circular cylinders inclination angle of the cylinder with respect to the mean free stream apparently does not affect the vortex induced oscillations. Bearman & Obasaju (1982) conducted a study to compare experimental results for fixed and forcibly oscillating square cylinders. They determined that the amplification of the fluctuating lift coefficient for a square cylinder at lock-in was much less than that of a circular cylinder subjected to similar conditions. Moreover, at low reduced velocities phase of the vortex shedding may actually damp out oscillations of a flexibly mounted cylinder. Below the lock-in range forced oscillations dominate the system, forcing the vortices to shed at approximately the cylinder frequency. Its only in the lock-in range that the cylinder executes vortex induced oscillations. Bearman (1984) reviewed the vortex shedding phenomena from oscillating bluff bodies. Ongoren & Rockwell (1988a) studied cylinders of various cross sections executing forced oscillations while submerged vertically in a water channel. Two different mechanisms of frequency synchronization based on whether the excitation is subharmonic or harmonic relative to the vortex formation frequency, were outlined. In a subsequent paper in the same year, they studied the effects of cylinder inclination with respect to the mean free stream, using a forced circular cylinder in a water channel. The authors contend that outside the synchronization range the symmetrical and anti-symmetrical modes compete to lock on to the near wake structure. The number of occurrences of each mode is a function of the excitation frequency and the inclination angle, Ongoren & Rockwell (1988b). Williamson & Roshko (1988)

provided the mechanism of vortex formation and the underlying physics for mode shifts. The authors concluded that the sudden phase shifts of the lift force with respect to the body motion can be attributed to the vortex pairing each half cycle occurring downstream of the bluff body. Parkinson (1989) resumed the phenomenology and the theoretical modeling tools available to understand the vortex induced oscillations and the galloping instability in case of flow past bluff bodies. Brika & Laneville (1993) studied a hollow slender cylinder in a wind tunnel and showed that the cylinder's steady response was hysteretic. Each branch in the hysteresis loop is associated to either the 2S or the 2P mode of vortex shedding. Abrupt change in the amplitude curve is attributed to the sudden mode shift. Khalak & Williamson (1999) conducted an experiment using low mass and low damping. They studied the effects of varying non-dimensional mass and non-dimensional damping. Govardhan & Williamson (2000) presented the transverse vortex induced oscillations of an elastically mounted rigid cylinder in a fluid flow. The authors point out that in a classical high mass ratio system the initial and lower amplitude branches can be distinctly identified due to a discontinuous mode transition. In case of lower mass ratio systems a further upper amplitude branch is clearly identifiable attributed to a second instance of mode transition. Extensive details about the vortex shedding mode formation and the transition from 2S to 2P can be found in Govardhan & Williamson (2000). Hémon *et al.* (2006) submitted experimental and numerical results on the aeroelastic behavior of slender rectangular and square cylinders subjected to a cross flow. Their study primarily focused on a flexible rectangular cylinder. They noted that a small increase in the free stream turbulence intensity actually reduces the critical galloping velocity. Cheng *et al.* (2003) have discussed the use of piezoelectric ceramic actuators installed on the bluff body surface. The actuators when operated would deform the cylinder surface thus modifying the fluid flow and structural vibration. Facchinetti *et al.* (2004) have investigated the coupled dynamic behavior of a circular cylinder using the classical wake oscillator model based on the one proposed by Currie & Hartlen (1970). The authors have demonstrated that the acceleration coupling in the forcing term of the wake oscillator best matches with the available experimental data. Morse & Williamson (2009) discovered the $2P_{overlap}$ mode using high resolution data from a forced oscillating cylinder at a fixed Reynold's number. They found that even when the cylinder oscillates with a constant amplitude and frequency, the cylinder wake can still shift from the 2P to $2P_{overlap}$ mode. Also, a cylinder subjected to a flow could keep on oscillating even if the vortex generation

frequency de-synchronizes with the cylinder oscillating frequency. This can be explained by the presence of a component of fluid forcing at the cylinder oscillation frequency which yields positive fluid excitation.

Common practice in studying VIV on cables and on slender structures consists in performing free motion tests in a wind tunnel on sectional models to define the lock-in region in terms both of vibration amplitudes and width of the synchronization range and the energy transferred by the wind in the mechanical system.

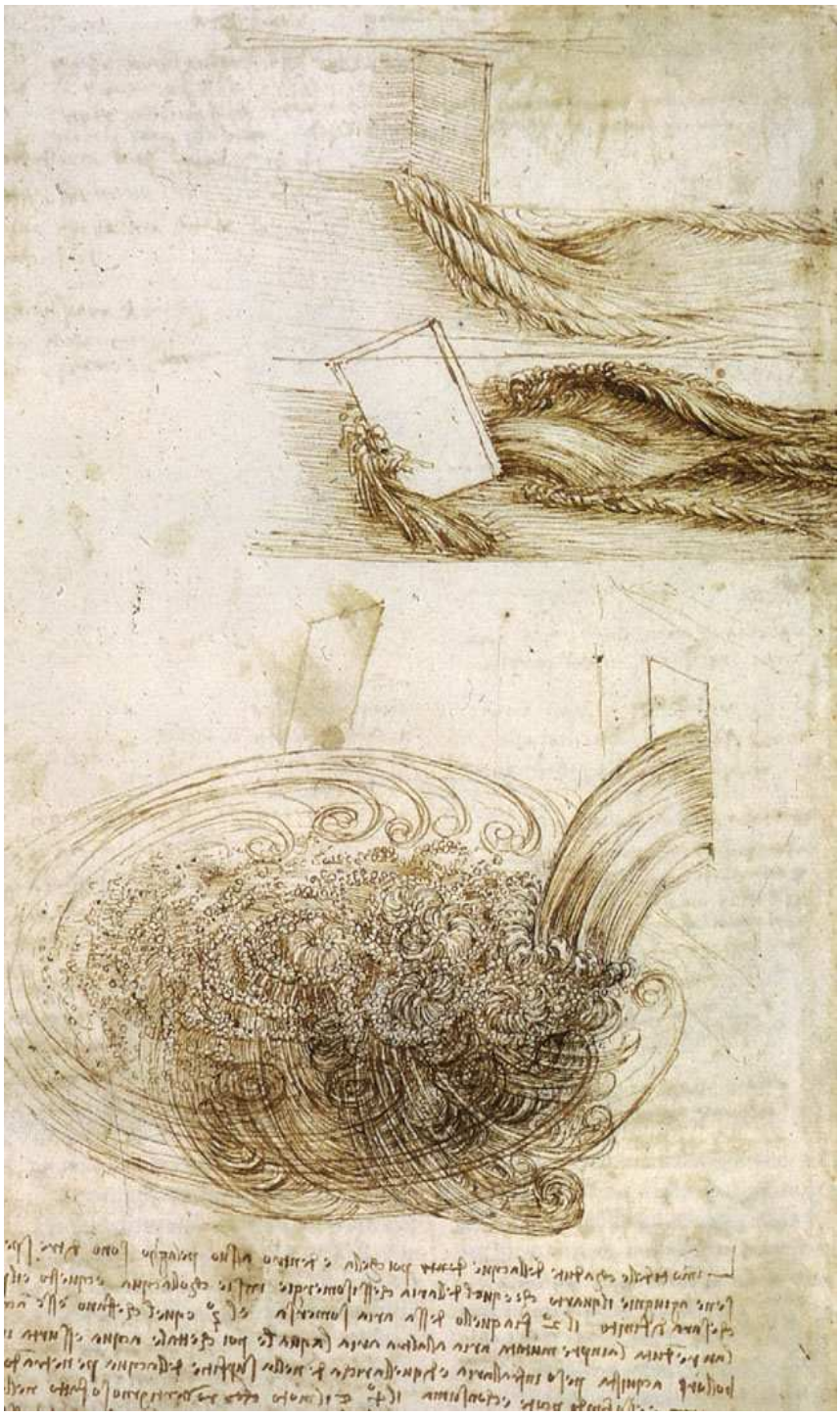

Figure 1.3: Flow Past a Bluff Body by Da Vinci. (www.cora.nwra.com)

1.3 Un-Limited Frequency Coalescence

Civil engineering structures like bridge decks may also execute self-excited oscillations and in turn respond to the aerodynamic forces thus generated. One of the oldest examples of suspended bridge deck failure due to frequency coalescence is the Angers Bridge in France, although the exact cause of failure in this case is not aeroelastic in nature. The Brighton Chain Pier Bridge, Fig.1.4 and the original Tacoma Narrows Bridge, Fig.1.5 are notorious examples of bridge failure due to aeroelastic effects.

Figure 1.4: Chain Pier Brighton, Artist: Clem Lambert. (en.structurae.net)

Aerodynamic performance of bridges is very sensitive to sectional shape and detailed structure of the section. Studies aimed at investigating the bridge deck behavior at lock-in wind speeds have increasingly found space in modern bridge construction projects. Recent developments in the long span suspension bridge deck design and huge on-going projects across the globe have strengthened the need to investigate this phenomenon. Storebaelt Suspension Bridge in Denmark is a real life example where vortex shedding downstream of the deck section caused low frequency oscillations. Subsequent investigations in a wind tunnel revealed lock-in at existing

Figure 1.5: Tacoma Narrows moments before the collapse.

wind speed conditions, Larsen *et al.* (2000).

Scanlan & Tomko (1977) showed conclusively that though helpful, the Standard Airfoil Theory has very distinct limitations in case of bridge deck sections. Aerodynamic flutter derivatives calculated even for stream-lined bridge deck sections showed limited resemblance with those of a symmetric airfoil. The most important difference as pointed out in Scanlan & Tomko (1977) is the difference between the added aerodynamic damping coefficient for an airfoil and for a bridge deck. Some streamlined bridge decks may exhibit similar coefficients as those of an airfoil, attention must be paid that any such resemblance is necessarily limited. Nakamura (1978) submitted a set of analytical formulas applied to the bi-modal bridge deck flutter. Larose & Mann (1998) presented an analytical model independent of the strip assumption to predict the gust loading effects on a streamlined bridge deck subjected to isotropic turbulence. The strip assumption is known to be a source of error in the analytical prediction methods used to predict the aerodynamic behavior of closed box girder bridge decks. Chen *et al.* (2000) investigated the effect of aerodynamic coupling between the modes on the flutter and buffeting response of a bridge deck. They solved the equations of motion of an aeroelastic bridge deck section using complex eigen

value analysis to study the self-excited forces and their effects on modal frequencies, inter-modal coupling and damping ratios as functions of wind velocity. The authors concluded that the symmetric vertical and torsional modes are the dominant modes for coupled flutter. The coupled self excited forces acting on the bridge deck are primarily responsible for the negative damping which in turn causes flutter. These coupling effects may cause flutter at lower velocities as predicted by the conventional mode by mode approach in case of relatively bluff bridge deck sections. Chen *et al.* (2002) proposed a method exploiting the general least square theory for identifying the flutter derivatives of a three degree of freedom bridge deck section. Banerjee (2003) submitted an analytical method for the free vibrations and flutter analysis of bridge decks using the normal modes method and generalized coordinates. Chen (2007) proposed a new frame work for estimating the modal frequencies, damping ratios and coupled oscillations of a two degree of freedom aeroelastic bridge deck system subjected to varying wind velocities. Matsumoto *et al.* (2007) resumed the evolution of our know-how about the flutter instability in bridge decks. The authors pointed out the most effective flutter derivatives which can be exploited to counter the flutter instability in such cases. Detailed discussion on flutter derivatives shall follow in Sec.3.1. Bartoli & Mannini (2008) showed that the contribution of structural damping in on-setting flutter cannot always be neglected depending on the dynamic and aerodynamic properties of the bridge deck. Neglecting the structural damping may result in an in-accurate prediction of the critical fultter velocity.

The present study explores the long term and transient stability phenomena in case of bridge deck sections. Most bridge deck sections, except very stream-lined, behave like bluff bodies and the airflow is essentially separated down-streams. Cross section aerodynamics of the bridge deck is often optimized by modifying shape and non-structural parameters. Sometimes dynamic parameters like the frequency ratio are also adjusted to increase the flutter critical wind speed. Prediction of the critical flutter speed remains one of the most important design procedures for modern long span suspension bridges.

Frequency Coalescence in Airfoil Sections

Aircraft wings and control surfaces have been known to oscillate since early days. Consider a simple rigid airfoil without sweep in a wind tunnel with a small angle of attack. In the absence of any flow, any forced vibration would damp out gradually.

As the flow speed in the wind tunnel increases, the rate of damping first increases. With further increase in the flow velocity, a point is reached at which the damping decreases rapidly. At the critical flutter speed an oscillation can just maintain itself with steady amplitude. At flow velocities beyond this critical value, a small accidental disturbance of the airfoil can serve as a trigger to initiate oscillations with an increasing amplitude. In such circumstances the airfoil suffers from oscillatory instability and is said to *'flutter'*.

The first recorded flutter victim was a Handley Page O/400 twin engine bi-plane bomber in 1916. Bairstow & Fage authored the first theoretical flutter analysis in 1916, Fig.1.6. They investigated binary flutter; twisting of the fuselage and motion of the elevators about their hinges, Garrick & Wilmer (1981). H. Reissner in 1926; developed a detailed analysis of wing torsional divergence, showing the importance of relative locations of the aerodynamic center of pressure and of the elastic axis, Garrick & Wilmer (1981).

Von Schlippe formulated the first ever flutter test in 1935 in Germany, Kehoe (1995). He plotted the amplitude of an airframe forced to oscillate at resonating frequencies as a function of airspeed. Increase in amplitude suggested reduced damping. Flutter was thought to occur at the asymptote of theoretically infinite amplitude as shown in Fig.1.7.

Theodorsen & Garrick (1940) compiled the results of the then existing basic flutter theory and the large number of experiments that were being conducted at that time. Kholodar *et al.* (2004) studied the effects of structural parameters and free stream Mach number on the Limit Cycle Oscillation (LCO) characteristics of a typical two degrees of freedom transonic airfoil configuration. They concluded that the stability of the limit cycle oscillations is very sensitive to the changes in the Mach number in the transonic range. Lee *et al.* (2005) studied a two degrees of freedom airfoil in sub-sonic flow with cubic non-linear stiffnesses at the supports. Exploiting the Quasi-Steady Aerodynamic Theory they formulated three fast frequency components to study the dynamics of fluid structure interaction. Their study showed that an initial excitation of the bending mode triggers the excitation of the torsional mode through non-linear interaction. Hémon *et al.* (2006) presented an extensive experimental study of coupled mode airfoil flutter with reference to the transient

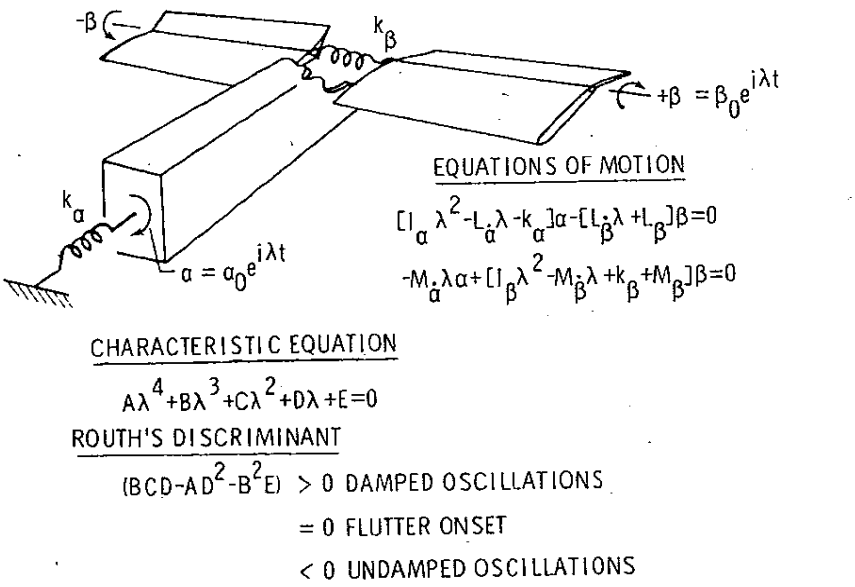

Figure 1.6: Historic Tail Plane Flutter Analysis given by Bairstow & Fage in 1916, Garrick & Wilmer (1981). Modern theoretical tools used to study flutter are based on Theodorsen's General Theory of Aerodynamic Instability. Theodorsen's method to solve the equation for flutter stability differs from his predecessors. This difference exists because he deals with pure sinusoidal motion applied to a case of un-stable equilibrium. He therefore, does not make use of the Routh's discriminant, Theodorsen (1935) .

growth of energy in the system. Experimental data showed that the maximum energy amplification attained in such a system does indeed vary with the magnitude of the imposed initial conditions. In these experiments however, upstream turbulence was very low. The airfoil was excited by physical mechanical means like dropping a fixed weight from a controlled height. Experimental results were later compared with the simulations using the Unsteady Airfoil Theory and were found to be in good agreement. Shams *et al.* (2008) presented a method for non-linear aeroelastic analysis of a slender airfoil. They showed that the Unsteady Linear Airfoil Theory based on the Wagner function agreed well with the results obtained from their test case. Limitations of the theory in predicting the physical phenomenon beyond the critical flutter limit was pointed out.

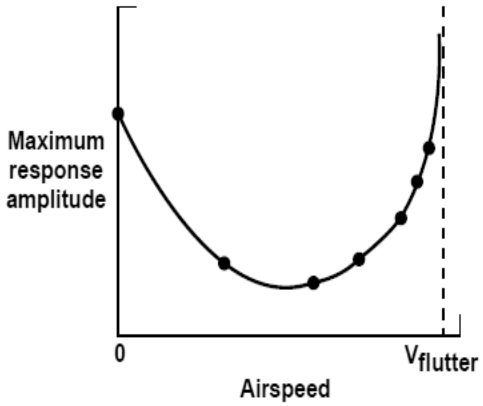

Figure 1.7: Von Schlippe's Historical Flight Flutter Test Method, Kehoe (1995).

Presenting a comprehensive chronological overview of the discoveries in this field is not the aim here. It would suffice to say that flutter has remained a subject of intense research ever since. Despite the tremendous advancement in our understanding of the flutter phenomena and the development of the state of the art flutter testing techniques, it keeps occurring. Recent examples of flutter related incidents in the aviation industry include Taiwan's IDF fighter, which crashed due to flutter of horizontal tail during high dynamic-pressure flight-test in 1992. Later in the same year, a prototype of the U.S. F-22 crashed in a flutter related accident. In September 1997, a U.S. Air Force F-117 crashed due to flutter excited by the vibration from a loose elevon. Every year many small airplanes, usually the home-built, continue to become casualties of flutter. Boeing started flutter testing of its 787 Dream liner in February 2010. As obvious, flutter still attracts tremendous potential for further research. It continues to remain a hugely important aspect of modern aircraft design.

In this work we shall investigate the by-pass tansition to flutter due to transient growth of energy in case of an airfoil with coupled two degrees of freedom. We shall demonstrate how the simple quasi-steady theory coupled with the Kussners aerodynamic admittance function can qualitatively predict the airfoil behavior. The airfoil experimental set-up is similar to the one described in Schwartz *et al.* (2009). Scope of this work is limited to two dimensional incompressible flow past a symmetric airfoil.

1.4 Problematic

Fluid structure interaction systems as outlined in the previous sections encompass a broad horizon of our daily lives. Given the natural tendency of things to move towards chaos, all efforts are spent to find out and understand any possible mechanisms which could lead a fluid structure system inch towards an un-stable state. As the title of the thesis suggests; purpose of this study is to investigate various fluid structure interaction systems with focus on their behaviors both in the long-term and short-term. The later is commonly referred to as Transient Behavior. Various standard measurements like the critical velocities and natural frequency evolution provide important information regarding the long-term response of a fluid structure interaction system. Careful caliberation, detection and measurement of these parameters plays an important role towards reliable scientific investigation. Findings from these experimental procedures are then put to use to study the more complex short-term or transient dynamic properties of the system which are inherently elusive and complicated to reproduce in a lab environment. For example, critical velocity measured is commonly used to normalize the mean free stream velocity while studying the transient behavior of such systems close to their linear stability limits.

Traditionally, investigations of the stability properties of a flow were treated as eigen value problems. It was established that exponentially growing eigen modes in a system cause the instability. In some cases however, a system may transition to an unstable state even in the absence of primary exponential instabilities as mentioned above. This type of instability mechanism is known as the 'by-pass transition'. Given all the above, it is needless to point out that although proven experimental techniques exist to study the long-term behavior of various systems, its awareness and anticipation of various crucial system parameters remains of profound practical importance. At the same time, as we shall see during the course of this study, transient behavior of a system has proven to be critical in understanding various new failure mechanisms as discovered in the field of fluid structure interaction and briefly summarized in the preceeding sections.

Recently, a number of theoretical and numerical studies have explored the possibility of exsitance of transient instability mechanism in case of fluid structure interaction systems. Schmid & de Langre (2003) applied the concept of transient growth of energy to coupled mode flutter, Type-II fluid structure system, Fig.1.1. The authors found that energy of a coupled two degree of freedom system can be

amplified by a factor of 10 by the transient growth. The magnitude of this transient amplification is large enough to qualify as a discrepancy from the threshold predicted by the linear stability theory. Noger & Hémon (2004) presented a study showing the existence of transient amplification of energy in case of automobiles. Hémon *et al.* (2006) presented experimental evidence of transient amplification of energy before airfoil flutter. The authors established that natural transient loading may trigger large amplitude oscillations at linear sub-critical flow velocities; in such systems. Needless to mention here that transient amplification of energy in fluid structure interaction systems has attracted some attention only recently. Very little experimental data exists, Hémon *et al.* (2006), to verify the theoretical predictions. More detailed experimental investigations are needed.

The present study is an experimental investigation of the long-term and transient behavior of fluid structure systems with two degrees of freedom. We shall present our findings based on three case studies under taken during the course of this work. Each case study is based on a bluff body subjected to a uniform incident flow. This report is divided into two parts based on the long-term and transient properties of the experimental setups. We shall discuss the long term behavior of a bluff body system executing vortex induced vibrations in the first part. Moreover, long term stability parameters for an airfoil and a bridge deck system are also included. The second part is dedicated to the transient behavior of all the three fluid structure systems. We have organized the fluid structure interaction systems into two types based on how the natural frequencies of the system behave as linear stability threshold is approached, Section1.1, Fig1.1.

We shall start our inquisition firstly by a Type-I system, Fig.1.1. The most simple Type-I fluid structure system is depicted by the classical flow past a bluff body setup. One of the most intriguing phenomenas related to the investigations of flow past a freely oscillating bluff body is the existence of hysteresis in the amplitude variation and the frequency capture depending on the approach to the resonance range - from lower velocities or from higher velocities. As cataloged in the previous sections, it appears that very few experimental studies have focused on the existence of hysteresis in case of freely oscillating square cylinders. Some data obtained from freely oscillating circular cylinders can be obtained from Feng (1968) and Brika & Laneville (1993). Cheng *et al.* (2003) have presented some data on a freely oscillating square cylinder. None of these works presents data concerning transient regime. The vortex

shedding oscillations of high mass ratio structure is therefore not well documented for a freely oscillating square section despite its obvious interest in civil engineering problems. In the present study we shall present results obtained from a freely oscillating square cylinder in a vertical wind tunnel. Reduced amplitude curves of the oscillating cylinder obtained under different experimental configurations provide insight to the long term behavior of such systems. Experimental data is compared with the results obtained by numerically simulating a theoretical wake-oscillator model. Wind tunnel measurements of the reduced growth rate in the transient regime are discussed in Part-II of the study. The experimental findings were used to validate a wake oscillator model presented by Facchinetti *et al.* (2004).

Type-II fluid structure interaction systems are studied for two cases. Firstly, the aeroelastic behavior of a linear two degrees of freedom bridge deck is studied in a horizontal wind tunnel. Most bridge deck sections are not streamlined so that flow around the cross section is necessarily separated. On the other hand most bridge deck sections are not very bluff so there may be a net lift/drag force acting on the deck section. In the present study, flow around the bridge deck section generates a net lift force pushing the bridge deck downwards in the wind tunnel test section. This new position is taken as reference for subsequent energy calculations. Extensive experimental evidence is provided to study the effects of frequency ratio on the evolution of maximum normalized energy of the system and the critical flutter speed. We shall define our frequency ratio and see how the maximum energy amplification of a bridge deck section can be controlled by manipulating the frequency ratio parameter. Accurate experimental evidence is also provided linking the critical flutter velocity and the frequency ratio of the system. The present work is limited to lower Reynolds Number and the turbulence level upstream of the test section is kept very low. We have studied a stream-lined bridge deck profile resembling that of the cable-stayed road bridge constructed over the valley of river Tarn near Millau in Southern France, Fig.1.2(b).

Secondly, another important fluid structure interaction system which exhibits Type-II frequency coalescence mechanism, Fig.1.1, but which is fundamentally different from the bridge deck is the airfoil system. As pointed out earlier with reference to Scanlan & Tomko (1977) Standard Airfoil Theory has distinct limitations when applied to bridge deck sections. End plates are used to ensure two dimensionality of the setup. This experiment builds onwards from the experimental study presented

in Hémon *et al.* (2006). We added an aluminum flap to the system to create an up-stream gust. The gust is allowed to excite the airfoil in the test section. This brings the experimental set-up closer to the real world scenario where aircrafts are often subjected to gusts in flight. Results obtained by this experimental procedure are compared with the already existing classical airfoil theories. The experiment is repeated for another airfoil setup with weak non-linearity in the system stiffness. Results obtained by both linear and non-linear experimental setups are compared to establish the existence of by-pass transition to flutter, Sec.6.3. Furthermore, a new cobmination of the standard quasi-steady theory and the Kussners aerodynamic admittance function is proposed to validate the transient energy amplification results obtained for the linear airfoil setup. Airflow over the profile has been treated as incompressible in the simulations. All the experimental results and our findings from the comparison shall be discussed in subsequent chapters.

In the end, our findings from the study, some suggestions regarding the possibilities for further investigations and a bibliography of the literature consulted shall conclude this study.

PART-I Long Term Behavior

Part-I of this thesis report is dedicated to the long-term behavior of different fluid structure interaction systems, Sec.1.4. As pointed out earlier, various standard measurements including the critical velocities and frequency evolution provide important information regarding the long term response. Accurate knowledge of these parameters is important because the results obtained in this part shall be used in the more complex transient study in Part-II. For example, awareness of the frequency evolution in the presence of dynamic wind conditions enables us to determine how the energy amplification due to transient growth is linked to the frequency ratio in case of bridge deck sections, Chapter 5.

We shall start with the long-term limit cycle behavior of a square cylinder oscillating freely in a high mass ratio environment. The present study differs from its predecessors in the sense that while the flow velocity and elastic system parameters are closely controlled, the square cylinder is allowed to oscillate freely under the effect of incident air flow. The existence of hysteresis in the reduced amplitude result is demonstrated using credible experimental data. Experimental results are compared with the findings from a wake-oscillator model. Discrepencies in the location of maximum amplitude and the frequency lock-in range are pointed out and discussed. Next, we move on to a similar long-term analysis of an airfoil and a bridge deck system. We submit our experimental setups with low structural damping and inherently protected from friction losses. An Aluminum flap is used to generate a single gust. All the measured system parameters are verified using results from numerical simulations. Our experimental findings are presented and discussed in terms of critical velocities, frequencies and dampings.

Chapter 2

Behavior of a Square Cylinder in a Wind Tunnel at Low Velocity

In this chapter we shall present experimental results obtained in a wind tunnel for an elastically mounted rigid square cylinder restrained to move in the transverse-wind direction. Structural supports of the set-up are assumed to behave linearly through out the amplitude envelope. Measurements consist of the time histories of oscillations using laser displacement sensors. All the structural parameters are estimated without airflow. The behavior of the vortex-induced oscillation is studied using two configurations. In the first case, the cylinder was brought to rest and then allowed to oscillate freely for each increment in velocity. In the second case however, the cylinder was not brought to rest for any velocity increment so as to study the memory effects on the cylinder amplitude. The classical mode switch can be observed in both the cases. Hysteresis is however found only in the later case. Results for both the cases are presented and discussed.

We know that, a bluff body when placed in a fluid stream; generates separated flow. In the creeping steady flow regime where $Re < 1$, viscous diffusion dominates most of the flow and Stokes solution applies to the system. A symmetrical un-separated flow surrounds the body. No significant changes take place until $Re > 5$. The flow remains stable but a re-circulation bubble appears behind the body. As the $Re > 48.5$, a typical Benard-Karman vortex street appears behind the bluff body, Godreche (1998). This vortex shedding and general wake turbulence induce fluctuating pressure on the body surface, in a direction away from the last detached vortex, which can in turn cause the body to oscillate. The body is set to oscillate

in a direction normal to the mean flow. Amplitude of the oscillation can vary from 1.5 to 2 body diameters. For large amplitude oscillations of a body in high mass ratio configuration, frequency of body oscillations is close to its natural frequency, Bearman (1984).

2.1 Experimental Methods

2.1.1 Experimental Set-up

The square cylinder has a cross section, D = 0.02 m and a span, b = 0.15 m. The cylinder is put in place in the test section using four linear springs mounted outside the test section. Specific chord wiring is used to restrain the cylinder such that it oscillates transverse to the air flow. Special attention is paid to keep the structural damping as low as possible. The experiment is conducted in a vertical axis Eiffel Wind Tunnel which has a closed circular test section of diameter 0.20 m. A centrifugal fan, down stream of the test section is used to produce the wind stream. This free stream flow velocity can be safely assumed to be uniform over the cylinder span given the comparison between the cylinder span and the test section diameter. Mean velocity in the test section varies from ≈ 2 m/sec to ≈ 7 m/sec for this experiment. Turbulence level of the upstream airflow is less than 1% over the velocity range during the course of this study, Amandolèse & Hémon (2010), Fig.2.1.

No endplates have been used in the experiments. Due to the aspect ratio of the cylinder ($b/D = 7.5$), flow around the longitudinal ends can have a significant effect on the vortex dynamics, the correlation of the induced fluid forces on the body and thus the vibrations. Meanwhile the proximity of both the ends of the cylinder with the test section wall could reduce the effect of the end conditions. As reported by Morse *et al.* (2008), for a circular cylinder the vortex-induced vibrations for attached and un-attached endplates are nearly the same.

2.1.2 Measurement System

Accurate measurement of low velocities is always difficult to achieve. In the present case, a nozzle is mounted down-stream of the test section. Bernoulli's Theorem is used to calculate the air flow velocity in the test section compared with the flow velocity in the nozzle section. Pressure readings in the test section and the nozzle section are obtained by using pairs of static pressure taps in each section. A

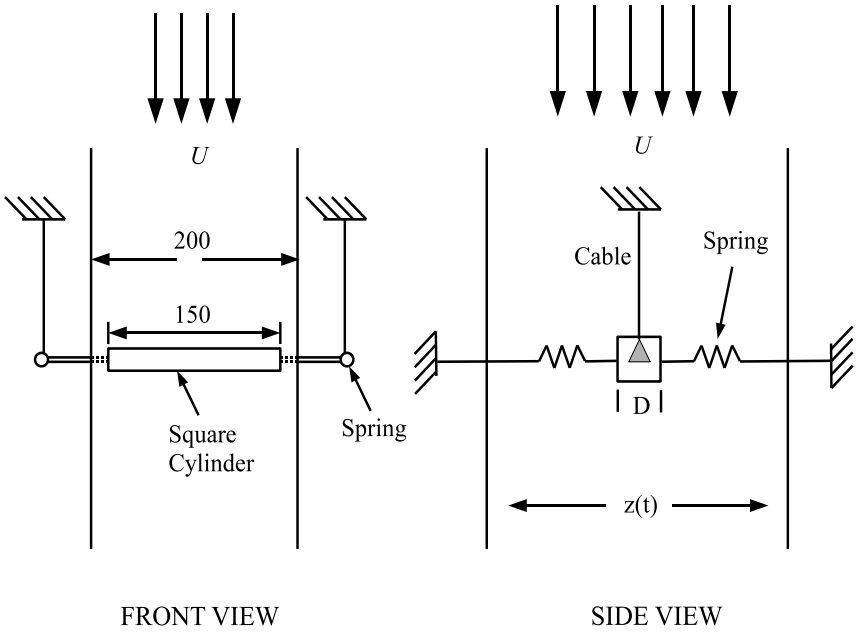

Figure 2.1: Sketch showing the principles of the experimental setup Amandolèse & Hémon (2010).

thermocouple is used to implement temperature correction. This technique allows us to measure low flow velocities with accuracy better than 1%, Amandolèse & Hémon (2010).

Measurements of the transverse displacement of the cylinder are obtained by a laser displacement sensor. The measurement resolution is $40\mu m$ and the accuracy is 1% of the full scale range. Signals from the laser displacement sensors are transmitted to an acquisition system named PAK provided by Mueller-BBM. It consists mainly of a 24-bit and 8-channel acquisition card and a signal processing software. Sampling resolution is 1024 Hz and the typical duration of data accumulation is 60 s. This duration was increased to 300 s for the frequency measurements of the LCO of the cylinder. Increasing the duration enabled us to obtain a better frequency resolution for the measurements. The physical degree of freedom $\hat{z}$ is provided by the recombination of the measured signals using the system kinematics, Amandolèse & Hémon (2010).

Strouhal number of the cylinder was measured while at rest using the spectral analysis of the unsteady wake. Measurements were obtained by a single component hot wire anemometer installed down-stream of the square cylinder at a distance equal to one length of the cylinder side. The Strouhal number was found to be 0.127 over the velocity range of the vortex shedding oscillation regime, Amandolèse & Hémon (2010).

2.1.3 Identification of Structural Parameters

We have a rigid square cylinder of side 'D'. The cylinder is constrained to oscillate in a direction normal to the mean flow direction as depicted in Fig.2.2.

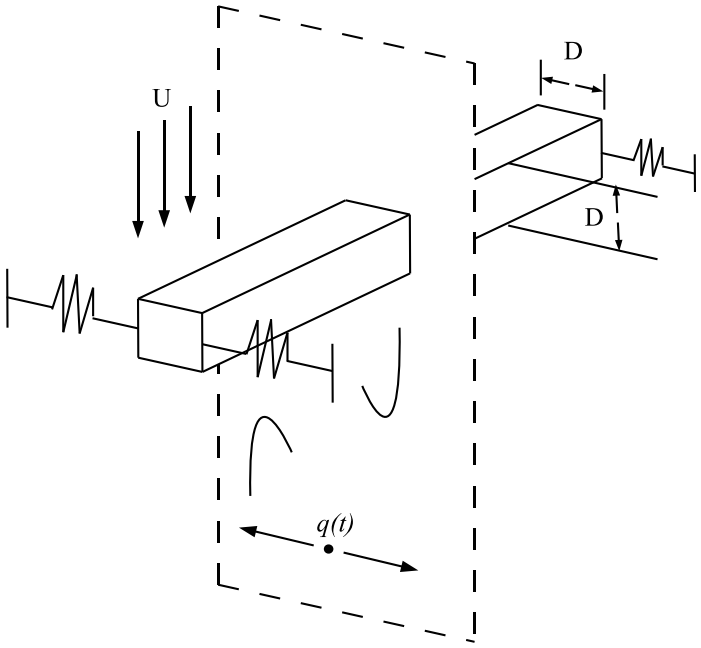

Figure 2.2: Schematic for Square Cylinder Coupled Wake Oscillator for 2D Vortex Induced Vibrations in a Vertical Wind Tunnel.

Flow is assumed to be uniform all along the cylinder length. The cross flow displacement 'z' of the cylinder can be described by the standard damped linear oscillator as in Eqn.2.1.

$$m\ddot{z} + r\dot{z} + kz = S \tag{2.1}$$

The un-damped natural frequency of the system is defined as:

$$f_o = \frac{1}{2\pi}\sqrt{\frac{k}{m}} \tag{2.2}$$

Structural parameters are identified under zero wind velocity. The natural frequency f_z and the system damping r_s are obtained by spectral analysis. Static Weight Calibration technique is used to calculate the stiffness *'k'*. Mass *'m'* is then calculated using:

$$m = \frac{k}{(2\pi f_o)^2} \tag{2.3}$$

The reduced velocity, U_r is given as: $U_r = \dfrac{\overline{U}}{f_o D}$ and the RMS amplitude, Z^* is given as: $Z^* = \dfrac{z}{D}$. Table 2.1 shows all the physical parameters of the experiment including geometrical dimensions, mass, stiffness, damping and wind tunnel velocity range. Table 2.2 has important non-dimensional parameters. The experimental system used for this study has a high mass ratio $\mu = 905$ and a low damping ratio $\eta = 0.0828\%$. Low damping ratio leads to a smaller Scruton Number, $S_c = 1.5$.

2.2 Limit Cycle Oscillations

The square cylinder exhibits vortex induced vibrations under the effect of the air flow. Generally, maximum amplitude for a circular cylinder with higher mass ratio is achieved for a reduced upstream velocity close to (1 / St). For the square cylinder however, it occurs at $U_r \approx 8$ which is slightly more than (1 / St) in our case. In the present study, limit cycle oscillations of a square cylinder are measured for reduced velocity ranging from $U_r \approx 6 \approx 25$.

Reduced RMS amplitude of the limit cycle oscillation, $Z^* = \dfrac{z}{D}$ is presented in Fig.2.4 as a function of the reduced velocity for a cylinder starting from rest for each incremental value of velocity. No significant oscillations occur for reduced velocity below 6. However, a typical VIV amplitude response can be observed for U_r ranging from 6 up to 13. At higher reduced velocity galloping oscillations appear which are not studied here. Hysteretic transition cannot be observed in this case. Long time analysis of the limit cycle regime clearly showed mode switching between the upper and the lower branches for $U_r \approx 10$. Different symbols in Fig.2.4 signify different experimental runs conducted at different times to ensure repeatability of the

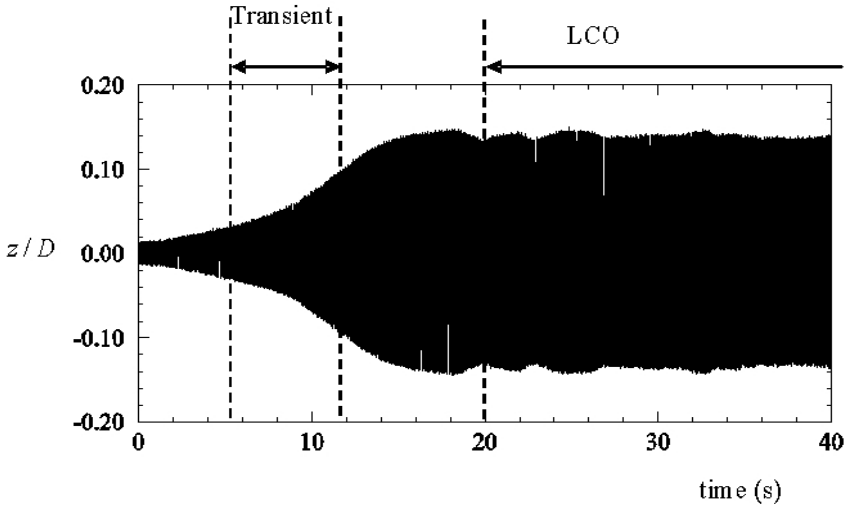

Figure 2.3: Time evolution of the cylinder motion amplitude at U=2.5155 m/s Amandolèse & Hémon (2010).

experimental procedure. Apart from the obvious dispersion of experimental points at higher reduced velocities we can safely assume that the resonant frequencies lie approximately in the same reduced velocity range for each experimental run.

In the VIV regime the amplitude data shown in Fig.2.4 are very similar to those carried out by Feng (1968) for a circular cylinder in airflow. Results obtained by Feng (1968) show two amplitude branches, which were later named as the 'initial' and the 'lower' branch in Khalak & Williamson (1999). The maximum oscillation amplitude occurs on the initial branch for a reduced velocity close to 10 which is significantly above the pure resonant point expected for a reduced frequency close to 8 ($\approx 1/St$). This off-set of the maximum value of amplitude from the expected value of reduced velocity, U_r can be attributed to the blockage effects in the wind tunnel test section.

A second series of experiments was conducted where the cylinder was not brought to rest so as to study the memory effects on the cylinder amplitude. Results are reported in Fig.2.5, where circular points represent experimental data recorded while increasing the velocity by a fixed increment and cross points represent data accumulated while decreasing the free stream velocity using a fixed decrement. As was the

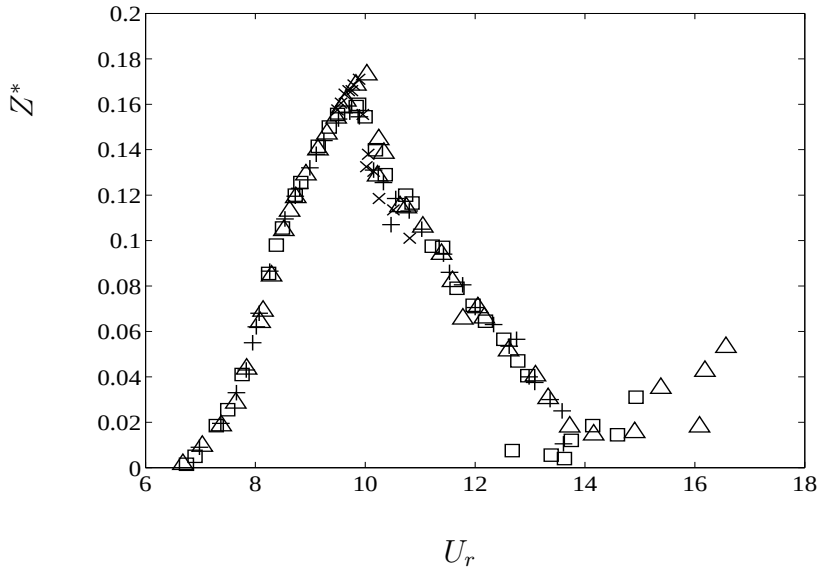

Figure 2.4: Reduced RMS Amplitude of the limit cycle oscillations versus reduced velocity; without Memory Effect.

case in Fig.2.4, reduced RMS amplitude of the limit cycle oscillation is presented as a function of the reduced velocity. We see that in this case also, the typical VIV response is observed for the same reduced velocity range, from 6 to 13.

Results, obtained from the experiments which allowed the memory effect, exhibit an upper and a lower branch with an abrupt transition for a reduced velocity ≈ 9.5. Williamson & Roshko (1988) used visualisations attributing the sudden change in magnitude to an abrupt mode switch which in turn can be explained by the abrupt shift in phase angle between the vortex shedding frequency and the cylinder oscillating frequency. They showed that the fluid stream just below the critical reduced velocity is extremely sensitive and a very small disturbance is enough for the system to go from one equilibrium state to another thereby causing an abrupt change in formation named as 'the mode-jump'. Brika & Laneville (1993) found that these amplitude branches correspond to different synchronized vortex wake patterns. The 'upper' branch in the amplitude response lies in the von Karman type 2S mode of the Williamson-Roshko map of wake patterns. The 'lower' branch however lies in the 2P mode regime in which two vortices of opposite sign are shed from each side of the cylinder at every oscillation cycle. The probability of the existence of 2S mode

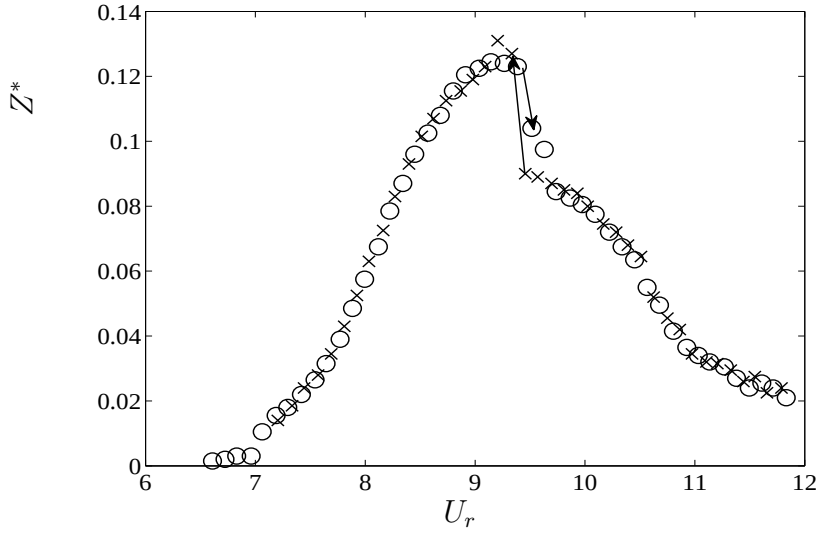

Figure 2.5: Reduced RMS Amplitude of the limit cycle oscillations versus reduced velocity; (o) increasing velocity, (x) decreasing velocity.

decreases as U_r is increased. A slight hysteretic effect can be observed for $U_r \approx 9.5$. Following the circular points as the reduced velocity is increased by a fixed increment, a relatively smooth mode switch to the lower branch can be noticed for a reduced velocity slightly above 9.5. Following the cross points while decreasing the free stream velocity using a fixed decrement, an abrupt mode switch takes place at reduced velocity slightly lower than 9.5. We can observe that the RMS amplitude routes for the square cylinder tend to superimpose except for a very brief interval of reduced velocity in the vicinity of the mode switch. The maximum oscillation amplitude found in this case is clearly less than 0.20D. This maximum amplitude is smaller than the maximum amplitude predicted for a circular cylinder in air flow by Brika & Laneville (1993) and later catalogued by Khalak & Williamson (1999). The amplitude levels presented in Fig.2.5 are also significantly lower than for the starting from rest configuration.

It is important to note here that the maximum amplitude location in both the cases is off-set from its expected value of (1 / St). This off-set may be attributed to the blockage effect in the test section. However, the fact that in case of the growth rate measurements of the same cylinder the maximum growth rate value lies very

close to (1 / St) adds to the complexity of apparently a simple phenomenon. We shall discuss the growth rate measurements in more detail in Sec.4.2.

2.3 Comparison with Theoretical Model

2.3.1 Theoretical Model

For a one dimensional case the equation of motion of a rigid cylinder oscillating in the transverse z-direction (normal to the flow) reads as Eqn.2.1, where, 'm' is the mass of the cylinder, 'r' is a viscous damping coefficient, 'k' is the stiffness of the setup and 'S' is the aerodynamic force resulting from the fluid structure interaction in this case, mainly due to vortex shedding.

The mass 'm' takes into account the cylinder mass and the fluid added mass m_f which models the inviscid inertial effects. Following Blevins (1990) we can precise:

$$m = m_s + m_f \quad ; \quad m_f = C_{M_a} \rho D^2 \frac{\pi}{4} \quad ; \quad \mu = \frac{m}{\rho D^2} \tag{2.4}$$

where, 'ρ' is the fluid density (in our case air), 'μ' is a dimensionless mass ratio and 'C_{M_a}' is the added mass coefficient. Similarly, following Blevins (1990) we can write the system damping:

$$r = r_s + r_f \quad ; \quad r_f = \gamma \Omega \rho D^2 \tag{2.5}$$

where 'γ' is a stall parameter as Skop & Balasubramanian (1997) and 'Ω' is a reference angular frequency. Assuming that the mean free stream velocity 'U' is zero, 'Ω' is the angular frequency of the structure oscillation and 'γ' is a function of the amplitude of oscillations related to the mean structural drag coefficient C_D, Blevins (1990). Blevins (1990) defines 'γ' for a circular cylinder as:

$$\gamma = \frac{1}{4\pi St} C_D \tag{2.6}$$

In our case however, 'Ω' is the vortex shedding angular frequency, $\Omega = \Omega_f = 2\pi St \frac{U}{D}$. 'St' is the Strouhal Number. Following Skop & Balasubramanian (1997) 'γ' shall be assumed to remain constant for the sake of simplicity. Govardhan & Williamson (2000) used two distinct formulations of the equation of motion for the *'total force'* and the *'vortex force'*. Following the same approach the fluid effects namely the added mass and added damping have been included directly in the

structural oscillatior in Eqn.2.1 through Eqn.2.4 & Eqn.2.5. The vorticity effects are modelled by the forcing term at the right hand side in Eqn.2.1. Structural angular frequency Ω_s is typically defined as $\Omega_s = \sqrt{\frac{k}{m}}$ and the reduced structural damping $\xi = \frac{r_s}{2m\Omega_s}$. Eqn.2.1 can be rewritten as:

$$\ddot{z} + \left(2\xi\Omega_s + \frac{\gamma}{\mu}\Omega_f\right)\dot{z} + \Omega_s^2 z = \frac{S}{m} \tag{2.7}$$

Standard van der Pol equation is used to model the fluctuating nature of the vortex street down stream of the oscillating square cylinder.

$$\ddot{q} + \left(\epsilon\Omega_f\left(q^2 - 1\right)\right)\dot{q} + \Omega_f^2 q = F \tag{2.8}$$

The fluid variable 'q' is defined as the reduced vortex lift coefficient. Mathematically, $q = 2\frac{C_L}{C_{Lo}}$. C_{Lo} is the reference lift coefficient measured on a fixed cylinder subjected to vortex shedding. 'F' shall be 'Az' for displacement coupling, '$A\dot{z}$' for velocity coupling and '$A\ddot{z}$' for acceleration coupling. Facchinetti *et al.* (2004) have presented a detailed study of the dynamics of such a coupled system. They estimated the near wake van der Pol parameter 'ϵ' and the coupling force scaling 'A' from the available experimental data. The oscillation amplitude at lock-in z_M is obtained from:

$$z_M = \frac{C_{Lo}/2}{S_G + 4\pi^2 St^2\gamma}\sqrt{1 + \frac{A}{\epsilon}\frac{C_{Lo}/4}{S_G + 4\pi^2 St^2\gamma}} \tag{2.9}$$

see Facchinetti *et al.* (2004) for algebraic details.

2.3.2 Den Hartog's Instability Criteria

It should be kept in mind here that the model proposed by Facchinetti *et al.* (2004) as discussed above is valid for circular cylinders. The present study however is based on the vortex induced vibrations of a square section cylinder. It is imperative to remark here that this basic difference in geometery has to be taken into account to be able to compare theoretical findings and experimental results later. Blevins (1990) suggested a simplified system to be considered, Fig.2.6.

The angle of attack 'α' can be calculated as $\alpha = tan^{-1}\left(\frac{\dot{z}}{U}\right)$ such that if $\alpha = 0$; $z = 0$ implying that the cylinder is at its equilibrium position. Also, if 'α' is very

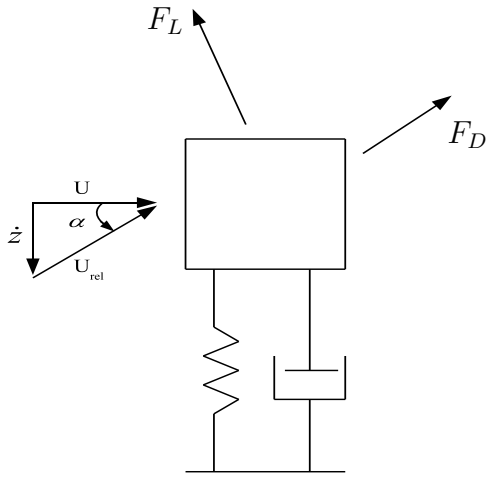

Figure 2.6: Single Degree of Freedom Galloping Model. Reproduced as Blevins (1990).

small $\alpha \approx \dfrac{\dot{z}}{U}$ and $U_{rel} \approx U$. Now from the Fig.2.6, the resultant vector is assumed positve downwards:

$$F_z = -F_L cos\,(\alpha) - F_D sin\,(\alpha) = \frac{1}{2}\rho U^2 DLC_z \tag{2.10}$$

where C_z is the vertical force coefficient

$$C_z = -\frac{U_{rel}^2}{U^2}\left[C_L cos\,(\alpha) + C_D sin\,(\alpha)\right] \tag{2.11}$$

Now because α is very small, advancing Eqn.2.11:

$$C_z\,(\alpha) = -C_L - \left(-\frac{\partial C_L}{\partial \alpha} + C_D\right)\alpha \tag{2.12}$$

In the last equation if $\dfrac{\partial C_z}{\partial \alpha} < 0$ or equivalently $\dfrac{\partial C_L}{\partial \alpha} + C_D > 0$, total damping of the system remains positive. The system remains stable. This is known as the *Den Hartog's Stability Criteria*. Equation 2.12 at $\alpha \approx 0$ gives $C_z = C_L$. Trivial algebraic manipulation of Eqn.2.10 and Eqn.2.12 yield:

$$F_z = -\frac{1}{2}\rho U^2 DLC_L + \frac{1}{2}\rho U DL\frac{\partial C_z}{\partial \alpha}\dot{z} \tag{2.13}$$

Comparing Eqn.2.1 and Eqn.2.13, retaining only lower order terms of α, we arrive at:

$$\gamma = \frac{1}{8\pi St}\frac{\partial C_z}{\partial \alpha} \tag{2.14}$$

where, $\frac{\partial C_z}{\partial \alpha}$ is 3 for a square cylinder in smooth flow and 3.5 for a square cylinder in turbulent flow, Blevins (1990).

Investigations by Facchinetti *et al.* (2004) revealed that using acceleration coupling in the forcing term of the wake oscillator best matches with the then available experimental results. The coupling terms were formulated to essentially allow only the linear functions of the wake variable 'q' and displacement 'z' and their temporal derivatives. In order to set the values of parameters 'A' and 'ϵ', the total lift coefficient was assumed to be the same as the vortex lift coefficient. Although Facchinetti *et al.* (2004) recommend acceleration coupling as the most suitable, it is important to keep in mind that the theoretical model was devised for systems with lower mass ratios. Since this experimental work involves higher mass ratio system we refer to the lock-in domain calculations as a function of mass ratio by the same authors. Given the seemingly asymptotic relationship between the upper and lower bounds of the lock-in region in the velocity coupling model at lower mass ratios, we can conclude that it is the velocity coupling model which is best suitable for our high mass ratio experimental setup. This study therefore focuses on the velocity coupling model.

Following the same approach as Facchinetti *et al.* (2004) and the references there in, we solved the model numerically as presented in Eqn.2.7 and Eqn.2.8 using the Fox and Goodwin iteration scheme. Details of the iteration scheme shall be described in Sec.3.1. System parameters are described in Table 2.1 and Table 2.2, Fig.2.7.

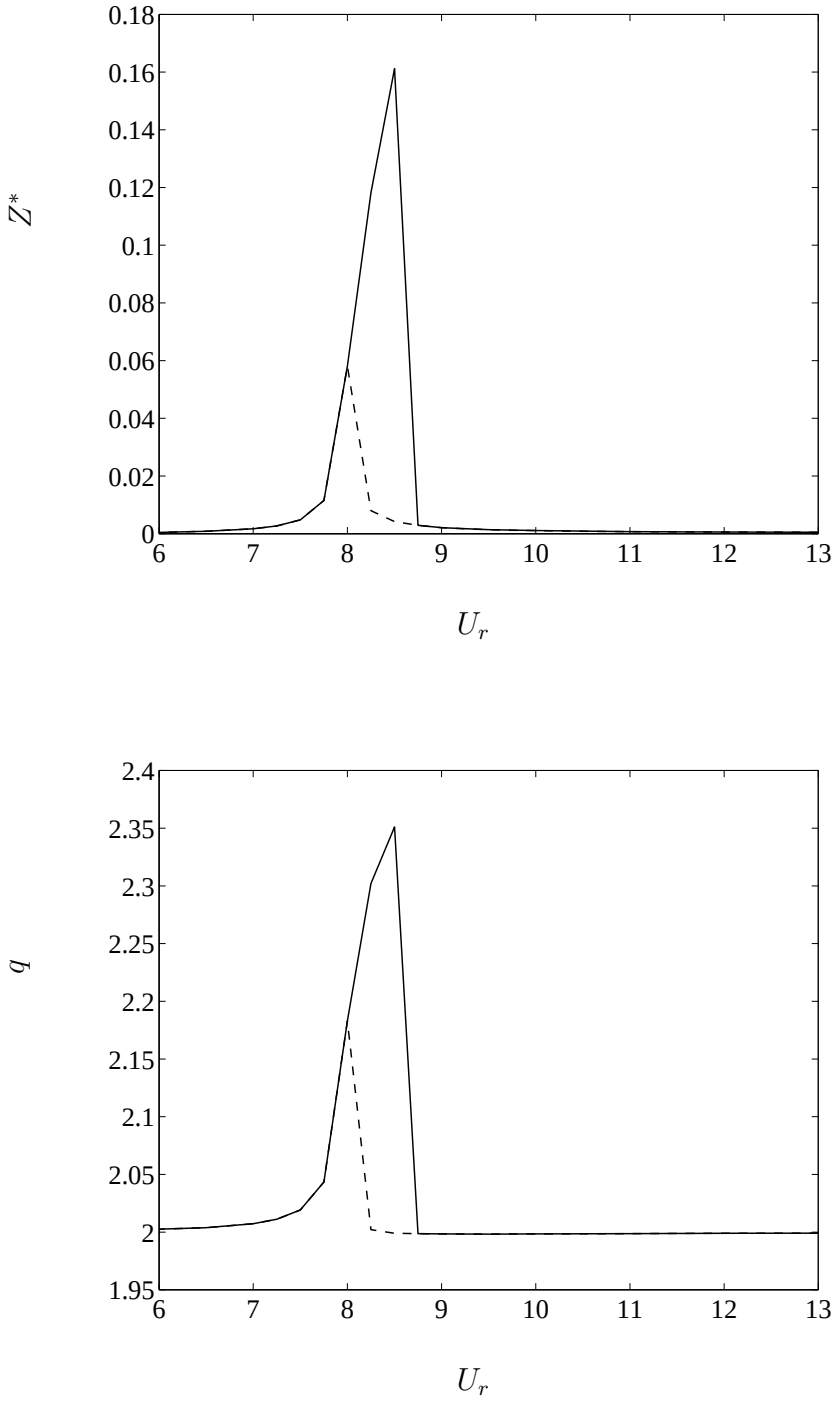

Figure 2.7: Hysteresis Standard Wake-Oscillator Model Solved Numerically using Velocity Coupling as in Facchinetti *et al.* (2004). (Solid-Line) Increasing Velocity, (Dashed-Line) Decreasing Velocity. Z* is the amplitude normalized with respect to the dimension 'D' of the Square Cylinder, Fig.2.2.

As discussed in Sec.1.1, experimental results presented in Fig.2.4 and Fig.2.5 can be explained by the Type-II frequency coalescence mechanism, Fig1.1. As obvious from Fig.1.1, no significant oscillations take place at lower reduced mean free stream velocities, U_r, when the two natural frequencies of the system are far apart. The fluid structure interaction mechanism is dominated by the inertial effects due to the in coming flow. As the U_r increases, the vortex shedding frequency down streams of the cylinder gets increasingly synchronized with the cylinder oscillating frequency. This results in an increasing energy transfer from the wake to the oscillating cylinder. Facchinetti *et al.* (2004) have stated that for a positive energy transfer of this sort, $0 < -\frac{\varphi}{\pi} < 1$, where φ is the phase angle between the vortex shedding frequency and the cylinder oscillating frequency. Increased energy transfer shows as higher cylinder oscillating amplitude. The cylinder exhibits a maximum oscillation amplitude for a critical flow velocity where the two frequencies of the system match exactly. As the mean free stream velocity is increased further, a sudden phase shift results in an abrupt change in the wake mode pattern, Khalak & Williamson (1999) and Brika & Laneville (1993). This point can be identified on the amplitude curves where there is a sudden change in amplitude. Facchinetti *et al.* (2004) observed that for such Type-II fluid structure interaction systems, phase between the structure and wake oscillators showed an overall jump of π passing through the lock-in range.

As the mean free stream velocity increases, a negative energy transfer takes place accredited to the sudden phase shift. Consequently, the cylinder oscillations amplitude decreases, Fig.2.4 and Fig.2.5, untill a second critical value of the reduced mean free stream velocity is reached. Experimental data presented in Fig.2.4 and Fig.2.5 depicts amplitude values for a velocity just below this second critical value. Beyond this second critical value of U_r, the two system frequencies split, Sec.1.1, Fig.1.1. If the mean free stream velocity is increased further, the secondary galloping instability sets in which is outside the scope of this work.

We shall now compare our experimental results as presented in Sec.2.2 with the theoretical wake-oscillator model outlined in Sec.2.3.1. As can be observed from Fig.2.8, the wake oscillator model predicts the location of maximum limit cycle amplitude closer to the expected value of (1 / St) for this case. However, the extent of frequency lock-in domain does not match the experimental result. We can safely state that the lock-in amplitude model in Eqn.2.9 provides acceptable results given that the added aerodynamic damping effect due to bluff-body cross section, Eqn.2.14

has been taken into account. de Langre (2006) states that the extent of the lock-in domain is infact controlled by the product AM; where 'A' is the coupling force scaling in the wake-oscillator model. Following Facchinetti *et al.* (2004), we determine A = 2.7 for our case. 'M' is a mass parameter such that: $M = \frac{C_{Lo}}{2}\frac{1}{2\pi^2 St^2 \mu}$. We shall address these findings in more detail in Sec.7.2.

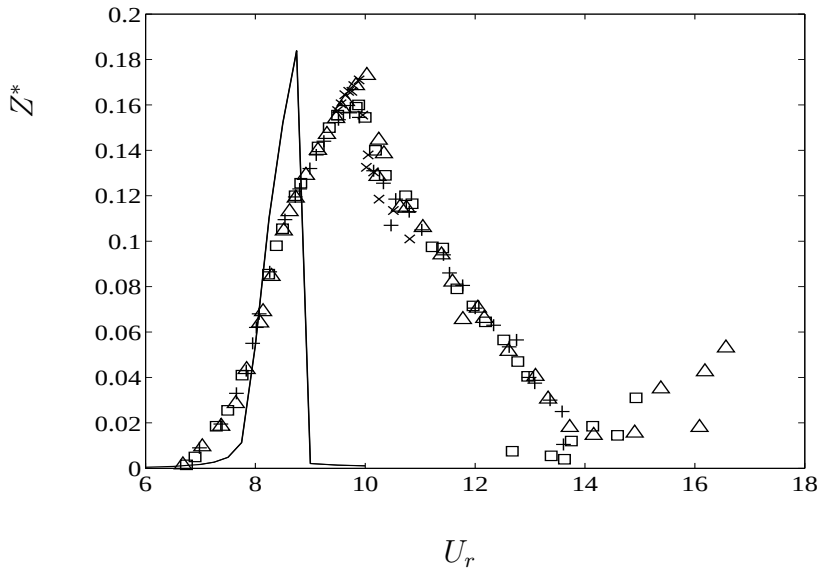

Figure 2.8: Reduced RMS Amplitude of the Limit Cycle Ocillations starting from rest configuration. (Solid Line) Velocity Coupling Simulations of the Wake Ocillator Model as presented in Facchinetti *et al.* (2004).

2.4 Discussion

We take this space to bring home the point that a similar experimental study involving a square cylinder oscillating freely in a high mass ratio environment apparently does not exist. Close coherence of the data points in Fig.2.4 exhibits the validity of the experimental procedure. Given the inherently elusive nature of the hysteresis phenomenon in such systems, we strongly believe that this study is a first step. Data from such experiments can be used to validate theoretical models as discussed in this chapter.

Table 2.1: Physical Parameters of the System

Diameter of the cylinder	D	20	mm
Length of the cylinder	b	150	mm
Stiffness of the setup	k	597.6 ± 35	N/m
Mass of the Cylinder	m	0.0654 ± 0.004	kg
Critical Damping	C_c	12.5 ± 0.75	N.s/m
Structural Damping	c	0.0104 ± 0.0008	N.s/m
Natural Frequency	f_o	15.21875 ± 0.01563	Hz
Wind tunnel Velocity	U	1.5 - 6.0	m/s
Air Density	ρ	1.205	kg/m^3
Kinematic Viscosity	ν	$15e^{-6}$	m^2/s

Table 2.2: Non-Dimensional Parameters of the System

Reynolds Number	Re	$\frac{UD}{\nu}$	2000 - 8000
Mass Ratio	μ	$\frac{m}{\rho D^2 b}$	905
Damping Ratio	η	$\frac{c}{c_c}$	0.000828 ± 0.000014
Scruton Number	Sc	$2\eta m^*$	1.498
Strouhal Number	St	$\frac{f_w D}{U}$	0.127
Skopp Griffin Parameter	S_G	$4\pi^2 St^2 Sc$	0.954
Reduced Velocity	U_r	$\frac{U}{f_o D}$	5-20

Chapter 3

Flutter in Two Degrees of Freedom Systems

Aeroelastic flutter plays a very important role in modern aircraft and suspended bridge deck design. We use the space in this chapter to recall the fundamental concept of Aeroelastic Flutter. Linear flutter modeling tools are briefly described. Although, comparatively straight forward, yet still the importance of the Quasi Steady Hypothesis cannot be under estimated. As we discussed earlier, accurate caliberation and measurement of different system parameters pertaining to the long term global behavior of the system is very important to conduct subsequent studies of the transient characteristics. This chapter is therefore devoted to the long term properties of our experimental setups. Different methods employed to measure system properties like dampings, stiffnesses and critical velocities are outlined in this chapter. As the reader shall find out; experimental findings have been satisfactorily validated.

3.1 Linear Flutter Modeling

Coupled mode flutter has been a subject of intense investigations for some time now. In this section we present salient features of classical coupled mode flutter.

Symmetric Airfoil Setup

Referring to Fung (1993), the equations of motion can be described as, Fig.3.1(a):

$$m\ddot{z} + 2m\eta_z\omega_z\dot{z} + k_z z + md\ddot{\alpha} = F_z$$
$$J_o\ddot{\alpha} + 2J_o\eta_\alpha\omega_\alpha\dot{\alpha} + k_\alpha\alpha + md\ddot{z} = M_o \tag{3.1}$$

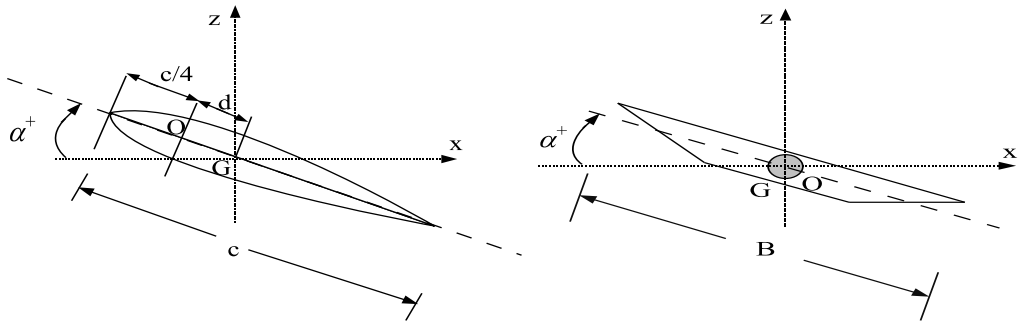

(a). Symmetric Airfoil (b). Stream-lined Bridge Deck

Figure 3.1: 'O' is the Axis of Rotation, 'G' is the Center of Gravity, 'd' induces coupling between the two Degrees of Freedom.

Assuming that the structural damping is small, Table 3.1, eigen values can be written in the form:

$$\lambda_\alpha = \omega_\alpha^2 = (2\pi f_\alpha)^2 = \frac{k_\alpha}{J_o} \quad ; \quad \lambda_z = \omega_z^2 = (2\pi f_z)^2 = \frac{k_z}{m} \tag{3.2}$$

The distance 'd' between the center of gravity 'G' and the axis of rotation 'O', Fig.3.1, can be determined using the following relation:

$$\lambda_1 + \lambda_2 = \lambda_z + \lambda_\alpha \left(\frac{1}{1 - \dfrac{md^2}{J_o}} \right) \tag{3.3}$$

where, λ_1 and λ_2 are the eigen values of the coupled system. The parameter 'd' is responsible for the inherent coupling between the two degrees of freedom.

Structural parameters are identified for each pure degree of freedom taken independently under zero wind velocity. Both the natural frequencies f_z and f_a are obtained by spectral analysis. Static Weight Calibration technique is used to calculate the stiffness k_z and k_α. The inertia J_o and mass m are then calculated using:

$$m = \frac{k_z}{(2\pi f_z)^2} \quad ; \quad J_o = \frac{k_\alpha}{(2\pi f_\alpha)^2} \tag{3.4}$$

Total energy is the sum of the system's Kinetic and Potential energies:

$$E(t) = \frac{1}{2}m\dot{z}^2 + \frac{1}{2}J_o\dot{\alpha}^2 + md\dot{\alpha}\dot{z} + \frac{1}{2}k_z z^2 + \frac{1}{2}k_\alpha \alpha^2 \tag{3.5}$$

Streamlined Bridge Deck Setup

In case of the bridge deck section, Fig.3.1(b), the model is supported at the center of gravity, d = 0. Consequently, the coupling term disappears. However, coupling between the two degrees of freedom in this case can be ascribed to the cross flutter derivatives associated to the aerodynamic damping terms in the right hand side of Eqn.3.1. The bridge deck profile is not symmetric, hence as the wind flows around the deck section a net lift force is generated which pushes the deck section down wards inducing an initial displacement from its rest position. This initial displacement remains constant with respect to time but it is a function of the mean wind velocity, $\overline{U}$. It is taken into account for all the energy calculations during the course of the present study. Equation 3.5 for the total energy takes the following form:

$$E(t) = \frac{1}{2}m\dot{z}^2 + \frac{1}{2}J_o\dot{\alpha}^2 + \frac{1}{2}k_z z^2 + \frac{1}{2}k_z {z_o}^2 - z z_o + \frac{1}{2}k_\alpha \alpha^2 \tag{3.6}$$

where z_o is the initial displacement induced by the incident wind.

Linear Aerodynamic Loading

We use Scanlan's flutter derivatives from Scanlan & Tomko (1977) to model the linear aerodynamic loading on the right hand side of Eqn.3.1:

$$\begin{aligned} F_z &= \frac{1}{2}\rho b c \overline{U}^2 \left(H_1\dot{z} + H_2\dot{\alpha} + H_3\alpha + H_4 z\right) \\ M_o &= \frac{1}{2}\rho b c^2 \overline{U}^2 \left(A_1\dot{z} + A_2\dot{\alpha} + A_3\alpha + A_4 z\right) \end{aligned} \tag{3.7}$$

The Aerodynamic Flutter Derivatives are also sometimes referred to as Aeroelastic Coefficients. They can be expressed by the Unsteady Airfoil Theory (UAT)

implying that the thin airfoil is in a non-stalled state executing small amplitude periodic oscillations along the two degrees of freedom. The incident airflow is assumed to be in-compressible and the viscous effects are neglected according to the established Kutta-Joukowski condition, Fung (1993). Two important pre-requisites are the reduced velocity, U_r and the reduced frequency, K which are commonly expressed as:

$$U_r = \frac{\overline{U}}{cf_z} \quad ; \quad U_r = \frac{\overline{U}}{cf_\alpha} \tag{3.8}$$

The reduced velocity is defined based on the profile chord and the frequency of each pure degree of freedom. All the aeroelastic coefficients of Eq.3.7 are expressed using the Theodorsen function, Theodorsen (1935), $C(K) = F(K) + iG(K)$, where K is the reduced circular frequency commonly expressed as $K = \frac{2\pi}{U_r}$. The real and imaginary parts of the Theodoresen Function are expressed using the modified Bessel Functions:

$$F = \frac{J_1\left(Y_0 + J_1\right) - Y_1\left(J_0 - Y_1\right)}{\left(Y_0 + J_1\right)^2 + \left(J_0 - Y_1\right)^2} \quad ; \quad G = \frac{-J_1\left(J_0 - Y_1\right) - Y_1\left(Y_0 + J_1\right)}{\left(Y_0 + J_1\right)^2 + \left(J_0 - Y_1\right)^2} \tag{3.9}$$

The functions ‘F’ and ‘G’ have been plotted against the reduced frequency ‘K’ in Fig.3.2.

The aeroelastic coefficients are now expressed as, Fung (1993):

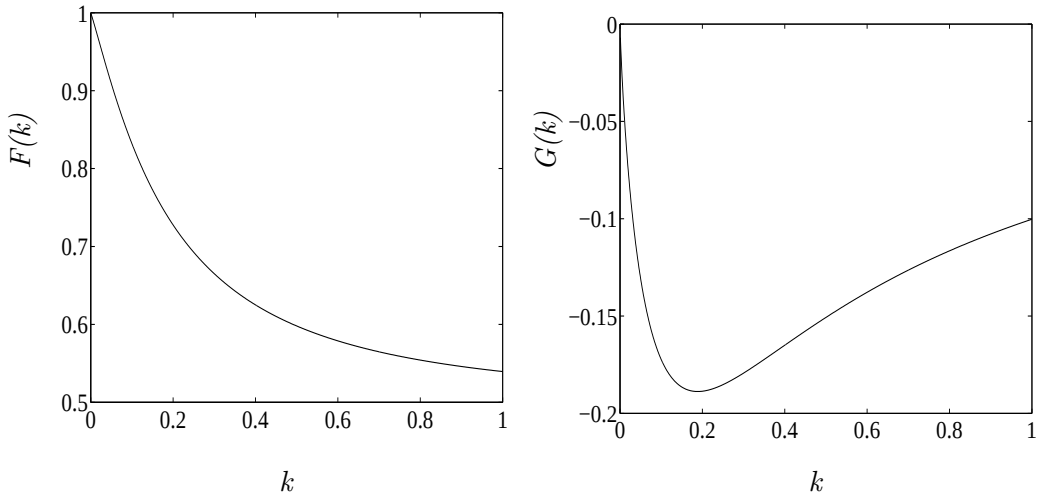

(a). Real Part (b). Imaginary Part

Figure 3.2: Real and Imaginary Part of the Theodoresen Function, $k = \frac{K}{2}$

$$H_1 = -\frac{1}{\overline{U}} C_z' F \qquad A_1 = -\frac{1}{\overline{U}} C_z' \frac{F}{2}\left(\frac{1}{2}+a\right)$$

$$H_2 = \frac{c}{\overline{U}} C_z'\left[\frac{1}{4}+\frac{G}{K}+\frac{F}{2}\left(\frac{1}{2}-a\right)\right] \qquad A_2 = \frac{c}{\overline{U}} C_z'\left[\frac{1}{8}\left(\frac{1}{2}-a\right)-\frac{G}{2K}\left(\frac{1}{2}+a\right)+\frac{F}{4}\left(a^2-\frac{1}{4}\right)\right]$$

$$H_3 = C_z'\left[F-\frac{KG}{2}\left(\frac{1}{2}-a\right)+K^2\frac{a}{8}\right] \qquad A_3 = C_z'\left[\frac{1}{16}\left(a^2+\frac{1}{8}\right)K^2+\frac{F}{2}\left(\frac{1}{2}+a\right)+\frac{KG}{4}\left(a^2-\frac{1}{4}\right)\right]$$

$$H_4 = \frac{C_z'}{c}\left[\frac{1}{4}+\frac{G}{K}\right]K^2 \qquad A_4 = C_z'\frac{K^2}{2c}\left[\frac{a}{4}+\frac{G}{K}\left(\frac{1}{2}+a\right)\right]$$

Figure 3.3: Aerodynamic Flutter Derivatives

Reissner (1926) analysed the wing torsional divergence demonstrating the importance of relative locations of the aerodynamic center of pressure and the elastic axis. The parameter *'a'* is the dimensionless distance between these two points of interest based on a reference length c/2. In our case a = -1/4 for the symmetric airfoil and a = 0 for the streamlined bridge deck section. In practice, flutter derivatives of suspended bridge deck sections are measured experimentally on a case to case basis. Measurement of the same for the bridge deck section in question is however, out of the scope of this work.

Numerical Simulations

As stated earlier, Sec.2.3, we used the Fox and Goodwin iteration scheme to numerically solve the governing equations 2.7 and 2.8. We shall use the same scheme to solve the equation 3.1, 3.5 and 3.6. Results from the numerical simulations shall be used to validate the measured structural parameters as in Fig.3.5 and Fig.3.10. The same numerical scheme is used to simulate the theoretic energy curve in Fig.6.14.

The Fox and Goodwin iteration scheme is a modified form of the widely known single step Newmark iteration method. In our case we shall implement the prediction-correction strategy in each iteration to solve the equations of motion. Unlike the standard Newmark scheme, Fox and Goodwin defined the constants as $\gamma = \frac{1}{2}$ and $\beta = \frac{1}{12}$. Assigning these values improves the precision of the method to the third order compared to a second order precision level obtained by the standard scheme. The stability condition in this case is typically defined as $\Delta t\omega \leq \sqrt{6}$. The inherent numerical damping in the scheme is reduced to zero given the fact that the phase error is shifted to the third order, Géradin & Rixen (1992). We implemented the Fox and Goodwin scheme using the following algorithm:

$$
\begin{aligned}
&\textit{Prediction} && \dot{x}^*_{n+1} = \dot{x}_n + (1-\gamma)\Delta t\ddot{x}_n \\
& && x^*_{n+1} = x_n + \Delta t\dot{x}_n + (\frac{1}{2} - \beta)\Delta t^2\ddot{x}_n \\
&\textit{Acceleration} && \ddot{x}_{n+1} = \frac{f\left(x^*_{n+1}, \dot{x}^*_{n+1}, t_{n+1}\right) - c\dot{x}^*_{n+1} - kx^*_{n+1}}{1 + c\gamma\Delta t + k\beta\Delta t^2} \\
&\textit{Correction} && \dot{x}_{n+1} = \dot{x}^*_{n+1} + \gamma\Delta t\ddot{x}_{n+1} \\
& && x_{n+1} = x^*_{n+1} + \beta\Delta t^2\ddot{x}_{n+1}
\end{aligned}
\tag{3.10}
$$

3.2 Wind Tunnel Setup and Measurement Techniques

3.2.1 Wind Tunnel Setup

All the experimental results discussed in this study were obtained using the fluid structure interaction lab facility at the Laboratoire d'Hydrodynamique, (LadHyX). Experiments were conducted on an airfoil and a bridge deck model separately. The models are flexibly mounted in an Eiffel type wind tunnel. The wind tunnel has a test section of 0.18m width. A 2500W centrifugal fan is installed down-stream of the test section. When operated the fan can create an airflow from $\approx 4m/s$ to $\approx 30m/s$ at maximum power. Air discharge from the fan exhaust is in the vertical direction. Contraction section of the wind tunnel is 0.5m long. A wire mesh and a honey comb structure at the inlet of the contraction section ensures a turbulence level of 1.5% at 10m/s.

The models used in the experiments were fabricated using a numerical milling machine to ensure close dimensional tolerance. The models are suspended in the test section primarily supported by two long flat Aluminum bands of dimensions 400mm x 20mm x 2mm. Two sets of vertical springs, one at each extremity of the models hold them exactly in place. Bending natural frequency of the models is controlled by adjusting the thickness of Aluminum bands near their clamping positions. Torsional frequency of the set-ups is controlled by using two sets of horizontal springs on each side. The models are restrained so that they can oscillate only in the rotational and vertical degrees of freedom when subjected to an air flow.

It must be pointed out here that there are no moving parts in the experimental set-ups so that there is no moving friction and the structural damping of the systems is very low. Sand particles are glued to the leading edge of the airfoil to ensure that the boundary layer separation takes place always at the same point. End plates were used to further the two dimensionality of the experimental set-up.

3.2.2 Measurement Techniques

Measurements are obtained using two laser displacement sensors for each degree of freedom. Measurement resolution used during the course of the experiments is $40\mu m$. The laser sensors have an accuracy better than 1% of the full scale range, $\pm 10mm$. Output signals from the laser displacement sensors are treated by a PAK

system provided by Muller BBM. It consists mainly of a 24-bit and 8-channel acquisition card and a signal processing software. Sampling frequency chosen for these experiments is 512Hz. The measurement system used is capable of conducting numerical post processing operations on the measured data to retrieve the physical quantites in terms of displacements and energy.

Mean wind velocity in the wind tunnel is measured by a pitot tube located downstream of the test section. The pitot tube is connected to an electronic manometer. Temperature corrections are incorporated using inputs from a thermocouple which measures ambient temperature. Velocity measurements with upto 0.2% accuracy are obtained.

3.3 Airfoil Setup

The airfoil model is a NACA 0015 airfoil of 0.12m chord and 0.17m span, Fig.3.4. The axis of rotation lies at its forward quarter chord point. This allows us to induce a separation 'd' between the center of gravity 'G' and the rotation axis 'O' of the airfoil, Fig.3.1(a). This distance 'd' is actually responsible for the inherent coupling between the two degrees of freedom of the airfoil set-up. Typical Reynolds Number of the experiments, based on the chord, is in the range 80 000 - 120 000.

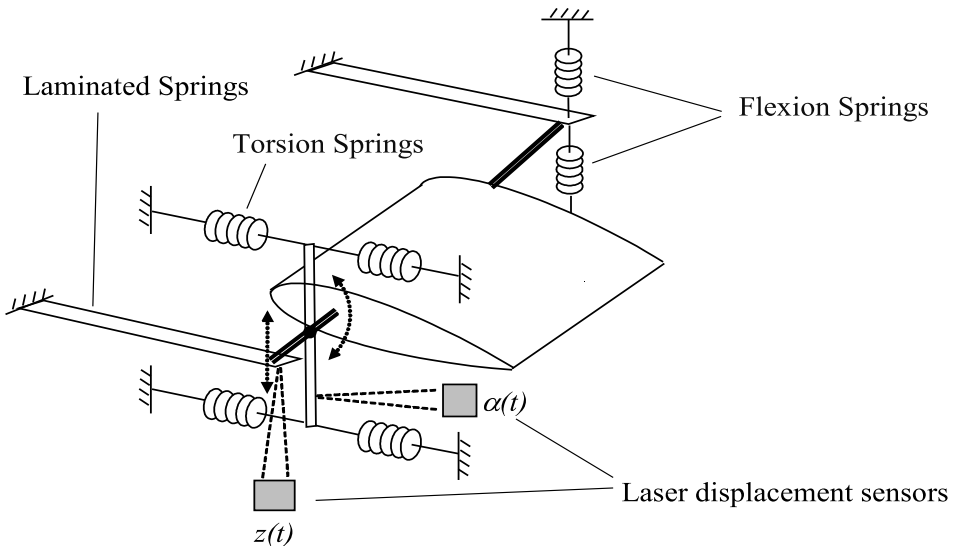

Figure 3.4: Airfoil Experimental Setup Schematic

3.3.1 Structural Parameters

Structural parameters are identified for each pure degree of freedom taken independently under zero wind velocity using Eqn.3.4 and Eqn.3.5. Computations curve in Fig.3.5 is obtained by numerically simulating Eqn.3.1. The technique used for simulations is described in Sec.3.1, Eqn.3.10.

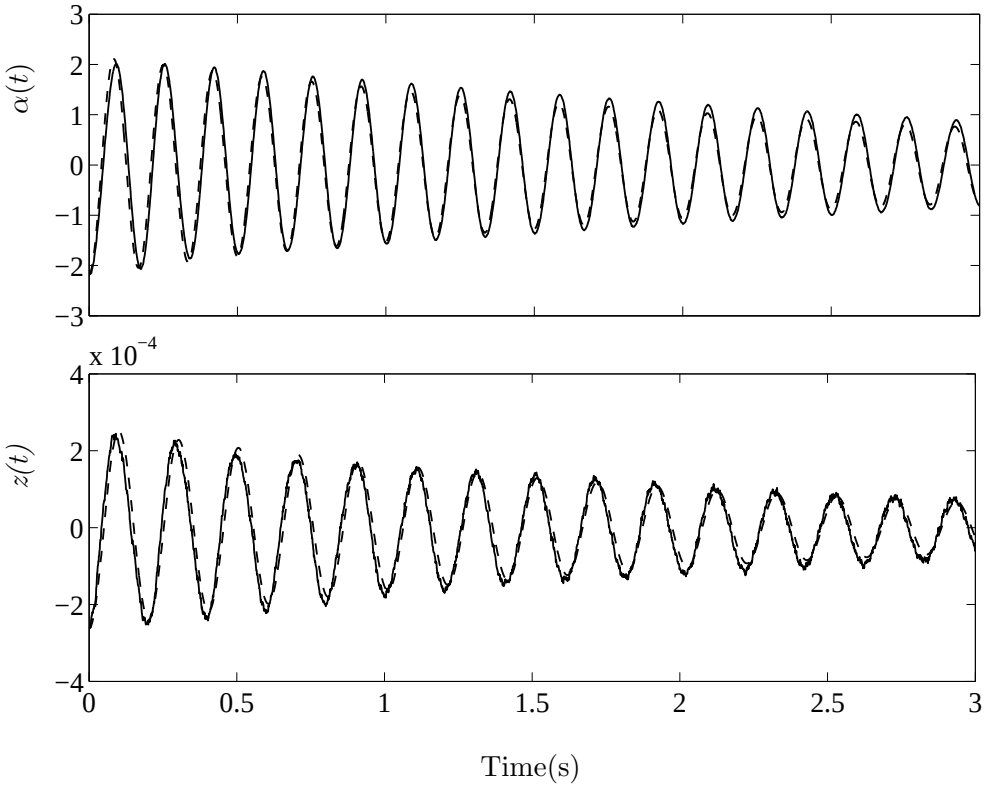

Figure 3.5: Time evolution of angular and bending displacement, Initial conditions: $\alpha_o = -2.173^o$, $z_o = -0.0003534$m. Linear Airfoil Setup (Table 3.1). (solid-line) Experiment, (dashed-line) Computation.

3.3.2 Critical Velocity

The most important parameter relative to the long term study of such fluid structure interaction systems is the critical velocity. If the incident wind velocity approaches this value, the system may suffer from the flutter instability. In order to demonstrate the calculation of critical velocity, following Hémon *et al.* (2006),

we shall start by rewritting Eqn.3.1, this time identifying the added aerodynamic damping terms:

$$\begin{aligned} \ddot{z} + 2\left(\eta_z + \eta_{az}\right)\omega_z \dot{z} + k_z z + d\ddot{\alpha} &= \frac{F_z}{m} \\ \ddot{\alpha} + 2\left(\eta_\alpha + \eta_{a\alpha}\right)\omega_\alpha \dot{\alpha} + k_\alpha \alpha + \frac{md}{J_o}\ddot{z} &= \frac{M_o}{J_o} \end{aligned} \tag{3.11}$$

combining with Eqn.3.7 and applying the quasi-steady hypothesis, we have the following form:

$$\begin{aligned} \ddot{z} + 2\left(\eta_z + \eta_{az}\right)\omega_z \dot{z} + \omega_z^2 z + d\ddot{\alpha} &= \frac{\rho b c U_r^2}{2 c f_z^2 m} C'_z \alpha \\ \ddot{\alpha} + 2\left(\eta_\alpha + \eta_{a\alpha}\right)\omega_\alpha \dot{\alpha} + \omega_\alpha^2 \alpha + \frac{md}{J_o}\ddot{z} &= 0 \end{aligned} \tag{3.12}$$

considering the system in Eqn.3.12 without any damping:

$$\begin{aligned} \ddot{z} + \omega_z^2 z + d\ddot{\alpha} &= \frac{\rho b c U_r^2}{2 c f_z^2 m} C'_z \alpha \\ \ddot{\alpha} + \omega_\alpha^2 \alpha + \frac{md}{J_o}\ddot{z} &= 0 \end{aligned} \tag{3.13}$$

if the eigen values of such a system become complex, natural frequencies of the two degrees of freedom shall become equal and the airfoil shall experience flutter. Mathematically,

$$det \begin{vmatrix} \lambda - \lambda_z & \lambda d + \dfrac{\rho b c U_r^2}{2 c f_z^2 m} H_3 \\ \dfrac{\lambda m d}{J_o} & \lambda - \lambda_\alpha \end{vmatrix} = 0 \tag{3.14}$$

now, we can find the smallest root U^2 of the following second order equation:

$$\left(\lambda_z + \lambda_\alpha + \frac{d\rho b c U^2}{2 J_o} C'_z\right)^2 - 4\lambda_z \lambda_\alpha \left(1 - \frac{m d^2}{J_o}\right) = 0 \tag{3.15}$$

the critical velocity is now given by:

$$U_c^2 = \frac{-2 J_o \left(-\left(\lambda_z + \lambda_\alpha\right) + \sqrt{4\lambda_z \lambda_\alpha \dfrac{\lambda_z + \lambda_\alpha}{\lambda_1 + \lambda_2}}\right)}{d\rho b c C'_z} \tag{3.16}$$

Using the system parameters as catalogued in Table 3.1, we solve the Eqn.3.16 for U_c which is found to be 18.58 m/s for this case.

3.3.3 Frequency

Normalized frequencies of the two degrees of freedom are shown in Fig.3.6. We can see that the two frequencies approach one an other as the incident mean wind velocity increases. The two frequencies finally merge at the critical velocity signalling the on-set of the flutter instability. This value of the flutter frequency can be calculated using

$$f_c^2 = \frac{1}{(2\pi)^2}\sqrt{\lambda_z \lambda_\alpha \frac{\lambda_1 + \lambda_2}{\lambda_z + \lambda_\alpha}} \tag{3.17}$$

substituting values in Eqn.3.17, we obtain the critical frequency value, $f_c = 5.99Hz$. This value is normalized with respect to the bending natural frequency f_z giving a dimensionless value 1.21, marked by the dashed line in Fig.3.6.

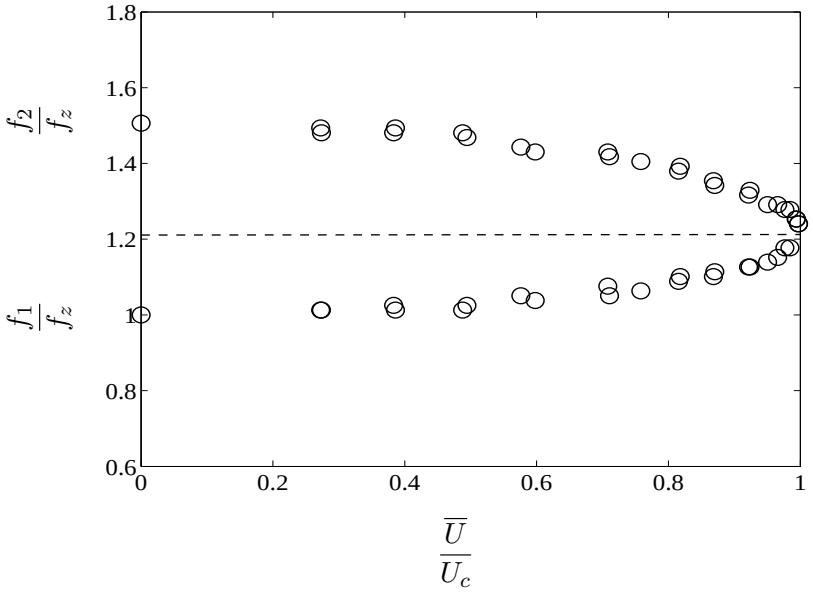

Figure 3.6: Frequency Ratios of the 2 modes versus velocity parameter; Schwartz *et al.* (2009).

3.3.4 Aerodynamic Damping

We know that aerodynamic damping plays a very important part in over all system dynamics. In order to fully observe the contribution of aerodynamic phenomena in the overall damping of the system, each degree of freedom is studied independently, Fig.3.7. The experimental setup was designed to keep the two structural dampings as low as possible. Applying the quasi-steady conditions, we know that the pure aerodynamic damping for each degree of freedom can be written as:

$$H_1 = \frac{-1}{\overline{U}} C'_z \quad ; \quad A_2 = \frac{-1}{8} \frac{c}{\overline{U}} C'_z \tag{3.18}$$

These aerodynamic dampings can be rewritten in a direct form by exploiting Eqns.3.1, 3.7 and 3.18 as follows:

$$\eta_{a_z} = \frac{\rho b c \overline{U}}{4 m \omega_z} C'_z \quad ; \quad \eta_{a_\alpha} = \frac{\rho b c^3 \overline{U}}{32 J_o \omega_\alpha} C'_z \tag{3.19}$$

C'_z was measured and found to be approximately equal to 2π. Aerodynamic damping curves obtained from Eqn.3.19 are compared with the experimental findings in Fig.3.7. Good agreement between the experimental points and the damping curves obtained by the quasi-steady theory validates the experimental procedure and the identification of structural parameters.

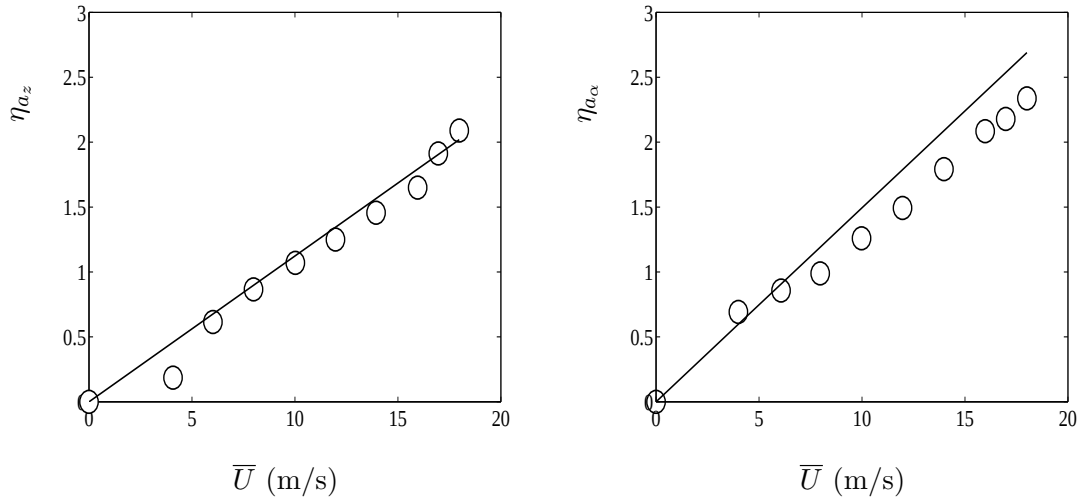

Figure 3.7: Aerodynamic damping versus velocity; (o) Experiment; (-) QST. Linear Airfoil Case (Table 3.1).

Table 3.1: Airfoil System Parameters

k_α, k_z	1.66 ± 0.05	881 ± 33	(N.m/rad) , (N/m)
g	0.655 ± 0.04		mm
δk	120 ± 5		N/m
$b,\ c$	0.12 ± 0.0001	0.17 ± 0.0001	m
f_α, f_z	6.9375 ± 0.0625	4.9375 ± 0.0625	Hz
f_1, f_2	4.9375 ± 0.0625	7.4375 ± 0.0625	Hz
η_α, η_z	0.2 ± 0.01	0.15 ± 0.01	(%)
J_o, m	$8.74e^{-4} \pm 0.25e^{-4}$	0.915 ± 0.05	$(kg.m^2), (kg)$
d	9.3 ± 0.3		mm

3.4 Bridge Deck Setup

The bridge deck section has a chord, B = 0.11 m and a span 0.17 m. The bridge deck model is supported at its axis of rotation which is located at its chord-wise geometric center, Fig.3.1(b). Bridge deck model mimicks the cable-stayed road bridge constructed over the valley of river Tarn near Millau in Southern France, Fig.3.8. Typical Reynolds number of the experiments, based on the chord, is in the range 35 000 - 160 000.

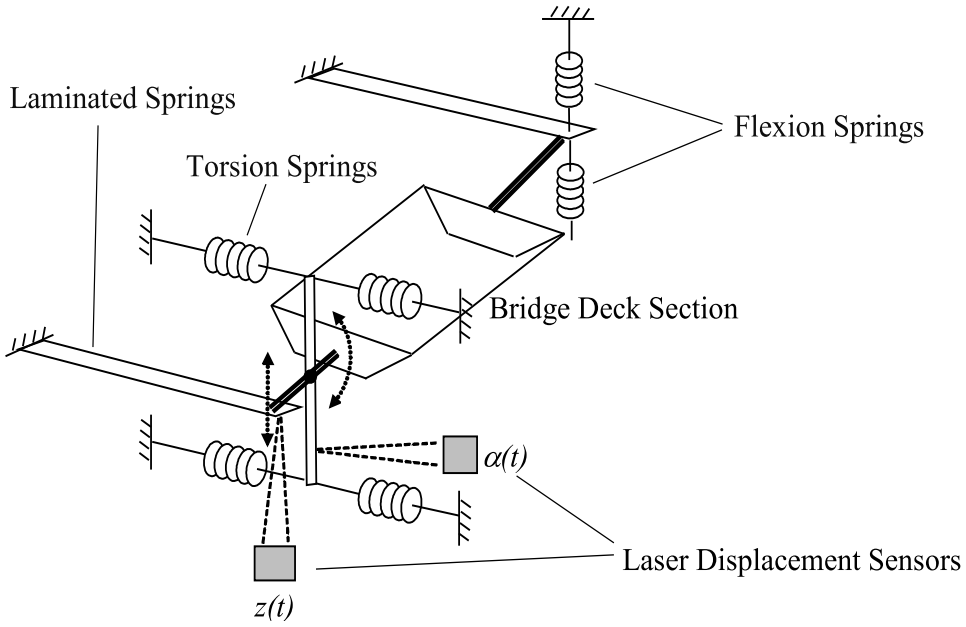

Figure 3.8: Bridge Deck Cross Section Schematic.

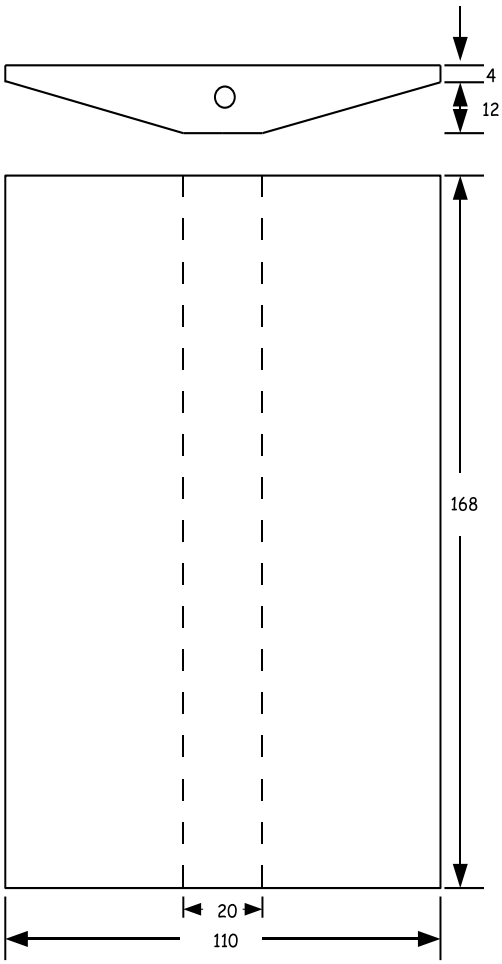

Figure 3.9: Bridge Deck Cross Section Schematic.

3.4.1 Structural Parameters

Structural parameters are identified for each pure degree of freedom taken independently under zero wind velocity using Eqn.3.4 and Eqn.3.5. Total energy is the sum of the system's Kinetic and Potential energies, Eqn.3.6 for bridge deck setup.

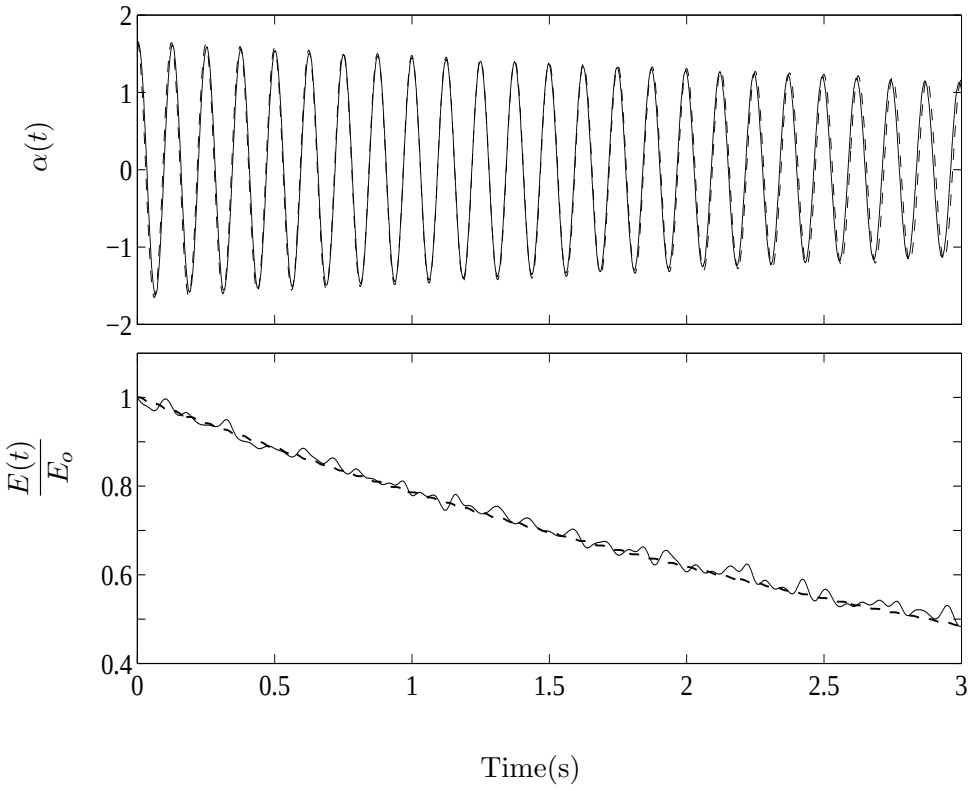

Figure 3.10: Time evolution of angular displacement and corresponding dimensionless total energy $\overline{U} = 0$, $\alpha_o = 1.66^{\circ}$, Bridge Deck Section, Case 2 (Table 3.2). (solid-line) Experiment, (dashed-line) Computation.

Measurement of these structural parameters is validated by comparing an experimental test for each case without wind with results from numerical simulation, as shown in Fig.3.10 for one of the cases. The numerical simulation technique is described in Sec.3.1, Eqn.3.10. Initial conditions for each independent case are provided by small mechanically induced offsets. For the pure vertical displacement case, the laminated springs also introduce a small angle of rotation. This is taken into account in the recovery procedure of the laser signal. Close agreement of the experimental

and simulation curves in Fig.3.10 verifies the correct detection and measurement of various structural parameters of the experimental setup.

3.4.2 Frequency Ratio

As part of our experimental investigations of the stream-lined bridge deck section; three different setups were used. All the three setups are distinctly identifiable on the basis of their frequency ratios. In this study the frequency ratio is defined as the ratio of the natural bending frequency of the bridge deck section to the pure torsional frequency.

$$r_F = \frac{f_z}{f_\alpha} \tag{3.20}$$

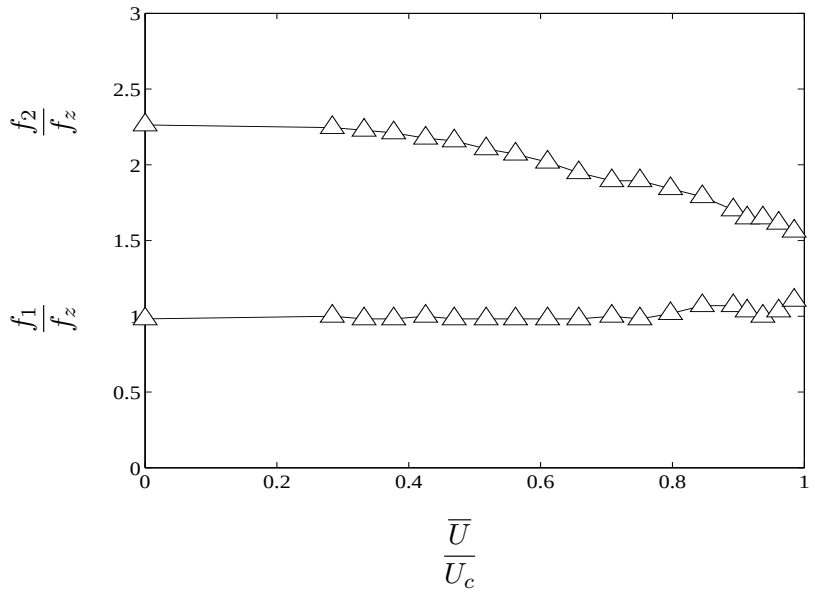

Figure 3.11: Frequency Ratios of the 2 modes versus Velocity Ratio.Case 3, (Table 3.2).

Recalling that the system is a Type-II (Class-1), Sec.1.1, Fig.1.1, fluid structure interaction system; in such two degrees of freedom cases one of the frequencies of the system remains almost constant while the second frequency changes as a function of mean free stream velocity. In this particular case, bending frequency (f_1) of the system remains quasi-constant. Torsional frequency (f_2) however changes. As the mean

free stream velocity is increased, torsional frequency moves towards the bending frequency until for a certain critical value of wind velocity, the two frequencies merge. In this result slight dispersion in the experimental points for the bending frequency can be observed in the vicinity of the critical velocity. A closer data resolution could not be obtained due to the practical constraints. If however, the velocity is increased further, the flutter in-stability sets in. The flutter frequency, f_c/f_z shall be the same as f_1/f_z.

Effect of Frequency Ratio on Critical Velocity

In our case for a frequency ratio 0.44, the maximum critical flutter velocity was 21.34 m/s as shown in Fig.3.12. This maximum velocity is close to maximum allowable operational velocity of the wind tunnel which is slightly more than 25 m/s. After credible energy evolution data had been obtained for this case, the system parameters were changed to obtain a frequency ratio value of 0.62. It is observed, as in Fig.3.12, that increasing the frequency ratio of the bridge deck section actually reduced the critical wind speed. Bridge deck systems with a higher frequency ratio shall have an equally lower critical wind speed making them susceptible to structural fatigue and a risk of complete failure at much lower incident wind speeds. The representation, $1-\left(\frac{f_z}{f_\alpha}\right)^2$, has been adopted to keep in line with Schmid & de Langre (2003).

Effect of Frequency Ratio on Aerodynamic Stiffness

We know that the aerodynamic added terms including the aerodynamic damping and aerodynamic stiffness play a very important part in overall system dynamics. Aerodynamic dampings have been discussed in Sec.3.4.3, Fig.3.14. Aerodynamic Stiffness, ${A_3}^{\#}$ is measured experimentally using the following expression, assuming that Quasi-Steady Theory holds:

$$A_3^{\#} = K^2 A_3^* = \frac{2J_o\lambda_\alpha\left(1-\left(\frac{f_z}{f_\alpha}\right)^2\right)}{\rho b B^2 U_c^2} \tag{3.21}$$

where $A_3^{\#}$ is inspired from Scanlan's flutter derivatives for which 'K' is the reduced angular frequency. Added stiffness is found to be quasi-constant for all the three frequency ratios. Experimental values of the aerodynamic stiffness are plotted as a function of the frequency parameter in Fig.3.13.

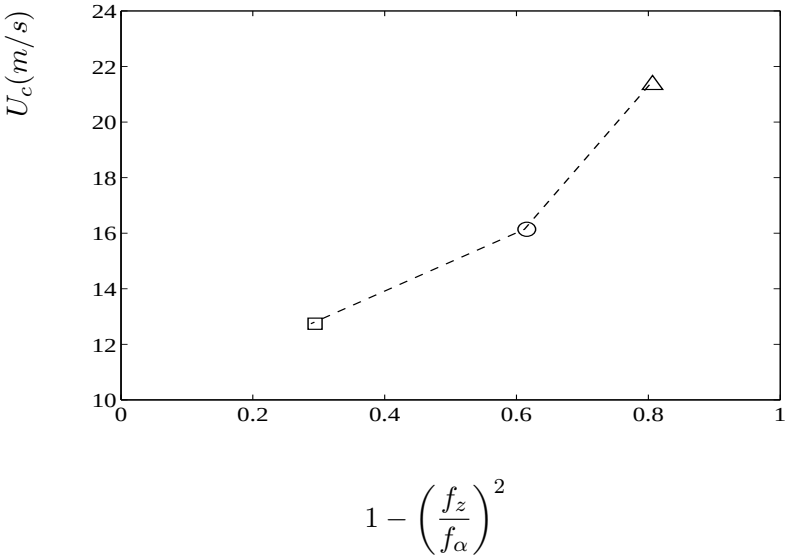

Figure 3.12: Dimensional Critical System Velocities versus Frequency Ratio; (❑) Case 1; (O) Case 2; (Δ) Case 3; (Table 3.2)

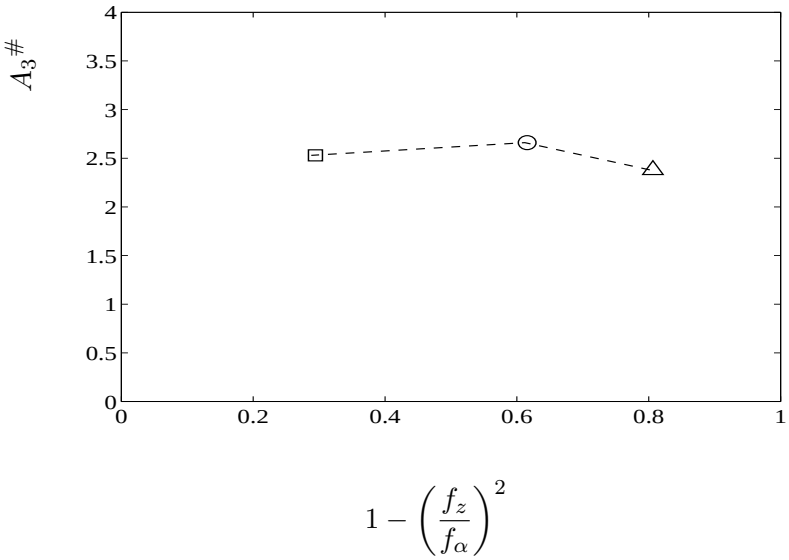

Figure 3.13: $A_3{}^{\#}$ versus Frequency Ratio at the respective critical velocities. (❑) Case 1; (O) Case 2; (Δ) Case 3; (Table 3.2)

3.4.3 Aerodynamic Damping

Recalling from Scanlan & Tomko (1977) and Sec.3.1, we know that the Standard Airfoil Theory as invoked above cannot be reliably used in case of a bridge deck section irrespective of the surface streamlining conditions. Therefore, for experiments conducted on the bridge deck section we use simple linear regression to observe the evolution of added damping with respect to the increasing mean wind velocity. The added damping is found to evolve linearly as expected from the Quasi-Steady Theory. Straight line in Fig.3.14 thus, represents the linear regression unlike in Fig.3.7 where the same is used to represent the Quasi-Steady Theory.

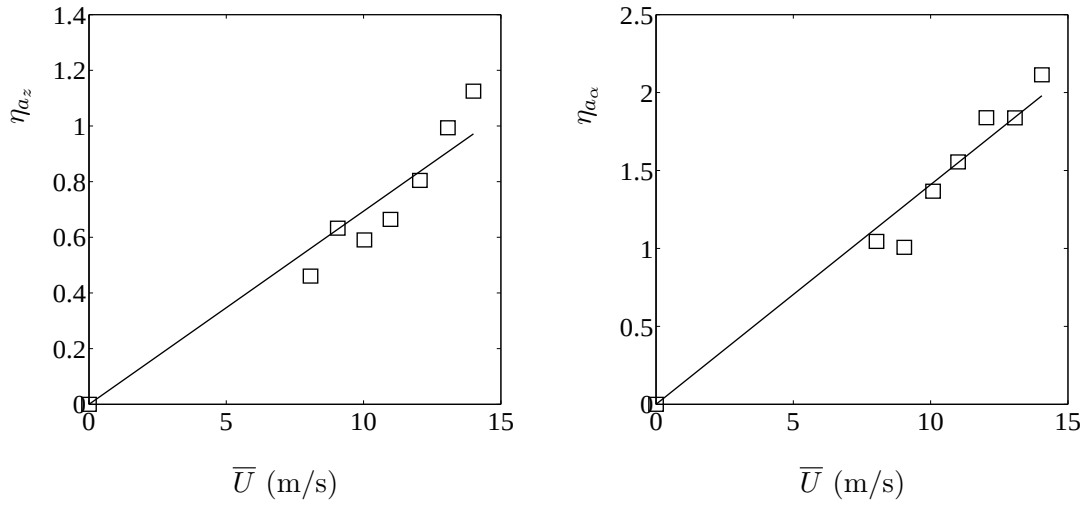

Figure 3.14: Aerodynamic damping versus velocity; (❑) Experiment; (-) Linear Regression. Bridge Deck Section Case 1 (Table 3.3).

3.5 Discussion

All the experimental results in this chapter have been reasonably validated using simple theoretical methods. As stated earlier, importance of such procedures cannot be under estimated for the fact that findings from these experiments shall be used in the more complicated transient energy growth studies. Any small discrepency can snowball into an un-acceptable error if proper attention is not paid to the fine details.

Table 3.2: Structural Parameters of Different Bridge Deck Sections Studied

	$\frac{f_z}{f_\alpha}$	f_α	f_z	k_α	k_z	J_o	m	$\eta_\alpha\%$	$\eta_z\%$
Case 1	0.84	8.00	6.75	1.85	1246.91	$7.32e^{-4}$	0.69	0.17	0.16
Case 2	0.62	7.12	4.43	1.33	519.36	$6.64e^{-4}$	0.66	0.3	0.08
Case 3	0.44	8.00	3.56	1.67	309.16	$6.61e^{-4}$	0.62	0.24	0.07

Table 3.3: Measured Parameters of Different Bridge Deck Sections Studied

	$\frac{f_z}{f_\alpha}$	U_c	$A_3^\#$
Case 1	0.84	12.74	2.53
Case 2	0.62	16.14	2.66
Case 3	0.44	21.34	2.38

PART-II Transient Behavior

As the name suggests, this part is reserved for the transient behavior of all the three fluid structure systems studied in Part-I. As pointed out earlier, Sec.1.4, researchers started paying attention to the existence of transient energy growth in fluid structure systems very recently. Experimental evidence published lately proves the existence of this phenomenon. Traditionally, spectral methods have been used to estimate structural constraints in such problems. However, recent research shows that such techniques may not always encompass all the exisitng phenomenon arising due to the combination of wind turbulence excitation and aeroelastic effects. This scenario becomes increasingly important in situations where a bridge deck may be exposed to high turbulent wind close to the ground level, for example. It is such real life scenarios which reflect the need for exhaustive temporal simulations. The time domain simulation tool enables us to treat wind gusts as a sudden transient excitation instead of a stationary excitation as largely assumed during typical spectral investigations. A very important favorable consequence of using temporal simulations is the fact that we can detect and study transient energy growth phenomenon as shall be discussed during the course of this part.

In this part we present an exhaustive experimental study demonstrating the existence of transient growth and techniques employed to objectively quantify our findings. Results have been compared with existing theoretical tools where available and where permitted by the time constraints. We shall start with the investigation of the transient behavior exhibited by a freely oscillating square cylinder. Growth rate of oscillations amplitude in the transient regime is measured and presented. Then we move on to a two degree of freedom bridge deck section studied in a wind tunnel. We demonstrate how the maximum energy amplification due to transient growth in such systems can be linked to the frequency ratio and the amplitude of the initial mechanical excitation. The bridge deck behavior is studied under the effect of both mechanical excitation and excitation by an upstream gust, separately. These results are followed by the experimental investigation of a non-linear symmetric airfoil. We present experimental results showing the by-pass transition to flutter instability due to transient growth in case of a non-linear airfoil setup. A new combination of the already existing quasi-steady theory and the Kussner's aerodynamic admittance function is proposed to validate the transient energy amplification results obtained from a linear airfoil setup subjected to an upstream gust. This combination enables us to circumvent the complex details of standard un-steady airfoil theory.

Chapter 4

Transient Behavior of a Square Cylinder

Before we go into the details of the transient behavior of the square cylinder, it is important to keep in mind that we are interested in the long term and transient behavior of the cylinder in the VIV regime. This vortex induced vibration region is in turn governed by the extent of the frequency lock-in domain as discussed earlier, Chapter 2.

Amandolèse & Hémon (2010) recently published interesting experimental data obtained using long time analysis of the limit cycle oscillations. Results presented by the authors depict that the oscillations frequency tends to approach the vortex shedding frequency at the beginning of the lock-in. As the reduced velocity is increased, the oscillations frequency increases settling eventually at a value slightly higher than the natural frequency of the cylinder, Fig.4.1. This frequency coalescence mechanism as demonstrated by the authors is in line with de Langre (2006) and validates our earlier discussion, Fig.1.1, Sec.1.1.

4.1 Measurement Procedure

We recall from Fig.2.3 that the square cylinder oscillating under the vortex shedding effect in a wind tunnel actually passes a transient stage before it achieves the limit cycle oscillations amplitude. One of the most straight forward technique to quantify the cylinder behavior in the transient regime is to measure the amplitude

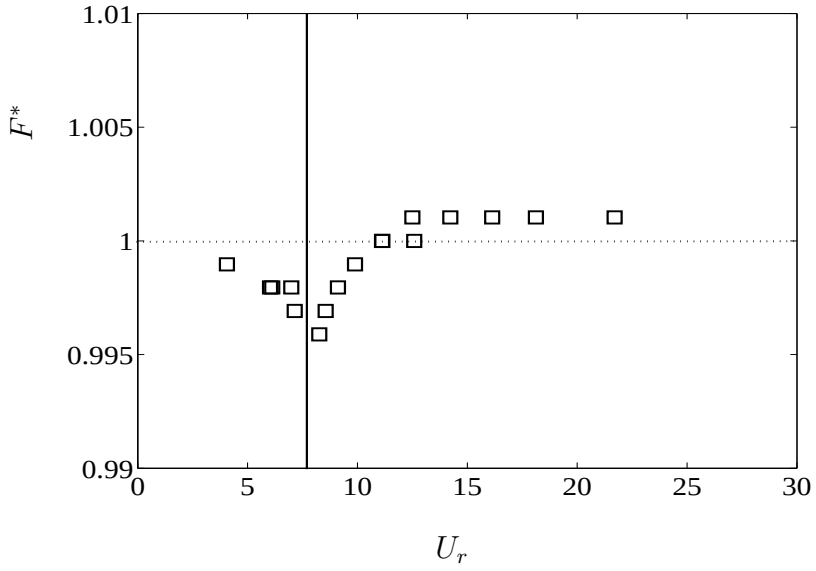

Figure 4.1: Reduced frequency of the LCO versus reduced velocity zoomed around the lock-in region, reproduced as Amandolèse & Hémon (2010)

growth rate for each value of up-stream velocity. The logarithmic decrement technique is used for this purpose. de Langre (2006) reported that the growth rate of amplitude of a cylinder executing vortex induced oscillations increases during the frequency lock-in range resulting in a higher oscillation amplitude. These measurements are however possible only for the starting from rest configuration of these experiments, Fig.2.4.

For each value of the mean free stream velocity, the cylinder is brought to rest and then allowed to respond to the incident wind. Data accumulation is triggered manually from as soon as the cylinder is let free untill the cylinder achieves limit cycle amplitude. Square of the cylinder displacement, $z^2(t)$ is plotted on a semi-logarithmic scale as a function of time, Fig.4.2. Corresponding values of time i.e. t_1 and t_2 are noted when the $z^2(t)$ curve intersects two consecutive base lines along the y-axis. We use the logarithmic decrement formula as Eqn.4.1 to calculate the reduced growth rate, $\delta(\%)$.

$$\delta(\%) = -100\frac{ln\frac{1}{10}}{4\pi f \Delta t} \tag{4.1}$$

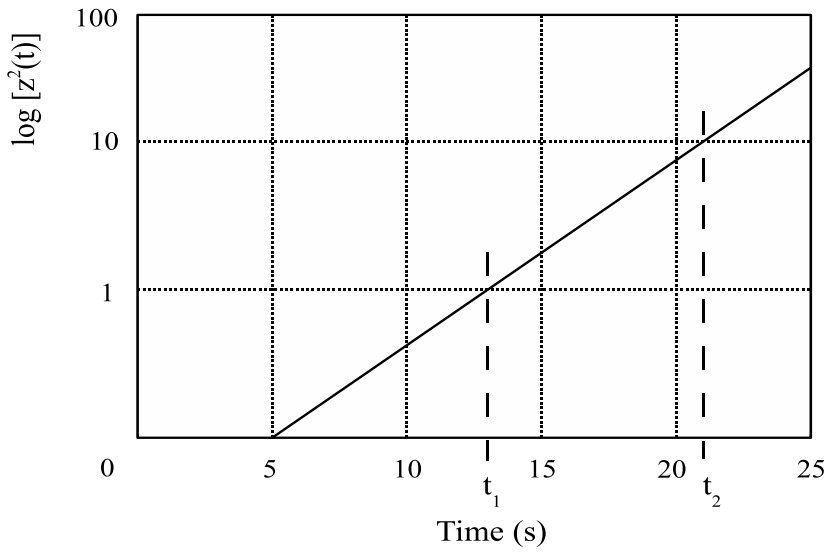

Figure 4.2: Logarithmic decrement technique used to measure the growth rate.

4.2 Growth Rate in the Transient Region

For the 'starting from rest' configuration, Fig.2.4, the transient behavior of the cylinder oscillation has been characterized by measuring the growth rate of the oscillations amplitude.

The growth rate $\delta(\%)$ has been identified in the VIV regime for reduced velocity ranging from ≈ 7 up to ≈ 14. Results are reported in Fig.4.3 where the growth rate is presented (as percentage of the cylinder critical damping) as a function of the reduced velocity. It must be noted that the growth rate values have not been corrected by the damping ratio of the cylinder motion in still fluid. To do so and to express a growth rate due to pure aerodynamics effect one has to subtract the damping ratio value $\eta = 0.0828\%$ from the growth rate data presented in Fig.4.3.

We can observe from Fig.2.3 that the amplitude of the square cylinder increases quasi exponentially. Experimental data presented in Figure 4.3 shows a sharp increase at the beginning of the lock-in, with a maximum slightly below 0.2% for a reduced velocity corresponding to the matching of the oscillations frequency with the vortex shedding frequency ($U_r \approx 1/St \approx 8$). Beyond, the growth rate then decreases in a slightly smoother way. This growth-rate behavior is in line with the frequency

coalescence results discussed earlier, Fig.4.1. Moreover, the same can be highlighted using classical couple mode-flutter analysis between the cylinder dynamics and the wake dynamics as reported in de Langre (2006).

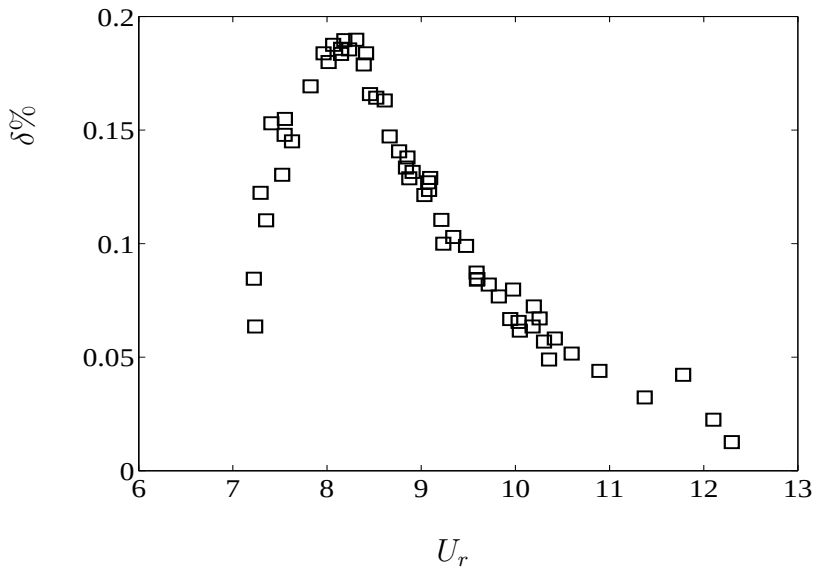

Figure 4.3: Growth rate of the oscillations (percentage of the critical damping) versus reduced velocity.

It is imperative to note here that contrary to the results presented and discussed in Sec.2.2, the maximum growth rate lies closer to the expected (1 / St). Hence, the off-set in the amplitude results cannot be explained by the blockage effect alone. In order to resolve this, we shall propose continuation of the present research work and some investigations of the wake-oscillator model in the following chapters.

4.3 Discussion

As emphasized in Chapter 2, our study finds an over all lack of experimental evidence concerning a square cylinder executing free vortex induced oscillations subjected to an airflow. Such evidence is needed to support the already existing theoretical models, de Langre (2006) for example.

Chapter 5

Transient Behavior of a Bridge Deck

5.1 Introduction

A spring mounted bridge deck section with two degrees of freedom is studied in a wind tunnel, Sec.3.2. The bridge deck profile is restrained such that it can oscillate only along the flexural and torsional degrees of freedom. Since the profile is hinged at its center of gravity there is no inherent structural coupling between the two degrees of freedom. However, coupling appears in the added aerodynamic terms in the expression for linear aerodynamic loading in such cases, Sec.3.1, Eqn.3.7. Also, given the physical structural constraints in the experimental setup, the two degrees of freedom cannot be mutually isolated. A small off-set in any one of the degrees of freedom induces a proportional off-set in the other. This fact has been kept in mind and appropriate algorithms have been implemented for the accquistion and post processing of experimental data to minimize error.

Experimental evidence is provided linking the frequency ratio, the critical velocity and the maximum transient energy amplification of a bridge deck section. The transient growth of energy is found to have significant effects on the behavior of the bridge deck. Energy amplification reaches up to 5 times the initial energy transmitted by the gust at a mean velocity just below the critical flutter velocity.

An Aluminum flap is used to generate the upstream perturbation which triggers the vertical and torsional oscillations in the flexible bridge deck system. This

perturbation is characterized using two component hot wire anemometry. Measurements consist of the time histories of oscillations in the two degrees of freedom using laser displacement sensors. Structural parameters are estimated without airflow. Time evolution of energy of the bridge deck section is measured and amplification is recorded for the deck section, first for a given set of initial conditions and then under the effect of the upstream perturbation.

It is important to keep in mind that the dynamics and aeroelasticity of a bridge deck are different from those of an airfoil. Hence, most of the existing theoretical tools commonly employed to study the airfoil behavior cannot be directly used in such cases.

Transient Growth

Before we discuss our experimental results in detail, it makes sense that we remind ourselves of the phenomenon of transient growth. This phenomenon until now has been a subject of immense scientific investigations in the field of hydrodynamic stability. Its effects in case of fluid structure systems started attracting some attention very recently, Schmid & de Langre (2003). It is already widely known that in case of viscous flows, transition to an unstable state is possible if an initial disturbance grows to activate any non-linear mechanisms in the system under consideration. In this thesis report however, we shall restrict our focus to the transient energy growth essentially in case of fluid structure interaction systems.

Let us start by considering any linear fluid structure system with coupled two degrees of freedom. In the absence of any external excitation the system tends to preserve its equilibrium state. Assuming now that at time t_o the system is excited using an external dynamic variable, incident wind for example. The system achieves an energy state E_o. If the system is stable the energy E_o decays with the passage of time and the system returns to its equilibrium state, Fig.5.1(a). On the other hand in case if the magnitude of the external excitation is beyond the linear stability limit, energy of the system grows exponentially in response ultimately resulting in system failure, Fig.5.1(b). In our experiments using linear models, the stability limit can be accurately known by measuring the critical velocity.

In real life scenarios however, the fluid structure interaction mechanism is not as simple. Speaking strictly of a solid object subjected to an incident airflow, if the

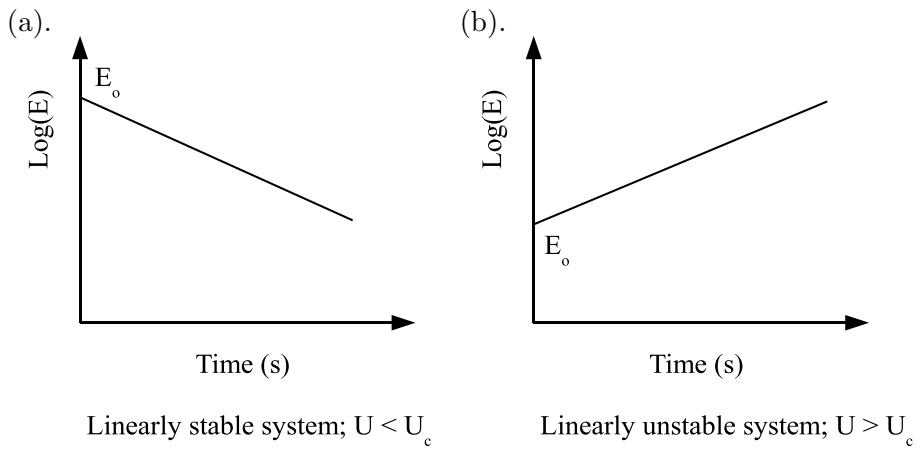

Figure 5.1: Energy evolution with respect to time.

magnitude of the up-stream velocity is closer to the critical system velocity, there exists a possibility that the energy of the system may amplify before it starts decaying in the stable region, Fig.5.2. Given the fact that energy of the system decays, the system remains stable in the long term. At the same time as pointed out earlier, magnitude of this energy amplification can be as high as 10 times the initial energy of the system, Schmid & de Langre (2003). Large amplitude oscillations induced as a result of this energy amplification may trigger non-linear instability even if the system is linearly stable at small amplitudes. Detailed discussion on this shall follow in Sec.6.1.

Mathematically, transient growth may be observed in dynamical systems having a set of non-orthogonal eigen functions. Any initial conditions expressed in terms of these eigen functions may experience short term amplification irrespective of the absence of unstable eigen values, Hémon *et al.* (2006). Schmid & Henningson (2001) have developed detailed mathematical formulations in this regard.

The purpose of the above discussion is to emphasize the existence of transient energy growth in real life fluid structure systems and the impact this may have over the short term system stability. We shall now move on to our experimental results.

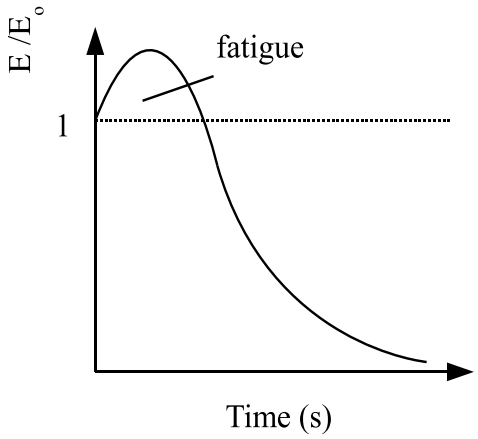

Figure 5.2: Energy evolution of a linearly stable system with respect to time

5.2 Transient Response to Mechanical Excitation

5.2.1 Mechanical Excitation

The mechanical excitation setup is used to induce an initial small value of pitching angle, α_o. A long vertical Aluminum strip is rigidly attached to the end of the bridge deck profile outside the test section. A restraining mechanism is designed using a hinge joint attached to a micrometer screw gauge. The vertical Aluminum bar can be pushed and locked in position using this setup, consequently imparting an initial angle of attack on the bridge deck profile inside the test section. The micrometer screw gauge allows the repeatability of different experimental runs with the same initial condition. Also, it ensures satisfactory accuracy of different initial conditions used, Fig.5.4. As the hinge joint is released, the bridge deck starts to oscillate. The data acquisition software enables automatic measurement and storage of experimental data for a pre-defined time interval. Energy of the bridge deck section is computed at the end of this recording period using Eqn.3.6, Sec.3.1.

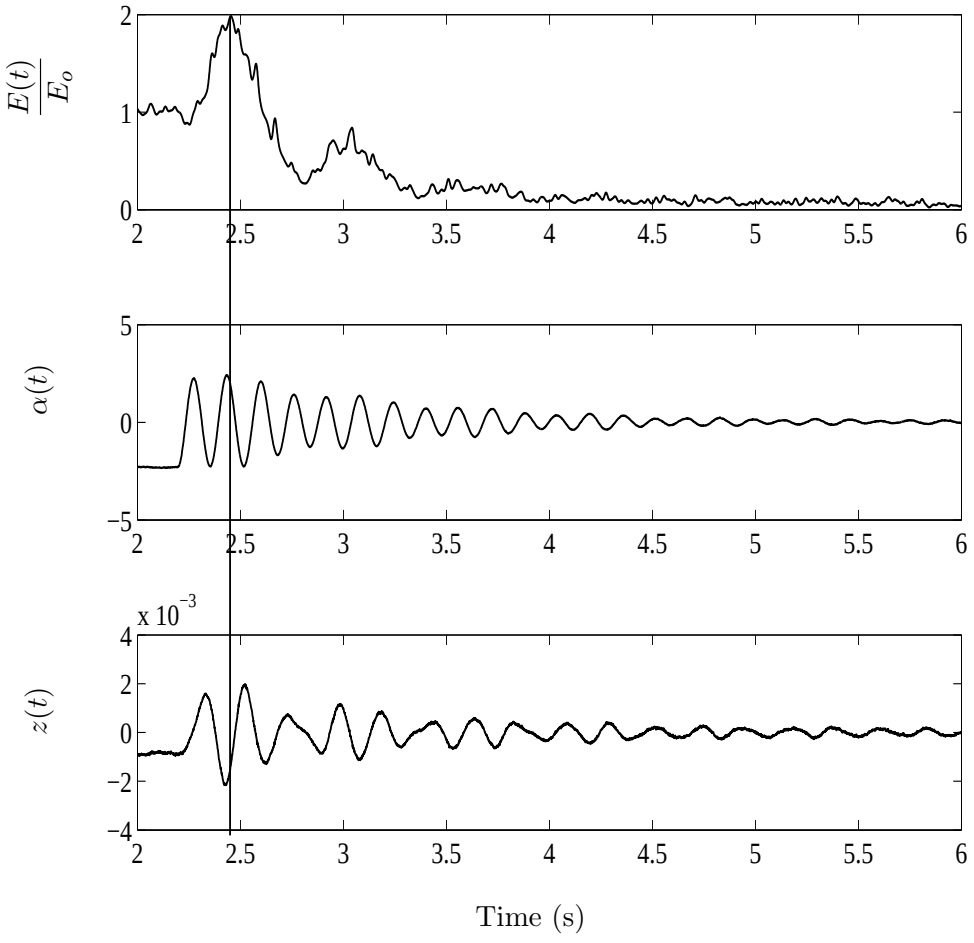

Figure 5.3: Time Evolution of Energy, Angular Displacement and Vertical Displacement of the Bridge Deck Section. Mechanical Excitation. $\overline{U}/U_c = 0.8$, Case 2, [Initial Conditions: $\alpha_o = -2.212^{\circ}$; $z_o = -0.0009191$] (Table 3.3).

The transient response of the bridge deck system due to the initial mechanical excitation can be observed from Fig.5.3. Transient response of the bridge deck sections is depicted as the maximum amplified energy at each value of up stream velocity normalized by a value of initial energy, E_o. In the present case, this value is deduced from the initial condition produced by the imposed initial pitch angle, α_o.

5.2.2 Effect of Excitation Amplitude

The effects of changes in the initial conditions on the maximum energy amplification are presented in Fig.5.4. A slight dispersive effect can be observed as the velocity approaches the critical velocity of the system or as the velocity ratio approaches 1. It can be deduced from Fig.5.4 that initial conditions with greater magnitudes result in a greater energy amplification of the system. Schmid & de Langre (2003) state that amplifying the initial perturbations may introduce non-linear effects. In the present study however, magnitude of the initial mechanical excitation is varied within a very small range i.e. $\approx 0.8^{\circ}$. The system is safely assumed to behave linearly for different initial conditions within this range. Hémon *et al.* (2006) have also studied the effect of initial conditions on the transient amplification of energy but in case of a linear two dimensional airfoil in a wind tunnel. Figures 5.5 & 5.6 show sets of experimental data points obtained from a number of series to validate the reliability of the experimental technique under similar initial conditions between distinct experimental series.

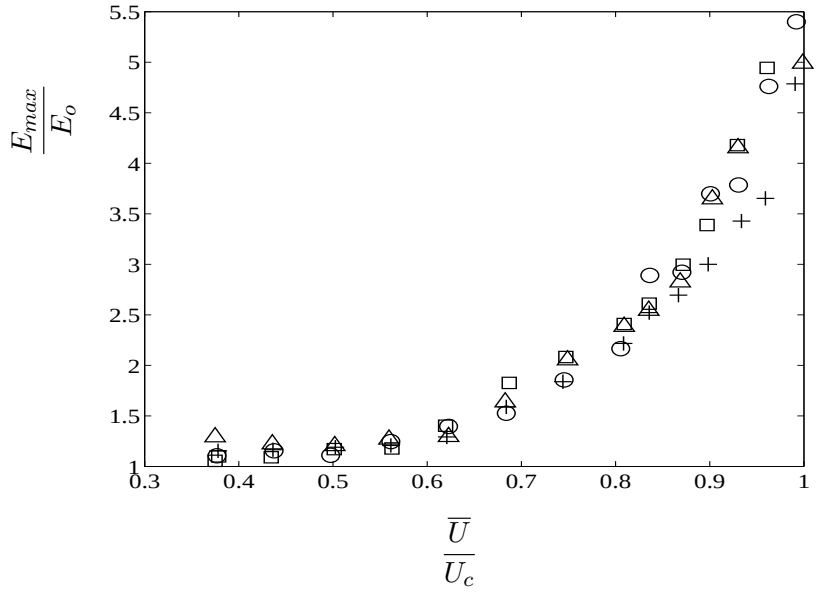

Figure 5.4: Amplification rate of energy versus velocity parameter for Case 2 (Table 3.2); (O) $\alpha_o = -2.6^o$; (❑) $\alpha_o = -2.5^o$; (Δ) $\alpha_o = -1.8^o$; (+) $\alpha_o = -2.1^o$; Mechanical Excitation

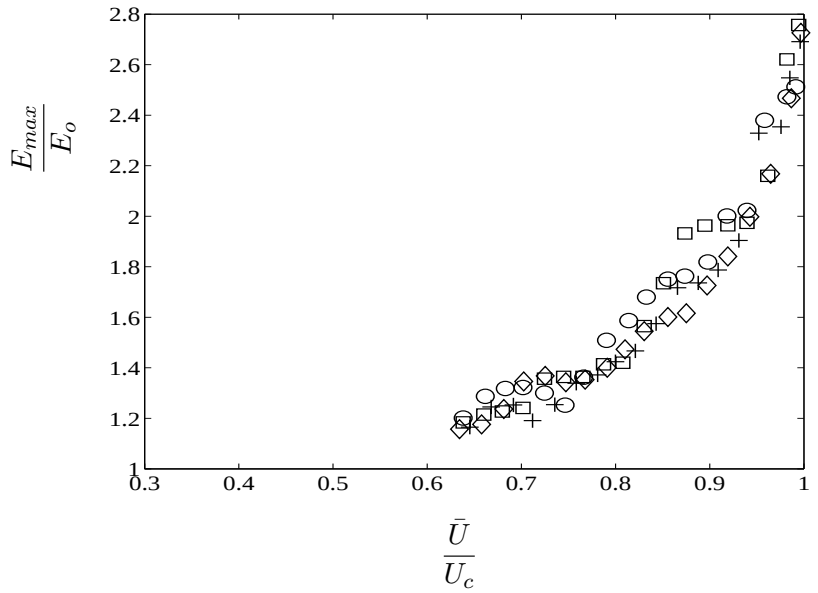

Figure 5.5: Amplification rate of energy versus velocity parameter for Case 1 (Table 3.2); Mechanical Excitation

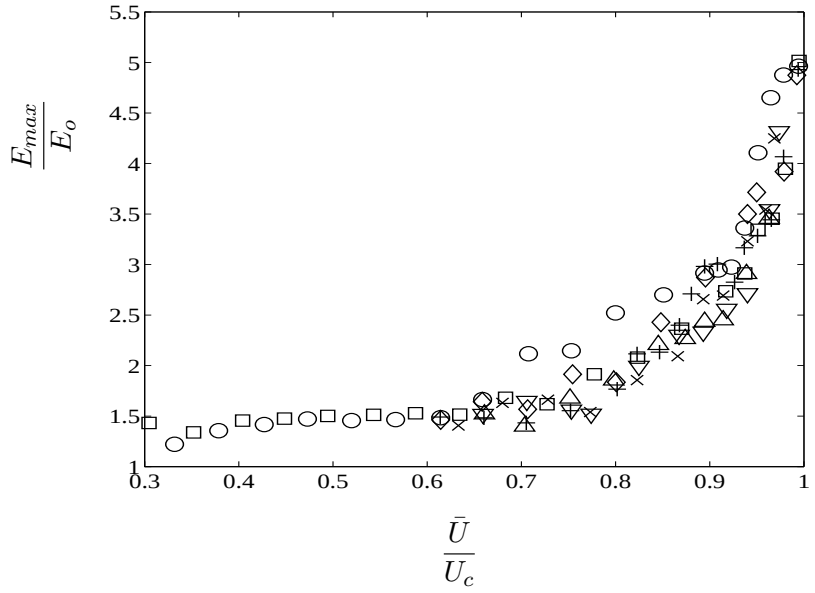

Figure 5.6: Amplification rate of energy versus velocity parameter for Case 3 (Table 3.2); Mechanical Excitation

5.2.3 Effect of Frequency Ratio

The 'frequency ratio' for this experimental study has been defined in Sec.3.4.2. Although the energy evolution curves for all the three cases of frequency ratios exhibit similar behavior however, all the three cases manage to attain three different maximum amplification values. Figure 5.7 shows that as the frequency ratio of the bridge deck section is increased, the maximum attainable energy amplification just below the critical upstream velocity decreases. It must be kept in mind that varying the frequency ratio automatically changes the flutter critical velocity of the bridge deck. Higher energy amplification for lower frequency ratio can be attributed to the corresponding higher dimensional value of the flutter critical velocity, Tab.3.3 & Fig.3.12. At the same time, a simple law like a linear evolution of the maximum energy amplification as a function of the square of the critical flutter velocity could not be established using these experimental results.

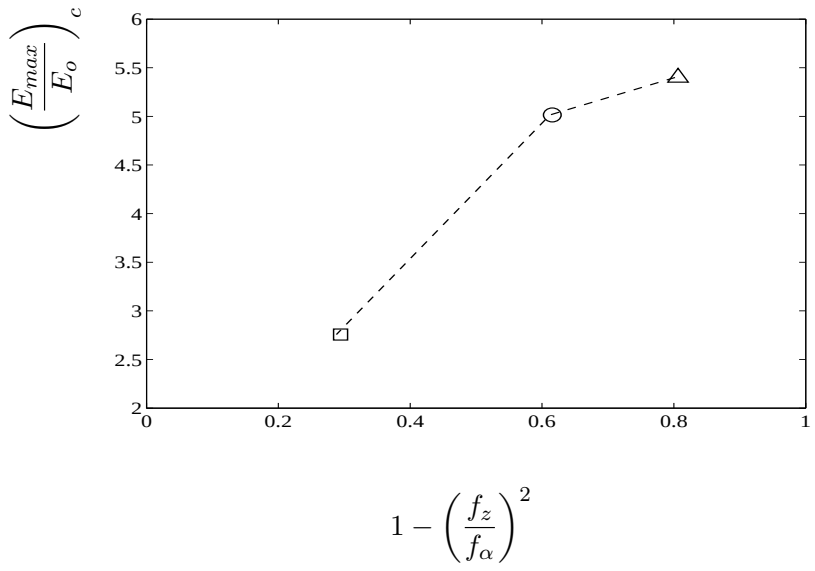

Figure 5.7: Maximum Energy Amplification versus Frequency Ratio. (❑) Case 1; (O) Case 2; (Δ) Case 3; (Table 3.2)

5.3 Gust Generation and Identification

In order to study the transient behavior of the system closer to the physical real world, a gust generating mechanism was incorporated in the experimental set-up.

Since in nature, gusts are not a harmonic entity, the aim was to generate a short singular gust up-stream of the test section and study the system transient behavior under the effect of this gust. An Aluminum flap (170mm x 45mm) was used. The flap is mounted on the floor of the wind tunnel. Initially, the flap remains aligned to the flow direction under the effect of a pre-tensioned spring. A rubber pad at the edge of the flap damps out vibrations due to impact with the wind tunnel floor and prevents the flap from bouncing. An accelerometer is attached to the flap. As the flap is let go by releasing the spring, signal from the accelerometer triggers the transient data accumulation. This approach ensures that the data is accumulated from the same relative time instant in each repetition of the experiment. Abrupt movement of the flap creates a short impulse $(u(t), w(t))$ which is added to the mean free stream flow, $\overline{U}$, Sec.6.4.1.

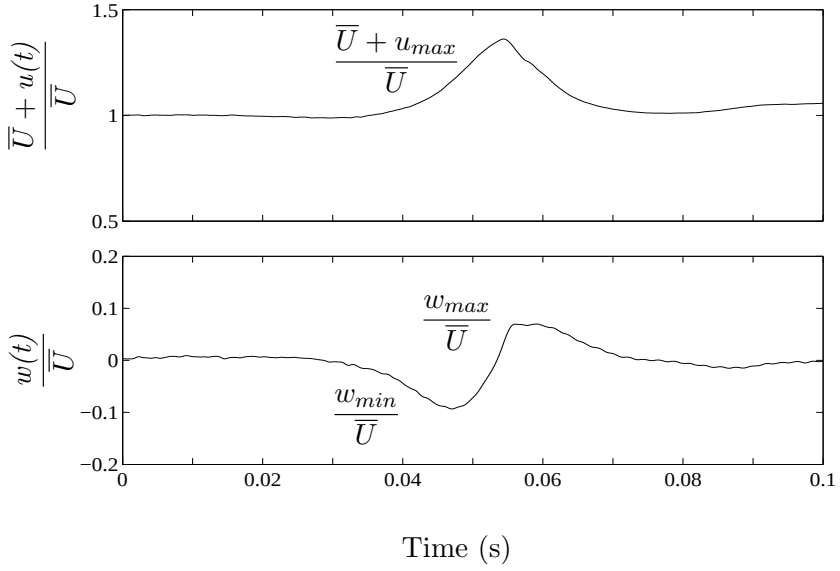

Figure 5.8: Measured Sample of Upstream Velocity Perturbation.

This impulse was calibrated using two component hot wire anemometry in an empty test section at the leading position of the bridge deck. The impulse thus created has a typical duration period of 0.02s which is below the typical period of the two degrees of freedom of the bridge deck set-up. For mean wind velocity greater than $\approx 12m/s$, we note that the gust components remain quasi-constant. It may also be noted that the gust profile generated by this experimental setup agrees to

the gust profile modelling described in Sec.6.4.2 and Sec.6.4.1.

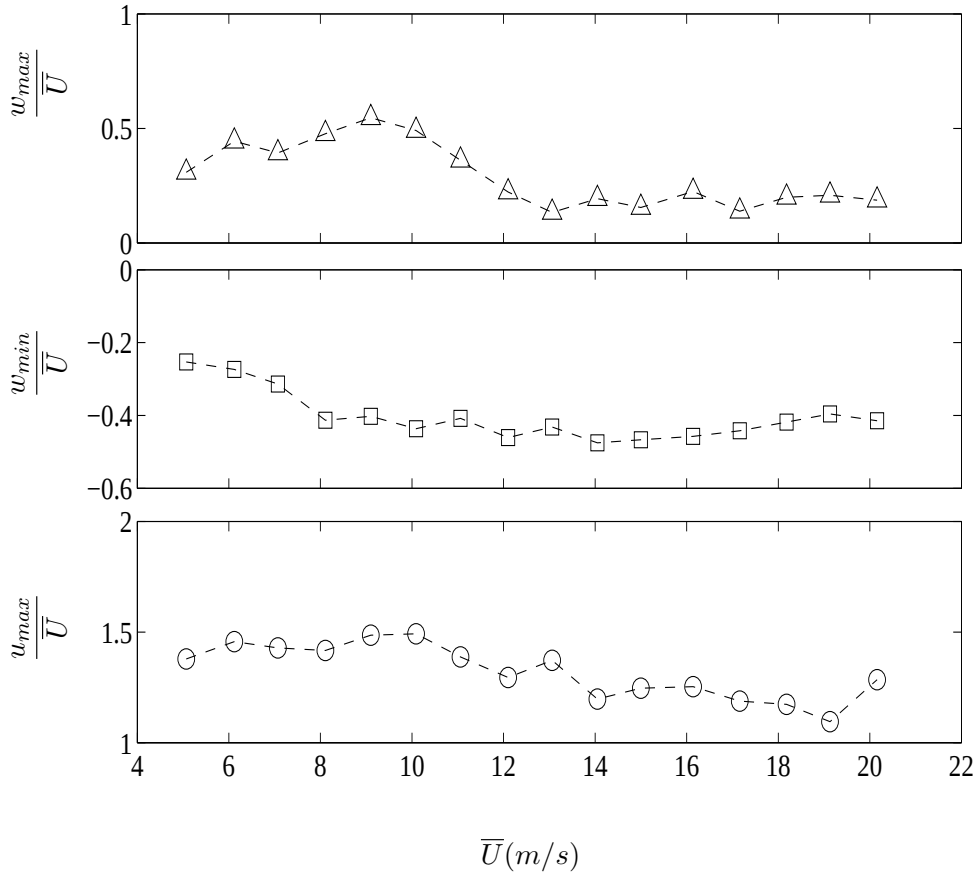

Figure 5.9: Characteristics of the instantaneous upstream velocity perturbation versus mean velocity at the leading edge position.

5.4 Transient Response to Gust Excitation

In the preceding sections we presented our findings from a series of experiments on a bridge deck section in a wind tunnel. The bridge deck system was excited mechanically while the wind velocity remained constant through out the interval of data accumulation. In this section we shall discuss results obtained from a more realistic bridge deck experimental setup involving up-stream gust. This gust impulse sets the system to oscillate upon interaction. We know from Sec.5.3 that the reduced gust components behave quasi-constantly for mean velocity greater than approximately 12m/s. However, out of the three bridge deck models studied, two have their velocity range greater then 12m/s, Tab.3.3. We shall therefore, discuss transient growth results for bridge deck models with velocity range greater than 12m/s.

As obvious in Fig.5.10 there is a clear wedge in the energy curve just before three seconds. Position of the wedge on the energy curve corresponds roughly with the maximum pitch and minimum plunge position of the bridge deck section. Total energy curve of the bridge deck model is normalized using the value at this point consequently setting it to 1.

A closer observation of Fig.5.3 and Fig.5.10 shall reveal that the gust excitation mechanism generates slightly different transient dynamics when compared with mechanical excitation. It can be seen that the maximum energy level for both the cases is achieved for different motion conditions. For mechanical excitation, Fig.5.3, the maximum energy amplification is obtained for almost a mximum pitch and minimum plunge. For the gust excitation however, the maximum energy is obtained with almost a mimimum pitch and maximum plunge.

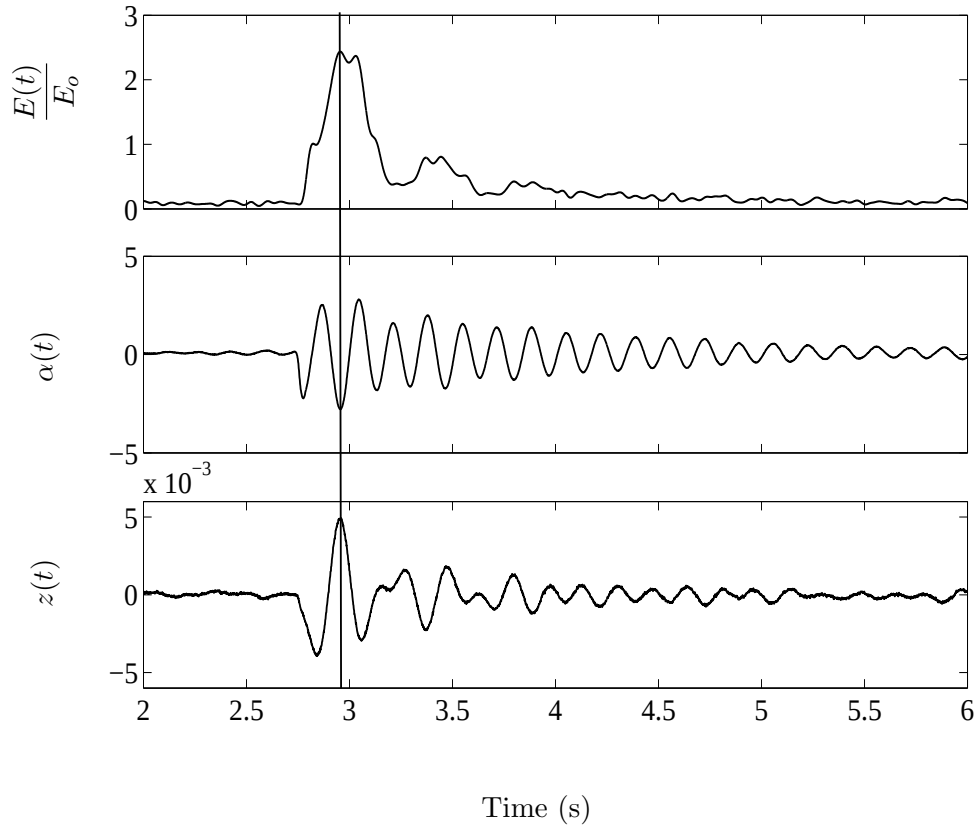

Figure 5.10: Time Evolution of Energy, Angular Displacement and Vertical Displacement of the Bridge Deck Section. Excitation by Flap. $\overline{U}/U_c = 0.91$, Case 3 (Table 3.3).

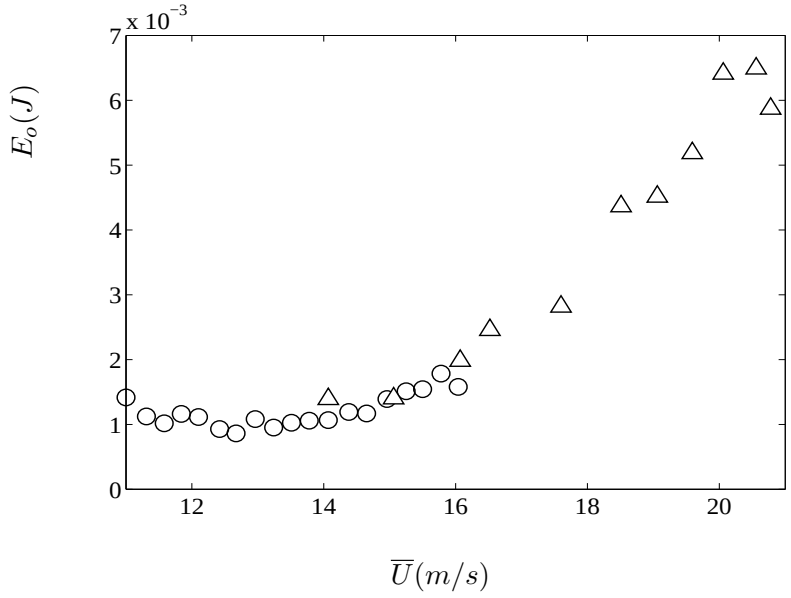

Figure 5.11: Value of Normalization Energy (J) versus Mean Velocity (m/s); (o) Case2; (Δ) Case 3. (Table 3.2); Excitation by flap.

Figure.5.11 depicts the dimensional values of normalization energy, E_o(J) plotted against the dimensional mean velocity, $\overline{U}$(m/s). We can observe that despite the distinct structural parameters of the two cases, values of E_o(J) collapse perfectly for the overlapping operational velocity range i.e. between ≈14m/s and ≈16m/s. This result reinforces the fact that the values of E_o(J) chosen for this set of experiments are representative of the gust effect at the bridge deck leading edge. Moreover, this value of initial energy E_o(J) follows an evolution as the square of the mean wind velocity.

Figure 5.12 shows the energy amplification behavior of two deck section systems subjected to an upstream gust. Gust monitoring through out the experiments was carried out as described in Sec.5.3. We see that the transient growth mechanism amplifies the initial energy of the system by a factor greater than five just below the linear stability limit. The experimental data points in this case show a considerably lesser cohesion when compared to the previous experiments conducted using fixed mechanical excitations. Still, the maximum energy amplification observed in this case is approximately of the same order as observed previously in case of mechanical excitations. This case is however closer to the real world scenario. Though the

experimental points are easily distinguishable, they follow approximately the same trend as we move along the horizontal axis.

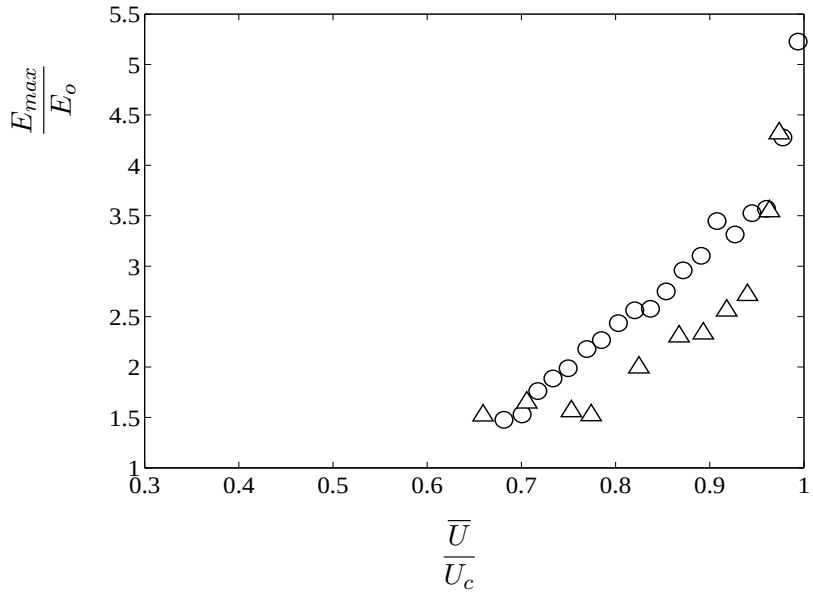

Figure 5.12: Amplification rate of energy versus velocity ratio; (O) Case2; (Δ) Case 3. (Table 1); Excitation by flap.

5.5 Discussion

This experimental study high lights the fact that suspended bridged decks exposed to turbulent wind conditions are prone to short term instabilities which may arise due to the transient energy growth in the system. Some authors have lately addressed the more general case of transient growth in fluid structure systems. Experimental results from this study including maximum energy amplification by transient growth follow previous theoretical results. We shall discuss some future aspects of the study in Sec.7.2.

Chapter 6

Transient Behavior of a Non-Linear Airfoil

6.1 Introduction

As the chapter name suggests, two degree of freedom coupled mode flutter of a symmetric airfoil is studied in a horizontal wind tunnel. A single upstream gust is used as the source of excitation for the airfoil. In addition to the experimental setup described in Sec.3.2 the model is modified to introduce a weak non-linearity in the system stiffness, Sec.6.2.1. Experiments are repeated for both the linear and non-linear airfoil models and the results are compared to show that the initial energy in such non-linear systems may get amplified to the un-stable range by the transient growth even below the linear stability limit of the dynamic system parameters. Various existing theoretical tools have been explored and a comparison is developed with a simple model validating the experimental results.

Non-Linear Systems and By-Pass Transition

In a linear case, transient growth may lead to an initial amplification of energy which would subsequently decrease as long as the system is under sub-critical conditions. Hémon *et al.* (2006) have shown that initial amplification of energy in such cases is strongly dependent on initial conditions. In a non-linear case on the other hand, if $U_{cnl} < \overline{U} < U_c$; where U_{cnl} is the non-linear critical mean free stream velocity and U_c is the linear critical mean free stream velocity; the resultant amplitude becomes very important, Fig.6.1. A small initial perturbation may not trigger an instability but a sufficiently large excitation may push the system in the un-stable

region even below the linear critical velocity.

In a non-linear case, i.e. when the airfoil support elasticity behaves non-linearly, the amplitude of the perturbation is an important parameter due to the sub-critical branch as illustrated in Figure 6.1(b), when the mean velocity is larger than the non-linear critical velocity U_{cnl} and below the linear critical velocity U_c. An initial small perturbation keeps the system in the stable region but for a larger initial perturbation, the system state may reach the unstable region, leading to flutter even below U_c. This scenario is called by-pass transition to flutter by amplitude effect.

Another possibility is the scenario when the transient growth results in the linear amplification of an initially small perturbation because the mean velocity is just below the linear critical velocity. As illustrated in Figure 6.1(c), two possibilities can exist. The transient amplification remains small and keeps the system stable, referred to as type B in Figure 6.1(c) or the transient amplification is such that the system response then reaches the sub critical branch, flutter instability is triggered (referred to as type C).

The latter is also a by-pass transition to flutter, but caused by transient growth of a small initial perturbation, the level of which would have lead to stability without this amplification. It is therefore different from a classic by-pass transition where the initial amplitude alone triggers the flutter instability. A similar mechanism is a possible scenario in the domain of transition to turbulence, Schmid & Henningson (2001).

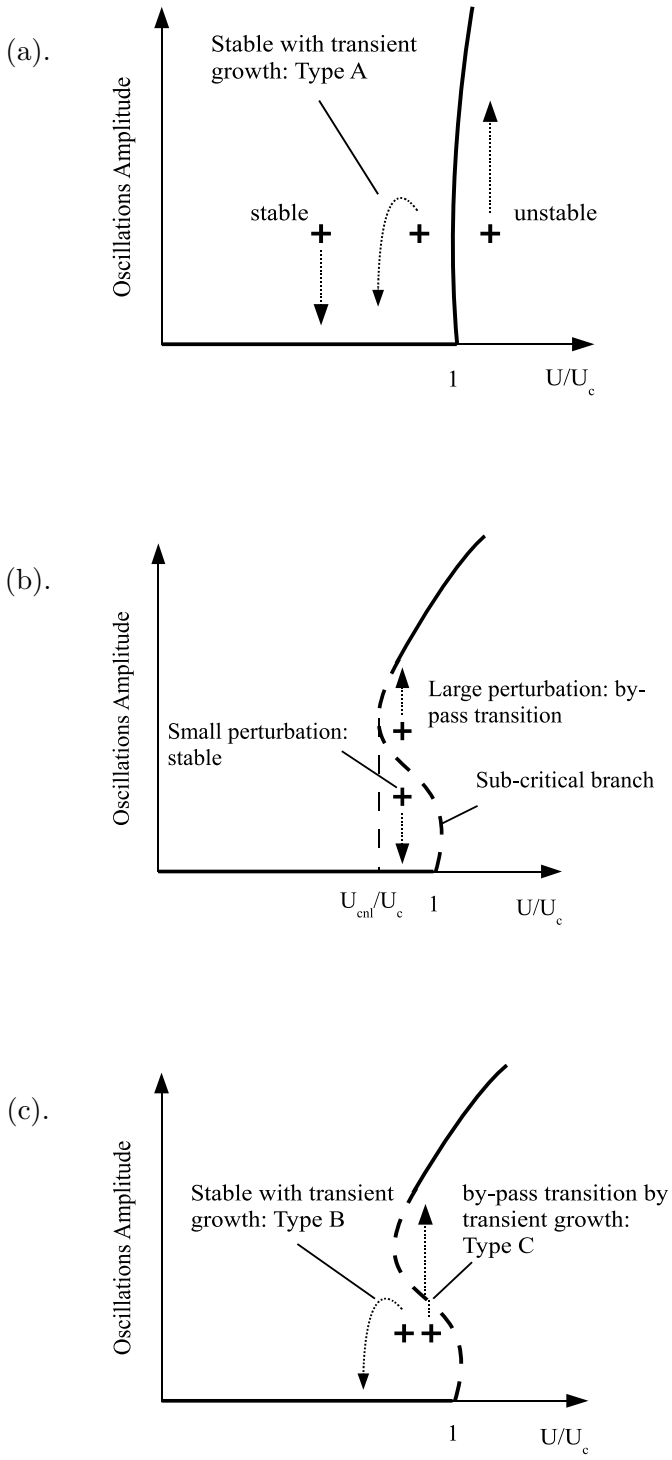

Figure 6.1: (a). Effects of an initial perturbation for a linear system; (b). Perturbation amplitude effect for a non-linear system; (c). Scenario of by-pass transition due to transient growth of an initial perturbation, Schwartz *et al.* (2009).

6.2 Experimental Techniques

6.2.1 Non-Linear Airfoil Setup

The non-linearity is located on the stiffness of the flexion due to the contact springs. Two parameters are needed, the gap 'g' between the position zero and the contact, and the resulting stiffness $k_{nl} = k_z + \delta k$ above this gap. In fact the non-linear system can be seen as a bi-linear system and the contact springs stiffness was chosen small enough so that the non-linearity is relatively small. The calibration

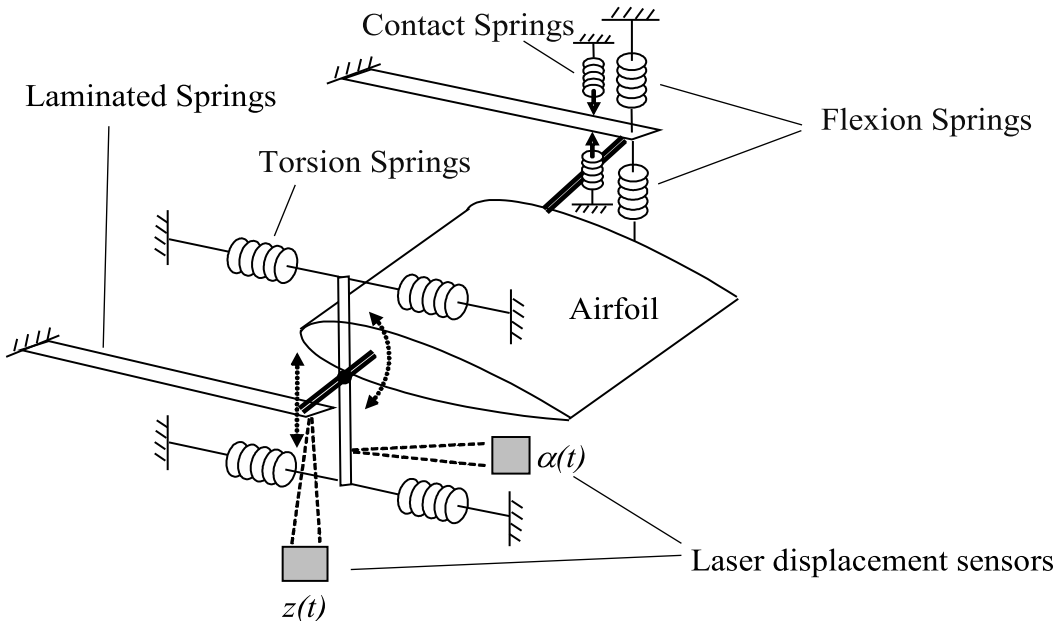

Figure 6.2: Kinematics of the flexible airfoil Schwartz *et al.* (2009).

is performed statically. This leads to a gap value g = 0.655 mm and an additional stiffness $\delta k = 0.136kz$. The non-linear feature of the flexural stiffness leads to an additional term on the energy that reads:

$$E_{nl}(t) = \frac{\delta k}{4}\left(\left(|z-g| + (z-g)\right)^2 + \left(|z+g| - (z+g)\right)^2\right) \tag{6.1}$$

This quantity is added to the energy, Eqn.3.5, when measurements are performed with the non-linear system.

6.2.2 Gust Generation and Identification

It is important to note here that the wind tunnel apparatus used in these experiments is different from the one used for bridge deck experiments, Chapter.5. The wind tunnel test section has been changed resulting in a corresponding new flap mechanism. We therefore discuss the results of the gust identification procedure for the sake of clarity and scientific consistency. Like the previous experimental setup an Aluminum flap is mounted on the test section floor 160mm up-stream of the airfoil. Two component hot wire anemometry is used to characterize the impulse, Sec.5.3. Horizontal component *u(t)* of the impulse comprises of a unique positive peak. The vertical component however, has a negative peak followed by a simultaneous positive peak. An example of the time evolution of both the orthogonal components is shown in Fig.6.3. It may be noted that the gust profile generated by this experimental setup agrees to the gust profile modelling described in Sec.6.4.1 and Sec.6.4.2.

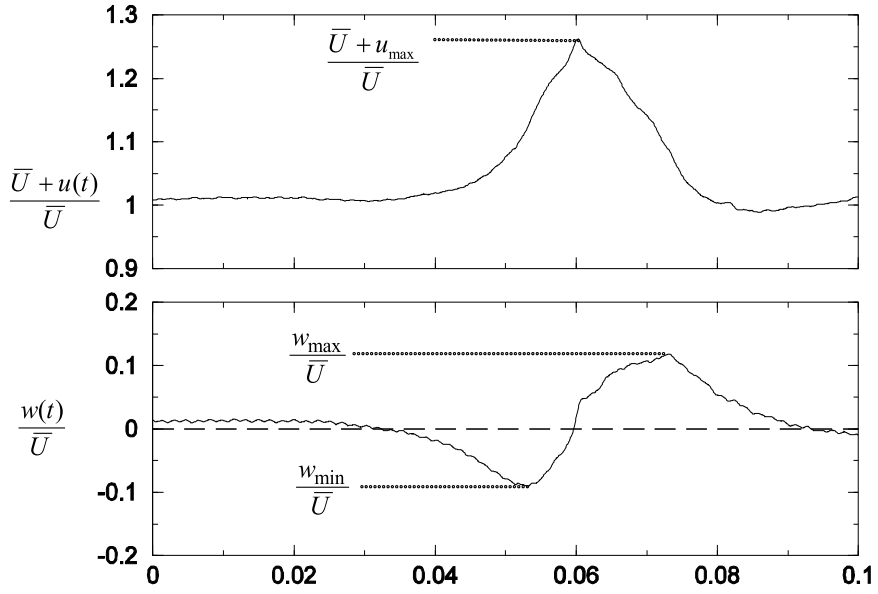

Figure 6.3: Gust Profile, Schwartz *et al.* (2009).

Effects of any changes in the mean velocity $\overline{U}$, on the behavior of the two component velocities are also investigated in Fig.6.4. These characteristic parameters of the upstream perturbation have been measured in the empty test section at the

position of the airfoil leading edge. The impulse thus created has a typical duration period of 0.05s which is below the typical period of the two degrees of freedom of the airfoil set-up. A comparison of the accelerometer and the hot wire signals gives us the time taken by the gust impulse to reach the leading edge of the airfoil. If the mean free stream velocity, $\overline{U}$ is maintained at 17m/s, the impulse takes 0.08s to reach the leading edge of the airfoil. This time interval decreases as the wind velocity increases in the test section. The gust parameters have been normalized with respect to the mean wind velocity in the test section.

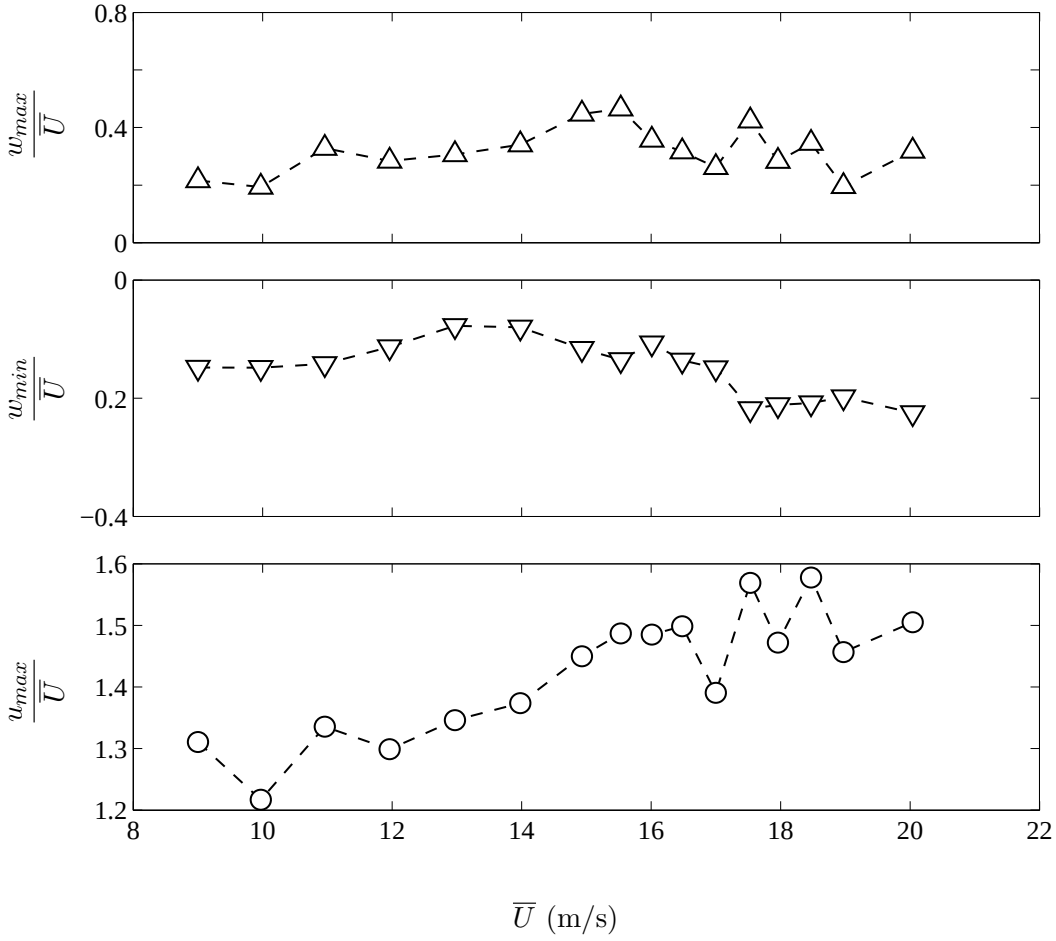

Figure 6.4: Instantaneous up-stream gust versus mean velocity at the leading edge position, Schwartz *et al.* (2009).

6.3 By-Pass Transition due to Transient Growth

The experimental results are mainly presented by comparing the behavior of the linear system, type A and behaviours of the non linear system, type B or C, Fig.6.1.

The first measured quantities are the periods of the system and their evolution versus the wind velocity as presented in Figure 6.5 in terms of frequencies. The linear critical velocity U_c has been previously estimated by experiments, Sec.3.3.2. In the non-linear system, the period depends on the amplitude of the motion. For the period measurements, plunge amplitude was then initiated manually during the recording so that the contact springs were always engaged. Since the gap 'g' is small, the amplitude necessary to reach contact remains small, of the order of 1mm. As the system is in fact weakly non-linear, the resulting period can be considered as a mean value between a linear system having a stiffness k_z and another linear system having a stiffness $k_{nl} = k_z + \delta k$, with less than 14% between them. This effect can be observed at $\overline{U} = 0$ where the non-linear system plunge frequency is just above that of the linear system (5.0625 Hz against 4.9375 Hz).

In the linear system at the onset of flutter the two frequencies coalesce. In the non-linear case, the coalescence of the two frequencies occurs at a velocity U_{cnl} which is lower than in linear case. For a velocity above U_{cnl} and below U_c a by-pass transition to flutter is therefore possible.

All data for the transient growth of energy is collected and finally presented in Figure 6.6, for the linear case, type A, and the non-linear cases, types B and C. The region covered by the unstable behavior of type C is shown with hachure. When the system is unstable the motion amplitude grows rapidly and it is stopped manually as the setup is not designed for high amplitude limit cycle oscillations.

Just below critical velocity with the linear system, the type A presents an amplification level that is 9 times the value of initial energy. With the non-linear system, the behavior follows the evolution of the linear system for low velocity. Then, approaching the value U_{cnl}, the energy growth rate is higher than in linear case and finally transition to flutter occurs, after an amplification larger than 7.

The comparison between linear and non-linear behavior is essential for the confirmation of the by-pass transition due to transient growth, because this is not a simple

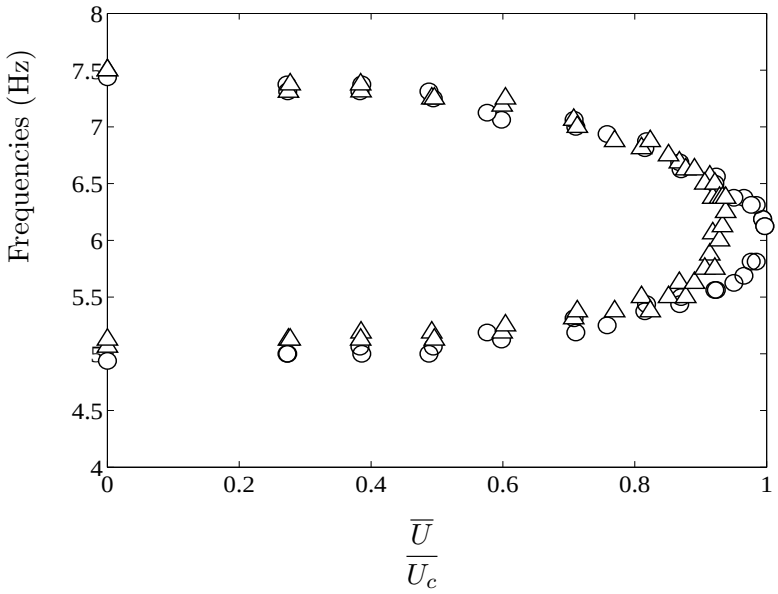

Figure 6.5: Frequencies of the 2 modes versus velocity parameter; (o) linear case; (Δ) non-linear case. Schwartz *et al.* (2009).

by-pass transition by initial amplitude effect. The initial perturbation produced by the flap generates a value of the energy which remains below the level of the energy for which the non-linear behavior occurs, i.e. the plunge 'z' remains below the value of 'g' at the initial instant.

This is shown in Figure 6.7 where we present time histories of the total energy in a linear case of type A and a non-linear unstable case of type C. Wind velocity is just below the linear critical velocity: the system is stable for the linear case, and by-pass transition to flutter occurs for the non-linear case. Before the perturbation is introduced, the background energy level is of the order $10^{-5}J$, a level where the linear system returns to the stable condition. The initial perturbation of level E_o is amplified by transient growth up to E_{max} for the linear case, while it triggers flutter in non-linear case. In the latter, the boundary of the non-linear behavior was determined statically. This energy level corresponds to the potential energy of the system when the displacement 'z(t)' reaches the value of 'g'. Beyond this gap, the contact springs are engaged and contribute to the stiffness of the airfoil, the system behaves non-linearly.

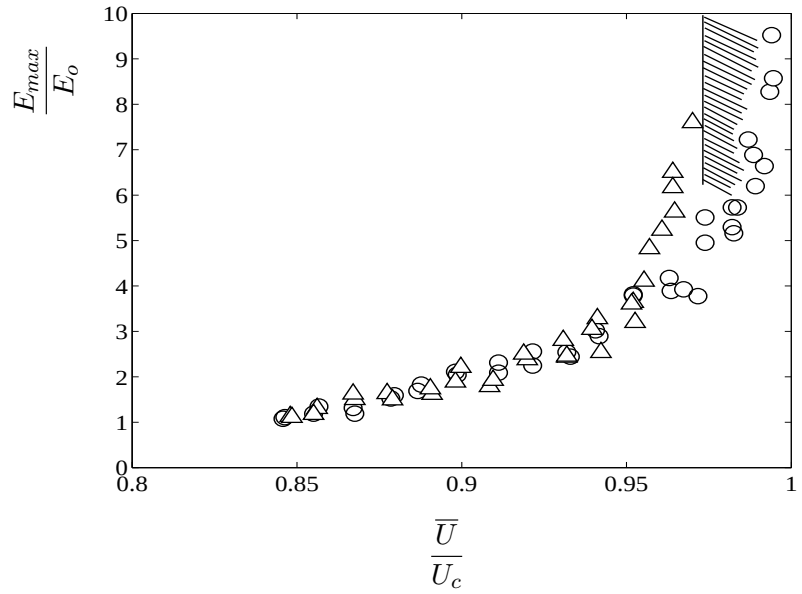

Figure 6.6: Amplification rate of energy versus velocity parameter; (o) linear, type A; (Δ) non-linear, type B; (hachure) non-linear, type C with by-pass transition caused by transient growth. Schwartz *et al.* (2009).

Figure 6.7 shows that the initial energy generated by the flap is well below the non-linear boundary, and that the transient growth is in fact responsible for transition to flutter.

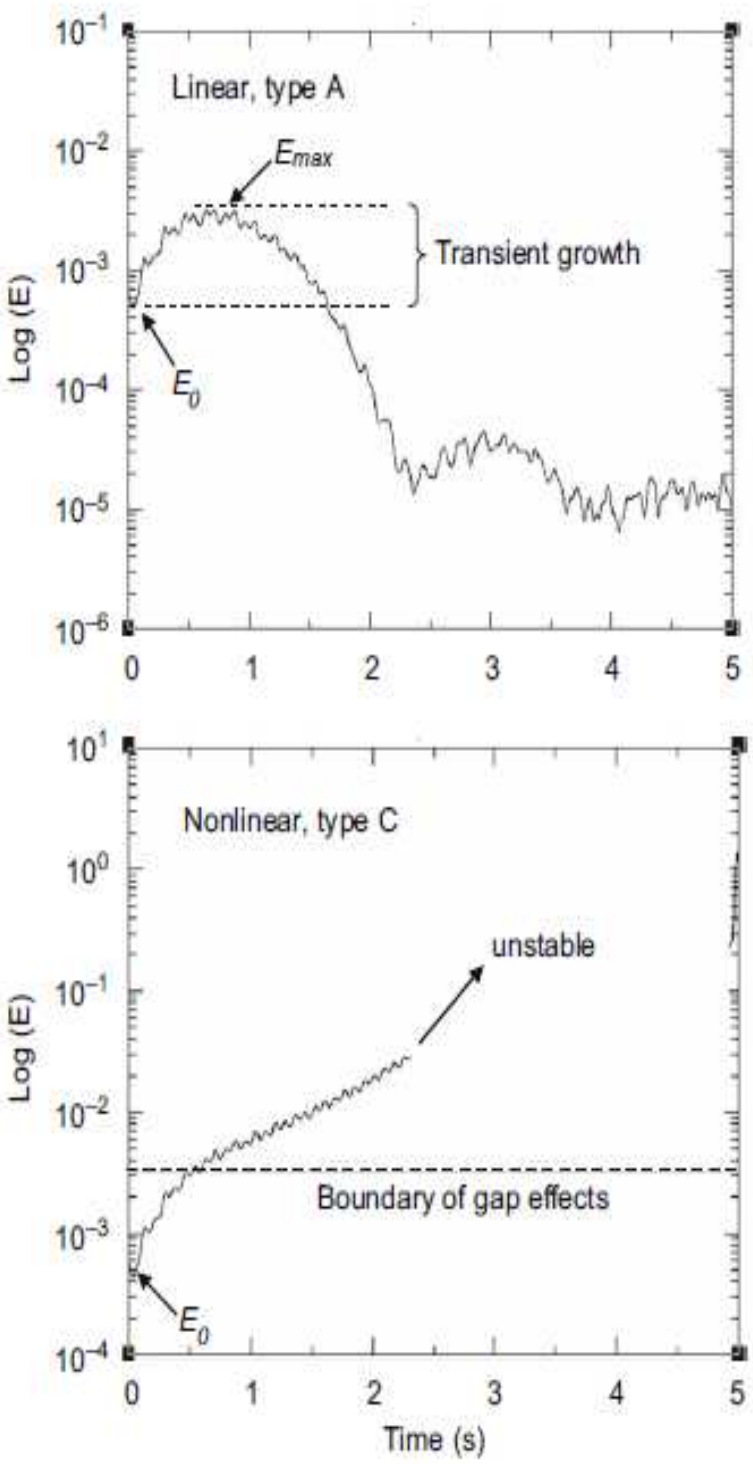

Figure 6.7: Energy time histories in linear and non-linear cases at $\frac{\overline{U}}{U_c} = 0.99$, Reproduced from Schwartz *et al.* (2009).

6.4 Theoretical Modeling

6.4.1 Gust Modeling

The atmospheric turbulence models can generally be categorized within two different approaches. The methods associated with a discrete gust representation are generally deterministic in nature. On the other hand, continuous turbulence models allow for a stochastic perspective. Hybrid methods also exist and are used in some cases such as the statistical discrete gust, Poirel & Price (1997).

Taylor and Von Karman pioneered the theory of isotropic stochastic turbulence. Isotropic implies that the properties of air are independent of the orientation at any point in space. The atmosphere is usually assumed to be homogeneous. Following Poirel & Price (1997), we assume that by superimposing a mean free stream velocity $\overline{U}$ on a fluctuation field, *(u, v, w)*, we can neglect the temporal gradients of turbulent velocity fluctuations for a coordinate system attached to the mean velocity $(\overline{x}, \overline{y}, \overline{z}, t)$. This is known as the *Taylor's Hypothesis* or *The Frozen Gust Assumption*. Now, since the temporal gradients are neglected, a transformation from a spatial to a time system of coordinates is permissible. For example the longitudinal component with a mean free stream velocity along the x-axis gives:

$$u\left(\overline{x}, \overline{y}, \overline{z}, t\right) = u\left(\overline{x}, \overline{y}, \overline{z}\right) = u\left(x - \overline{U}t, y, z\right) \tag{6.2}$$

where *x, y* and *z* form the body fixed system of coordinates. Hence at any fixed point on the airfoil, the longitudinal gust is considered as a function of time only.

In two dimensional flows, we consider only the vertical and longitudinal components of atmospheric turbulence velocity field. The vertical component acts as an external forcing function. On the contrary, the longitudinal turbulent field excitation also known as *Head on Turbulence*, is parametric as it acts on the airspeed. Furthermore, the gust is assumed to interact with the airfoil in a uniform fashion in the span wise direction to eliminate the three dimensional complexities from the model. Any irregularities along the vertical axis are also neglected.

The vertical and the horizontal components in this case were defined using the standard Gaussian Distribution Functions. The horizontal component is a symmetric gauss distribution function:

$$u = a * exp\left[-\left(\frac{x-b}{c}\right)^2\right] \tag{6.3}$$

where 'a' is the amplitude, 'b' is the centroid location and 'c' is the full duration at half maximum (FDHM). For the vertical component we simply add two symmetric Gaussian Distribution Functions:

$$w = -a_o * exp\left[-\left(\frac{x-b_o}{c_o}\right)^2\right] + a_1 * exp\left[-\left(\frac{x-b_1}{c_1}\right)^2\right] \tag{6.4}$$

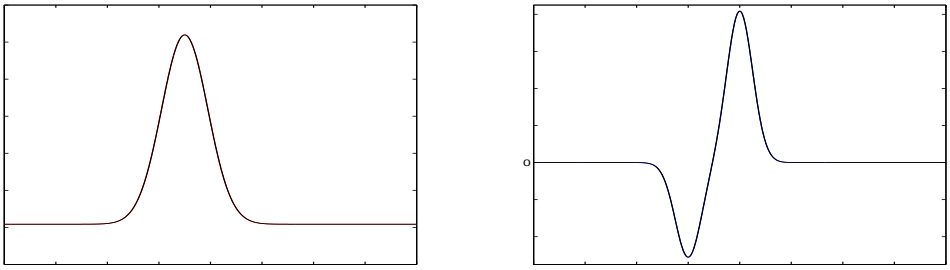

Horizontal Component Vertical Component

Figure 6.8: Upstream Gust Components Modeled using Gauss Distribution Function.

6.4.2 Unsteady Airfoil Theories

An airfoil subjected to an un-steady, in-compressible fluid resultantly experiences un-steady aerodynamic forces which constitute a very important design feature in case of structures exposed to incident wind. These un-steady aerodynamic excitations or loadings due to gust effects have been investigated by Wagner (1925), Kussner (1936), Sears (1941) and many other researchers of this field. A gust is usually ascribed as a non-uniformity in the ambient flow which is otherwise assumed to be isotropic, Sec.6.4.1. Such non-uniformities in the ambient flow are assumed to comprise of small disturbances superimposed on a uniform steady flow. An important theoretical tool to model gust loading are the aerodynamic admittance functions. [1] Fung (1993) has cataloged work by Wagner, Sears and Kussner in sufficient detail.

1. Aerodynamic admittance is the response of a system subject to un-steady excitation normalized with the load under steady state flow conditions, Filippone & Siquier (2003).

Response of an airfoil subjected to an upstream gust is studied under the assumptions outlined in Fung (1993).

Wagner's function enjoys fundamental significance in the Unsteady Airfoil Theories. The function models circulation growth or lift about an airfoil starting from rest and reaching a certain uniform velocity with a small angle of attack. The situation can be accurately modelled using a single step function, Fig.6.9. The circulation growth is assumed to be uniform over the airfoil as it traverses through a two dimensional in-compressible fluid. Wagner formulized the circulatory lift as Eqn.6.5:

$$L(\tau) = -2\pi\rho bUw\Phi(\tau) \quad where \quad \Phi(\tau) = \mathcal{L}^{-1}\left(\frac{C(-is)}{s}\right) \tag{6.5}$$

$\Phi(\tau)$ is the Wagner's aerodynamic indicial admittance function. Details of the modelling procedure for Eqn.6.5 can be consulted in Fung (1993). W. P. Jones formulated an approximate expression for a two dimensional airfoil. We use the same expression, Eqn.6.6 to plot the Wagner's function in Fig.6.9.

$$\Phi(\tau) = 1 - 0.165e^{-0.041\tau} - 0.335e^{-0.32\tau} \tag{6.6}$$

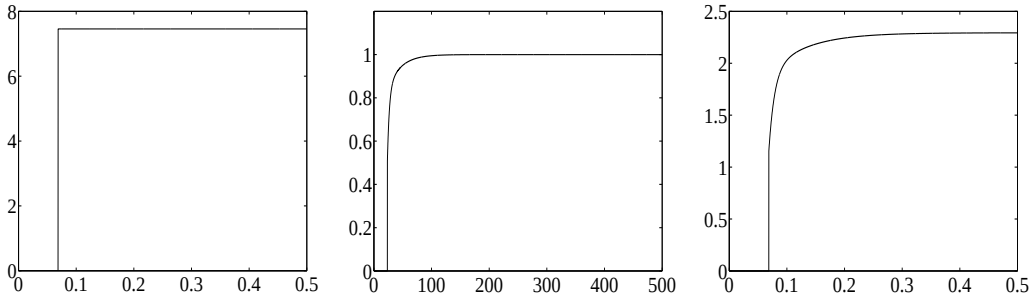

$w\ (t)$ $\Phi(\tau)$ $\dfrac{F'(t)}{\frac{1}{2}\rho U^2 bc}$

Figure 6.9: Wagner's Single Step Behavior.

It is imperative to note that the vertical gust component *w(t)* is plotted as function of time, the Wagner's function $\Phi(\tau)$ is plotted as a function of non-dimensional time τ and the normalized fluctuating lift component $F'(t)$ is plotted as a function

of time.

We know that gust loading pattern of the simpliest airfoil cannot actually be modelled by the single step velocity profile in Fig.6.9. However, the significance of this simple model for theoretical purposes cannot be over stated. A slightly more accurate representation of a free stream gust is presented in Fig.6.10. We use a sequence of step functions to model a velocity profile with a negative peak and a subsequent positive peak. Such a gust profile is closer to real life scenario. Wagner's function approximation by W. P. Jones, Eqn.6.6 is used to obtain the fluctuating lift component in Fig.6.10.

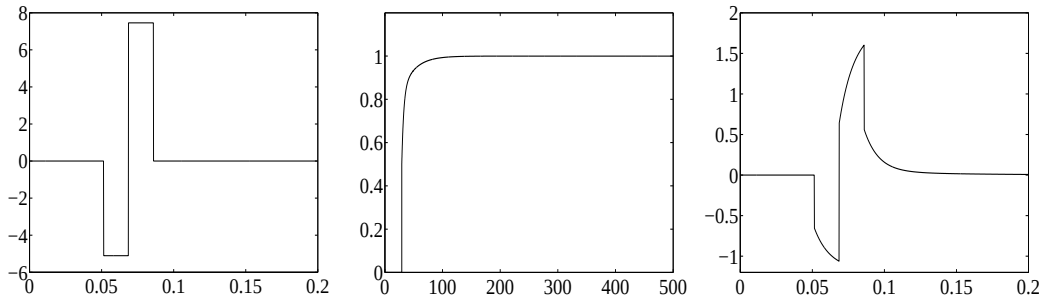

$w\ (t)$ $\Phi(\tau)$ $\dfrac{F'(t)}{\frac{1}{2}\rho U^2 bc}$

Figure 6.10: Wagner's Multi-Step Function Behavior.

Sears (1941) calculated the lift and moment of a rigid airfoil subjected to a gust with sinusoidal intensity distribution. He modeled lift as a function of reduced frequency which in turn depends on the ratio of airfoil chord and gust wavelength. For such a case, the total lift acts at the quarter chord point of the airfoil at all times. Sears expressions for lift and moment appear in Eqn.6.7:

$$L = \pi\rho cUWe^{iwt}S(k) \quad ; \quad M = L\frac{c}{4} \tag{6.7}$$

where $S(k) = [J_0(k) - iJ_1(k)]\,C(k) + iJ_1(k)$ is Sears Admittance Function based on C(k), the Theodoresen Circulation Function, Sec.3.1. Substituting the expression for Theodoresen's Function and simplifying we have:

$$|S(k)|^2 = \left(J_0^2 + J_1^2\right)\left(F^2 + G^2\right) + J_1^2 + 2J_0J_1G - 2J_1^2F \tag{6.8}$$

Sinusoidal gust form, typical sears function profile for our case and the resultant fluctuating lift component are plotted in Fig.6.11. Since, by definition, the Sears function is a function of reduced frequency, Eqn.6.8, it remains constant for this case.

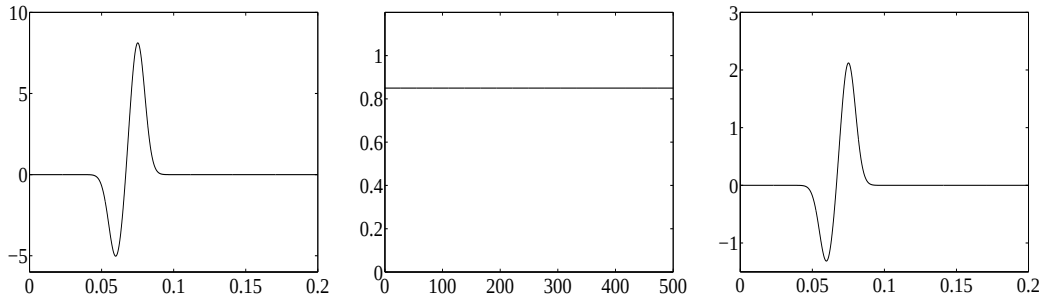

$w\ (t)$ $S(\tau)$ $\dfrac{F'(t)}{\frac{1}{2}\rho U^2 bc}$

Figure 6.11: Sears Function.

Kussner derived an admittance function which provides lift on an airfoil as it penetrates into a sudden vertical gust. Lift induced by a variable gust can be expressed as a Duhamel integral, Fung (1993):

$$L(\tau) = \frac{1}{2}\rho bcU^2 C_z' \int_0^\tau \frac{w(\sigma)}{U}\Psi'(\tau - \sigma)d\sigma \tag{6.9}$$

where Ψ is the Kussner's admittance function. R. T. Jones provided an approximate expression for two dimensional elliptic airfoils, Eqn.6.10, Fung (1993):

$$\Psi(\tau) = 1 - 0.5e^{-0.13\tau} - 0.5e^{-\tau} \tag{6.10}$$

The fluctuating lift force component exerted by the gust is now computed numerically using the Duhamel integral in Eqn.6.9.

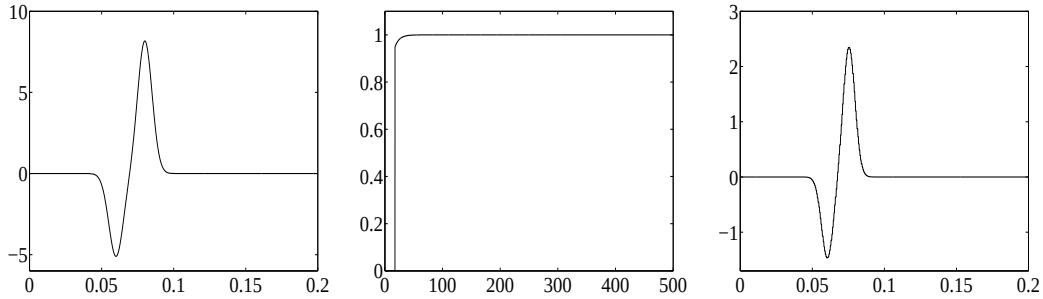

Figure 6.12: Kussner's Airfoil Theory.

Fig.6.12 exhibits the vertical component of the up-stream gust as a function of time, the Kussner function varying with respect to the non-dimensional time, τ and the normalized fluctuating component of lift force exerted by the gust.

In this section, we have catalogued all the theoretical tools used in common practise to understand the aerodynamic behavior of an airfoil subjected to an upstream gust. Without going into the complicated mathematical details we can see from Sec.6.2.2 and Sec.6.4.1 that the admittance functions proposed by Wagner and Sears cannot be used in this study. Firstly, because although Wagner's step assumption simplifies the problem to a large extent, yet a step function profile cannot be used to model a gust as observed in these experiments. Moreover, Sears' admittance formulation is based on the assumption that the gust behaves sinusoidally. This is also not the case in our experiments. Infact the experimental setup has been designed essentially to create only a single gust, Sec.5.3. A rubber padding was used on the flap so that it can be prevented from bouncing which would have created a somewhat continuous gust form otherwise. Kussner's admittance formula on the other hand is developed for the case of an airfoil penetrating a sudden gust which is about the case in our experiments.

It is for the reasons described above that the linear aerodynamic load model, Eqn.6.15 in Sec.6.4.1 depicts only the Kussner's aerodynamic admittance function. Moreover, results described in Sec.6.5 depict a theoretical curve obtained by plotting

Eqn.6.15. The Kussner's admittance function was incorporated following Eqn.6.9 and Eqn.6.10.

6.4.3 Slender Body and Quasi-Steady Hypothesis

We shall assume that the airfoil can be considered as a *'slender body'* with respect to its longitudinal axis and that the *'Quasi-Steady Hypothesis'* holds. Such hypotheses hold if the characteristic size of the section is small when compared with the turbulence length scale.

Effect of Upstream Turbulence

Under such circumstances, the forces due to turbulence can be defined as a function of the turbulence components in one point representative of the section and can be evaluated defining an instantaneous velocity corresponding to the resultant of the mean wind velocity and of the turbulence components. Holding the two hypotheses and assuming that the turbulence components are small with respect to the mean wind velocity: $u(t) << \overline{U}$ and $w(t) << \overline{U}$. The forces can be separated into a mean vector $\overline{F}$ and a fluctuating part $F'(t)$. Then Eq.6.11:

$$\begin{aligned} F_z &= \frac{1}{2}\rho \overline{U}_a^2 c C_z\left(\alpha_a\right) \\ M_o &= \frac{1}{2}\rho \overline{U}_a^2 c^2 C_M\left(\alpha_a\right) \end{aligned} \tag{6.11}$$

actually has:

$$\begin{aligned} F_z &= \overline{F_z} + F_z'(t) \\ M_y &= \overline{M_y} + M_y'(t) \end{aligned} \tag{6.12}$$

Effect of Airfoil Motion

Variations in the coefficients of aerodynamic forces are functions of the angle of incidence traced by the apparent velocity.

Assuming α is very small in Fig.6.13, simple substitutions in Eqn.6.11 & Eqn.6.12 provides us the following comprehensive form:

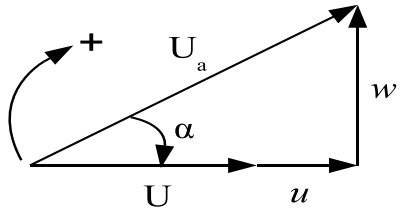

Figure 6.13: Velocity Triangle.

$$F'_z = \frac{1}{2}\rho\overline{U}^2 c\left[2\frac{u}{\overline{U}}C_z + \frac{w}{\overline{U}}C'_z\right]$$
$$M'_y = \frac{1}{2}\rho\overline{U}^2 c^2\left[2\frac{u}{\overline{U}}C_M + \frac{w}{\overline{U}}C'_M\right] \tag{6.13}$$

where modeling of the orthogonal velocity components u and w is explained in Sec.6.4.1. Meanwhile, applying the Quasi-Steady Theory assumption Fung (1993), we know from Eqn.3.9 and Fig.3.2 that as the reduced frequency 'K' approaches zero, the real part of Theodoresen Function 'F' approaches 1 and the imaginary part 'G' approaches zero. The aerodynamic flutter derivatives in Fig.3.3 are reduced to the form:

$$H_1 = \frac{-1}{\overline{U}}C'_z \quad H_2 = 0 \quad H_3 = C'_z \quad H_4 = 0$$
$$A_1 = 0 \quad A_2 = \frac{-1}{8}\frac{c}{\overline{U}}C'_z \quad A_3 = 0 \quad A_4 = 0 \tag{6.14}$$

Linear aerodynamic loads experienced by the airfoil can now be written from Eqns.3.7, 6.12 & 6.13 as follows:

$$F_z = \frac{1}{2}\rho bc\overline{U}^2\left(H_1\dot{z} + H_2\dot{\alpha} + H_3\alpha + H_4 z\right) + \frac{1}{2}\rho bcU^2 C'_z\int_0^\tau \frac{w(\sigma)}{U}\Psi'(\tau-\sigma)d\sigma$$
$$M_o = \frac{1}{2}\rho bc^2\overline{U}^2\left(A_1\dot{z} + A_2\dot{\alpha} + A_3\alpha + A_4 z\right) + \frac{1}{2}\rho\overline{U}^2 c^2\left[\frac{w}{\overline{U}}C'_M\right] \tag{6.15}$$

where $\Psi(\tau)$ is Kussner's aerodynamic indicial admittance function which varies with non-dimensional time, $\tau = \dfrac{2\overline{U}}{c}t$, Sec.6.4.2.

6.5 Linear System Experiment versus QST

Circular points in Fig.6.14 represent transient energy growth for the linear airfoil setup, Sec.3.3. Each circular point denotes the value of maximum energy of the system normalized with respect to a reference value for each increment in the mean free stream velocity. We see that as the mean free stream velocity approaches the linear critical velocity, energy amplification in the system increases exponentially. It reaches a value of $\approx 9 \approx 10$ for a mean velocity just below the linear critical velocity. This result is in line with Schmid & de Langre (2003). The authors studied a generic case of coupled mode flutter and established that energy amplification in case of linear systems by transient growth mechanism may be as large as 10. For damped systems, maximum energy amplification scales inversely to the square of the damping constant, Schmid & de Langre (2003).

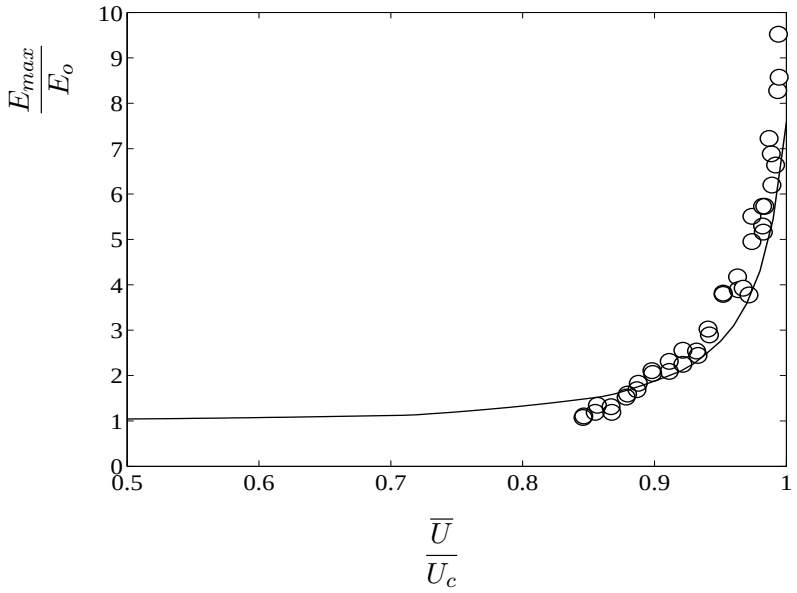

Figure 6.14: Maximum Normalized Energy versus Velocity Parameter. 'o' Experimental Points, (Solid Line) Computations.

Solid line in the figure is obtained by numerically simulating the on-going fluid structure interaction phenomena using Eqn.6.15. Long term response of the airfoil can be obtained by the first term on the right hand side in Eqn.6.15. The gust effect is modelled in the second term including the Kussner's admittance function. Normally, such a scenario would have been treated using the full un-steady airfoil theory. What we propose here is that the long term response of the airfoil can be reliably predicted using the quasi-steady theory as outlined in Sec.6.4.3. The short term impulsive response to the up-stream gust can be incorporated into the model using the Kussner's admittance function, Eqn.6.9. The important advantage associated with this approach is that system dynamics can be studied without going into the complex mathematical details of the un-steady airfoil theory, Hémon *et al.* (2006). The numerical simulation technique used in this case is described in Sec.3.1, Eqn.3.10. Excitation by the up-stream turbulence effects was modeled using symmetric Gauss Distribution Functions as described in Sec.6.4.1.

We can see from Fig.6.14 that although this new combination of the quasi-steady theory and the Kussner's admittance formulation slightly under-estimates the maximum energy amplification near critical flutter velocity, it models the aeroelastic phenomena fairly accurately.

6.6 Discussion

Detailed experimental evidence is provided showing the existence of by-pass transition to flutter instability in case of a non-linear airfoil setup; due to transient growth. Moreover, a new combination of the standard quasi-steady theory and the Kussner's admittance formulation is proposed to model the effects of a single abrupt gust on a symmetric airfoil. Experimental results and the simulation curve agree well.

Chapter 7

Conclusions and Perspectives

7.1 Conclusions

To conclude, this study deepened our understanding of the transient phenomena in different fluid structure interaction systems. We conducted experiments and validated our findings using simple theoretical tools. The study emphasizes the importance of accurate caliberation of different long term system parameters before they can be used for much complicated short term transient behavior of the systems. Another important aspect that comes to light is the significance of time domain simulations necessary for better comprehension of short term energy amplification phenomenon. This significance can be attributed to the fact that time domain simulations allow us to take into account different combinations of the turbulence excitation and aeroelastic effects. The study allows us to see some inherently complicated phenomena like hysteresis in case of vortex induced oscillations of a bluff body and the by-pass transition to flutter instability due to transient growth in case of non-linear airfoil systems.

We started with the vortex induced oscillations of a square cylinder in a wind tunnel at low wind velocities. An overview of the existing literature shall reveal that although various authors have written extensively on the underlying mechanisms of vortex induced vibrations, none of the studies caters for a square section cylinder allowed to respond freely to the incident flow; as is the case in this thesis report. Experimental set up was designed to ensure nearly two dimensional transverse oscillations. The free vibration approach was chosen due to the lack of existing experimental evidence for such systems. This approach is closer to a practical real

world system due to the fact that it provides direct evidence of non-linear fluid structure interaction mechanisms as shown and discussed. We conducted the experiments primarily using two different configurations. In the first case, the square cylinder was brought to rest for each increment in the upstream velocity. Oscillations growth rate during the transient phase was measured. In the second case however, the memory effect was allowed to play for each increment in velocity through out the velocity range. We were able to capture the ever elusive hysteresis in the reduced amplitude curve. It is important to underline the fact that although hysteresis is known to exist, this study is the first of its kind given the unique experimental conditions chosen for this case. The experimental results were compared with the simulation results of a theoretical wake oscillator model. Our study shows that while the wake oscillator model could predict the maximum lock-in amplitude fairly accurately, there remain some questions regarding the location of the maximum amplitude on the reduced velocity axis and the extent of the frequency lock-in range. We shall discuss possible explanations in the next section.

As stated earlier, this study reiterates the importance of the awareness of the long term behavior of fluid structure systems, indicating its direct implications on our understanding of the transient behavior of the same. A significant part of this study is therefore dedicated to the long term system analysis. An efficient experimental setup is proposed capable of generating just a single upstream gust which can be measured and incorporated into the theoretical model using simple algebraic tools. Special attention was paid to the fact that structural damping in the experiments remains very low. Sliding friction was eliminated by avoiding any moveable parts from the setups. Important structural parameters are measured and verified using simple theoretical tools. We observed how the frequency ratio of a linear two degree of freedom system effects the long term stability parameters including the critical velocity and aerodynamic stiffness.

The second part of this study presented the main focus of our research i.e. transient energy growth. The logarithmic decrement technique is used to measure the growth rate of oscillations amplitude in the transient regime. As discussed before, this study sets a foundation stone for the growth rate measurements of oscillating bluff bodies under similar circumstances. The experimental results are consistent with previously published findings, Amandolèse & Hémon (2010) and with previous

theoretical studies, de Langre (2006).

Transient energy growth was investigated in case of a spring mounted bridge deck section subjected to an upstream gust. Since the bridge deck section is not symmetrical, the incident airflow displaces the deck section downwards due to the resultant lifting force. This initial displacement is a function of the mean free stream velocity. All the subsequent energy calculations take this initial displacement into account. This study established experimental proof for the first time indicating the existance of transient energy amplification in such fluid structure systems. Experimental results support Schmid & de Langre (2003) on the fact that larger initial excitation results in larger energy amplification of the system due to the transient growth phenomenon. Experimental evidence is provided linking the frequency ratio, the critical velocity and the maximum energy amplification of a bridge deck section in a wind tunnel.

This study introduced another phenomenon, namely the by-pass transition to flutter instability due to transient growth in case of two degrees of freedom non-linear airfoil systems. A weak non-linearity was introduced in the system stiffness. Energy of the system was calculated while taking into account the non-linear effect. Experimental results from similar linear and non-linear experimental setups were compared to pin-point the existence of by-pass transition to flutter due to transient energy growth. During the course of this study we explored a number of aerodynamic admittance models as presented by Wagner, Sears and Kussner. The Kussner function was chosen for its closer co-relation to our experimental setup. We presented a new combination of the existing quasi-steady theory to model the long-term behavior and the Kussners aerodynamic admittance formulation to model the upstream gust effect. Results show that we can obtain an acceptable comparison without going into the intricate details of the unsteady airfoil theory.

7.2 Perspectives

Different authors have published their work in attempts to enhance the wake-oscillator model since it was proposed by Currie & Hartlen (1970). Such models are based on the reduced vortex lift coefficient manipulated in the form of a standard van der Pol equation to model the effects of the vortex shedding on the solid object. The solid object in turn is modelled in the form a standard damped spring mass

system. Focring terms in both the equations impose the necessary coupling. An important aspect associated with using this type of theoretical models is the fact that the ratio between the coupling force scaling 'A' and the near wake van der Pol parameter 'ϵ' has to be fixed independently for each case of a bluff body executing vortex induced vibrations. This ratio governs the maximum limit cycle amplitude at lock-in. The extent of the lock-in domain is controlled by the product of the coupling force scaling 'A' and the mass parameter 'M', de Langre (2006). While our experimental results validate the model's ability to predict the maximum lock-in amplitude; the comparison reflects an important draw back regarding the extent of the lock-in range. Also, a closer inspection of our experimental results in Fig.2.4 and Fig.2.5 shall reveal that the maximum lock-in amplitude lies at a slightly higher value of the reduced velocity then the expected (1 / St). The wake oscillator model proposes that this maximum amplitude should lie indeed at reduced velocity closer to (1 / St). This discrepency in the location of the maximum lock-in amplitude and the extent of the lock-in domain may be connected. A plausible explanation for the off-set in the maximum amplitude could be the blockage effect in the wind tunnel test section. However, the fact that the maximum growth rate, Fig.4.3 lies closer to the (1 / St) value contradicts this hypothesis. A two pronged approach may be helpful in this regard. A detailed investigation of the blockage effects in this case may yield new experimental evidence. But this will take intense consistent efforts given the highly coupled nature of the solid oscillations and the vortex shedding phenomenon. At the same time extending the model to consider higher order terms in the forcing functions could improve the accuracy of theoretical curves. Another important tool which could be used is a visualization study. The ability to simply see the vortex shedding patterns in real time could shed some more light on any existing phenomena near resonance.

Results presented regarding the transient energy growth in suspended bridge deck sections add valuable insight to our understanding of the aerodynamic bridge deck behavior. However, it is important to note that despite the extensive efforts we could not establish a linear relationship between the maximum transient energy amplification and the frequency ratio. This was largely due to the fact that changing fundamental system parameters like the frequency ratio changes the operational mean velocity range. The maximum operational wind velocity is physically governed by the available experimental tools, maximum fan power for exmaple. Needless to mention that working at higher wind velocities may pose a possible health/safety

concern. A future experimental study can be possibly directed towards this objective. Another important point regarding this study is that, as mentioned before, traditional theoretical tools cannot be directly used to qualify the transient experimental results. A literature overview would show that common practise in this respect is to measure aerodynamic coefficients for each bridge construction project individually. This was however, not the prime objective of this study. A theoretical study may be organized in future keeping in mind that although similar, the aerodynamic behavior of a bridge deck section is fundamentally different from that of an airfoil. Same aerodynamic coefficients cannot be used for both the cases, Scanlan & Tomko (1977). It is common practise in bridge deck design to keep the aerodynamic center at the axis of rotation which in turn lies at the chord wise geometric center of the deck section. Consequently, the coupling parameter 'd' and the parameter 'a' in Sec.3.1 become zero.

This study presented new experimental data establishing proof of the existence of by-pass transition to flutter instability due to transient growth in non-linear airfoil systems. We presented a new combination of the existing quasi-steady theory and the Kussners aerodynamic admittance function. Although the model under estimates the maximum energy amplification, it agrees with the experimental data to an acceptable limit. We hope that this model could be further evaluated and adopted for future transient energy studies of similar fluid structure systems.

Bibliography

Amandolèse, X. & Hémon, P. 2010 Vortex induced vibrations of a square cylinder in wind tunnel. *Compte Rendus Mecanique* **338** (1), 12–17.

Banerjee, J. R. 2003 A simplified method for the free vibration and flutter analysis of bridge decks. *Journal of Sound and Vibration* **260** (5), 829–845.

Bartoli, G. & Mannini, C. 2008 A simplified approach to bridge deck flutter. *Journal of Wind Engineering and Industrial Aerodynamics* **96** (2), 229–256.

Bearman, P. W. 1984 Vortex shedding from oscillating bluff bodies. *Annual Review of Fluid Mechanics* **16**, 195–222.

Bearman, P. W. & Obasaju, E. D. 1982 An experimental study of pressure fluctuations on fixed and oscillating Square-Section cylinders. *Journal of Fluid Mechanics* **119**, 297–321.

Blevins, R. D. 1990 *Flow Induced Vibrations*. Van Nostrand Reinhold, New York.

Brika, D. & Laneville, A. 1993 Vortex-induced vibrations of a long flexible circular cylinder. *Journal of Fluid Mechanics* **250** (-1), 481–508.

Chen, A., He, X. & Xiang, H. 2002 Identification of 18 flutter derivatives of bridge decks. *Journal of Wind Engineering and Industrial Aerodynamics* **90** (12-15), 2007–2022.

Chen, X. 2007 Improved understanding of bimodal coupled bridge flutter based on Closed-Form solutions. *Journal of Structural Engineering* **133**, 22–31.

Chen, X., Matsumoto, M. & Kareem, A. 2000 Aerodynamic coupling effects on flutter and buffeting of bridges. *Journal of Engineering Mechanics* **126**, 17–26.

Cheng, L., Zhou, Y. & Zhang, M. M. 2003 Perturbed interaction between vortex shedding and induced vibration. *Journal of Fluids and Structures* **17**, 887–901.

Currie, I. G. & Hartlen, R. T. 1970 Lift oscillator model of vortex induced vibration. *Journal of Engineering Mechanics Division of ASCE* **96**, 577–591.

Facchinetti, M. L., de Langre, E. & Biolley, F. 2004 Coupling of structure and wake ooscillators in Vortex-Induced vibrations. *Journal of Fluids and Structures* **19** (2), 123–140.

Feng, C. C. 1968 *The Measurement of Vortex Induced Effects in Flow Past Stationary and Oscillating Circular and D-Section Cylinders*. The University of British Columbia, Canada: Masters Thesis, Deptt of Mechanical Engg.

Filippone, A. & Siquier, J. 2003 Aerodynamic admittance of a two dimensional body. *The Aeronautical Journal* pp. 405–418.

Fung, Y. 1993 *An Introduction to the Theory of Aeroelasticity*. New York: Dover Publications.

Garrick, I. E. & Wilmer, H. Reed III 1981 Historical development of aircraft flutter. *Journal of Aircraft* **18**, 897–911.

Godreche, C. 1998 *Hydrodynamics and Nonlinear Instabilities*. New York: Cambridge University Press.

Govardhan, R. & Williamson, C. H. K. 2000 Modes of vortex formation and frequency response of a freely vibrating cylinder. *Journal of Fluid Mechanics* **420**, 85–130.

Géradin, M. & Rixen, D. 1992 *Theorie des Vibrations (Application a la Dynamique des Structures)*. Paris: Masson Paris.

Hémon, P., de Langre, E. & Schmid, P. 2006 Experimental evidence of transient growth of energy before airfoil flutter. *Journal of Fluids and Structures* **22** (3), 391–400.

Kehoe, M. W. 1995 A historical overview of flight flutter testing. *NASA TM-4720* .

Khalak, A. & Williamson, C. H. K. 1999 Motions, forces and mode transitions in Vortex-Induced vibrations at low Mass-Damping. *Journal of Fluids and Structures* **13** (7-8), 813–851.

Kholodar, D. B., Dowel, E. H., Thomas, J. P. & Hall, K. C. 2004 Limit cycle oscillations of a typical airfoil in transonic flow. *Journal of Aircraft* **41** (5), 1067–1072.

Kussner, H. G. 1936 Zusammenfassender bericht uber den instationaren auftrieb von flugeln. *Luftfahrtforschung* **13**, 410–424.

de Langre, E. 2006 Frequency lock-in is caused by coupled-mode flutter. *Journal of Fluids and Structures* **22** (6-7), 783–791.

Larose, G. L. & Mann, J. 1998 Gust loading in streamlined bridge decks. *Journal of Fluids and Structures* **12** (5), 511–536.

Larsen, A., Esdahl, S., Andersen, J. E. & Vejrum, T. 2000 Storebaelt suspension bridge - vortex shedding excitation and mitigation by guide vanes. *Journal of Wind Engineering and Industrial Aerodynamics* **88** (2-3), 283–296.

Lee, Y. S., Vakakis, A. F., Bergman, L. A., McFarland, D. M. & Kerschen, G. 2005 Triggering mechanisms of limit cycle oscillations due to aeroelastic instability. *Journal of Fluids and Structures* **21** (5-7), 485–529.

Matsumoto, M., Mizuno, K., Okubo, K., Ito, Y. & Matsumiya, H. 2007 Flutter instability and recent development in stabilization of structures. *Journal of Wind Engineering* **95**, 888–907.

Mizota, T. & Nakamura, Y. 1975 Unsteady lifts and wakes of oscillating rectangular prisms. *Proceedings of the ASCE* **101** (EM6), 855–871.

Morse, T. L., Govardhan, R. N. & Williamson, C. H. K. 2008 The effect of end conditions on the Vortex-Induced vibration of cylinders. *Journal of Fluids and Structures* **24** (8), 1227–1239.

Morse, T. L. & Williamson, C. H. K. 2009 Fluid forcing, wake modes, and transitions for a cylinder undergoing controlled oscillations. *Journal of Fluids and Structures* **25** (4), 697–712.

Nakamura, Y. 1978 An analysis of binary flutter of bridge deck sections. *Journal of Sound and Vibration* **57** (4), 471–482.

Noger, C. & Hémon, P. 2004 Transient growth of energy and aeroelastic stability of ground vehicles. *Compte Rendu Mécanique* **332**, 175–180.

Ongoren, A. & Rockwell, D. 1988*a* Flow structure from an oscillating cylinder part 1. mechanisms of phase shift and recovery in the near wake. *Journal of Fluid Mechanics* **191** (-1), 197–223.

Ongoren, A. & Rockwell, D. 1988*b* Flow structure from an oscillating cylinder part 2. mode competition in the near wake. *Journal of Fluid Mechanics* **191**, 225–245 M3 – 10.1017/S0022112088001570.

Otsuki, Y., Washizu, K., Tomizawa, H. & Ohya, A. 1974 A note on the aeroelastic instability of a prismatic bar with square section. *Journal of Sound and Vibration* **34**, 233–248.

Parkinson, G. 1989 Phenomena and modelling of flow induced vibrations of bluff bodies. *Progress in Aerospace Science* **26**, 169–224.

Poirel, D. C. & Price, S. J. 1997 Post-Instability behavior of a structurally Non-Linear airfoil in longitudinal turbulence. *Journal of Aircraft* **34** (5), 619–626.

Reissner, H. 1926 Neurere probleme aus der flugzeugstatik. *Zeitschrift fuer Flugtechnik und Motorluftschiffahrt* **17**, 137–146.

Sarpkaya, T. 1979 Vortex induced oscillations, a selective review. *Journal of Applied Mechanics* **46**, 241–258.

Scanlan, R. H. & Tomko, J. J. 1977 Airfoil and bridge deck flutter derivatives. *ASCE Journal of the Engineering Mechanics Division* pp. 1717–1737.

Schmid, P. & Henningson, D. S. 2001 *Stability and Transition in Shear Flows*. New York: Springer.

Schmid, P. & de Langre, E. 2003 Transient growth before Coupled-Mode flutter. *Journal of Applied Mechanics* **70** (6), 894–901.

Schwartz, M., Manzoor, S., Hémon, P. & de Langre, E. 2009 By-pass transition to airfoil flutter by transient growth due to gust impulse. *Journal of Fluids and Structures* **25** (8), 1272–1281.

Sears, W. R. 1941 Some aspects of non stationary airfoil theory and its practical applications. *Journal of Aeronautical Sciences* **18**, 104–108.

Shams, Sh., Lahidjani, M. H. S. & Haddadpour, H. 2008 Nonlinear aeroelastic response of slender wings based on wagner function. *Thin-Walled Structures* **46** (11), 1192–1203.

Skop, R. A. & Balasubramanian, S. 1997 A new twist on an old model for Vortex-Excited vibrations. *Journal of Fluids and Structures* **11** (4), 395–412.

Theodorsen, T. 1935 General theory of aerodynamic instability and the mechanism of flutter. *NACA Technical Report 496* .

Theodorsen, T. & Garrick, I. E. 1940 A theoretical and experimental investigation of the flutter problem. *NACA Technical Report 685* .

Wagner, H. 1925 Uber die entstahung des dynamischen auftriebes von tragflugeln. *Zeitschrift fur Angewandte Mathematik und Mechanik* **5**, 17–35.

Wilkinson, R. H. 1974 *On the Vortex Induced Loading on Long Bluff Cylinders*. Faculty of Engineering, University of Bristol, England: PhD Thesis, Faculty of Engineering, University of Bristol, England.

Williamson, C. H. K. & Roshko, A. 1988 Vortex formation in the wake of an oscillating cylinder. *Journal of Fluids and Structures* **2**, 355–381.

Appendix

Vortex Induced Vibrations of a Square Cylinder in a Wind Tunnel. Manzoor, S., Hémon, P., Amandolèse, X. Proceedings of ASME 3^{rd} FEDSM 2010, FEDSM-ICNMM2010-30067.

On the aeroelastic transient behavior of a streamlined bridge deck section in a wind tunnel. Manzoor, S., Hémon, P., Amandolèse, X. Submitted, Journal of Fluids and Structures.

By-pass transition to airfoil flutter by transient growth due to gust impulse. Schwartz, M., Manzoor, S., Hémon, P., de Langre, E. Journal of Fluids and Structures, 2009, 25(8), 1272-1281.

Transient temporal response of a flexible bridge deck submitted to a single gust. Manzoor, S., Amandolèse, X., Hémon, P. Submitted, 13^{th} International Conference on Wind Engineering, Amsterdam.